

University of Montana

ScholarWorks at University of Montana

Graduate Student Theses, Dissertations, &
Professional Papers

Graduate School

2013

MECHANISMS AND CYTOTOXIC EFFECTS OF NQO1-DIRECTED LAVENDAMYCIN DERIVATIVES AND MITOCHONDRIA-TARGETED ANTHRACENYL ISOXAZOLE AMIDES AS NOVEL ANTITUMOR AGENTS

Alison King Kearns

The University of Montana

Follow this and additional works at: <https://scholarworks.umt.edu/etd>

Let us know how access to this document benefits you.

Recommended Citation

Kearns, Alison King, "MECHANISMS AND CYTOTOXIC EFFECTS OF NQO1-DIRECTED LAVENDAMYCIN DERIVATIVES AND MITOCHONDRIA-TARGETED ANTHRACENYL ISOXAZOLE AMIDES AS NOVEL ANTITUMOR AGENTS" (2013). *Graduate Student Theses, Dissertations, & Professional Papers*. 4132. <https://scholarworks.umt.edu/etd/4132>

This Dissertation is brought to you for free and open access by the Graduate School at ScholarWorks at University of Montana. It has been accepted for inclusion in Graduate Student Theses, Dissertations, & Professional Papers by an authorized administrator of ScholarWorks at University of Montana. For more information, please contact scholarworks@mso.umt.edu.

**MECHANISMS AND CYTOTOXIC EFFECTS OF NQO1-DIRECTED
LAVENDAMYCIN DERIVATIVES AND MITOCHONDRIA-TARGETED
ANTHRACENYL ISOXAZOLE AMIDES AS NOVEL ANTITUMOR AGENTS**

By

ALISON KING KEARNS

Bachelor of Science in Nutritional Sciences, Pennsylvania State University, University
Park, Pennsylvania, 2007

Dissertation

presented in partial fulfillment of the requirements
for the degree of

Doctor of Philosophy
in Biomedical Sciences

The University of Montana
Missoula, MT

Summer 2013

Approved by:

J.B. Alexander Ross, Dean of The Graduate School
Graduate School

Dr. Howard D. Beall, Chair
Department of Biomedical and Pharmaceutical Sciences

Dr. Douglas Coffin
Department of Biomedical and Pharmaceutical Sciences

Dr. Keith Parker
Department of Biomedical and Pharmaceutical Sciences

Dr. Mark Pershouse
Department of Biomedical and Pharmaceutical Sciences

Dr. Kent Sugden
Department of Chemistry and Biochemistry

**MECHANISMS AND CYTOTOXIC EFFECTS OF NQO1-DIRECTED
LAVENDAMYCIN DERIVATIVES AND MITOCHONDRIA-TARGETED
ANTHRACENYL ISOXAZOLE AMIDES AS NOVEL ANTITUMOR AGENTS**

Chairperson: Dr. Howard D. Beall

Cancer is a common, complex, and oftentimes fatal disease. Despite extensive research in the field of cancer drug discovery, there are still improvements to be made in the design of effective anticancer agents. This project involved three separate but related studies that fall under the category of anticancer drug discovery as a whole. The overall goal of this project was to design and investigate the mechanisms of action of new antitumor agents to be used against solid tumors. First, we developed a series of anthracenyl isoxazole amides (AIMs) designed to bind to G-quadruplex DNA and inhibit telomerase. Results from this study demonstrated an alternative mitochondrial mechanism of action of the AIMs not yet fully described in the literature. Investigation of lead compound AIM 1 showed localization of the AIM in mitochondria with resulting induction of apoptosis, generation of mitochondrial superoxide, disruption of mitochondrial membrane potential, and activation of caspase-9. The second goal of this project was to assay a series of 4-isoxazoly-1,4-dihydropyridines (IDHPs) that function as P-gp inhibitors to determine their contribution to enhanced cytotoxicity of the AIMs when co-dosed together *in vitro*. Because so many anticancer agents are substrates for P-gp and are therefore limited in their ability to reach intended targets, the development of P-gp inhibitors is an important area of research. Results from this study indicate that IDHPs are a viable class of P-gp inhibitors that can be co-dosed with P-gp substrates to increase substrate cytotoxicity. The third goal of this study was to determine the NQO1 substrate potential of a series of lavendamycin derivative quinolinequinones and assess their corresponding antitumor potential. Surprisingly, few of the quinolinequinones tested showed preferential specificity for NQO1-expressing cells compared to NQO1-null cells. However, in our series of aryl-substituted quinolinequinones, the active molecules appear to be the quinone derivatives and not derivatives of hydroquinones or semiquinones. These data suggest a mode of action that differs from that of previously studied lavendamycin analogues that are activated by NQO1 reduction. While this project focused on the general targeting of solid tumors, the type of tumor explicitly studied varied from brain cancer to breast cancer and encompassed multiple drug targets. Collectively the results of this study are expansive and offer much to the field of targeted drug discovery.

KEY WORDS

Cancer, antitumor agents, targeted drug discovery

ACKNOWLEDGEMENTS

First and foremost I would like to thank all members of the Department of Biomedical and Pharmaceutical Sciences as well as those in the Center for Environmental Health Sciences for their support, encouragement, and enthusiasm towards my research and career. I would like to say a special thank to Pam Shaw who was an absolutely vital part of the research team and who helped me become confident in my research skills and always had the answer when I couldn't find it on my own.

I would like to thank my dissertation advisor, The World's Best Boss, Dr. Howard Beall for always being available, knowing when to push me and when to pull back, for being supportive of my goals and my research, and for being my mentor and my friend (BFF).

I would like to thank and acknowledge the members of my dissertation committee Dr. Douglas Coffin, Dr. Keith Parker, Dr. Mark Pershouse, and Dr. Kent Sugden. I will always be grateful for your support and guidance.

I am so lucky to have amazing friends that have stood by me through all of life's changes. Lindsey, I will never forget that phone call as I was speeding down the highway on my way back to Montana. You have always supported me in every decision I have made and for our friendship, I am grateful. Jess, I am so happy that we have maintained a long distance friendship and want to say thank you for your cheer leading and never ending support. Emily, I had no idea when we first met in the lab that our relationship would be what it is today. You are the only one that I have trusted to take over work for me when I was unavailable and that I have consulted when I had questions relating to lab. Outside of work, I consider you one of my dearest friends. Thank you for always saying the right things, for listening when I needed to talk, and for inspiring me to be a better person every day.

Lastly, this work would not have been possible without the encouragement and support I received from my father, the first Dr. Kearns. Thank you for telling me when I was a child that I was capable of big things, for never questioning the decisions that I have made for myself, for taking all of my phone calls (including those at 4am), and for always believing in me when maybe I had doubts, myself. Thank you for always reminding me about the bigger picture and for inspiring me every day. Dad—I love you more than words can express.

TABLE OF CONTENTS

CHAPTER 1: Introduction

Brain cancer	
Overview.....	1
Glioblastoma classification and development.....	2
Apoptosis	
Overview.....	4
The extrinsic apoptotic pathway.....	5
The intrinsic apoptotic pathway.....	6
Non-apoptotic methods of cell death.....	9
Pharmacologic targeting of the apoptotic pathway.....	10
G-quadruplex	
Overview.....	12
Telomeric G-quadruplex.....	13
hTERT.....	17
G-quadruplex in gene promoters.....	22
G-quadruplex ligand features and druggability.....	23
Barriers to effective drug treatment	
Overview.....	26
P-glycoprotein.....	27
P-glycoprotein inhibitors.....	30
Alternative anticancer drug targets.....	31
NQO1	
Overview.....	32
NQO1 structure and function.....	33
Quinones as NQO1 substrates.....	34
Conclusions.....	38
Hypothesis and specific aims.....	39
References.....	41

CHAPTER 2: Cytotoxicity and mechanisms of antitumor anthracenyl isoxazole amides (AIMs) as G-quadruplex ligands

Abstract.....	50
Introduction.....	51
Materials and Methods.....	55
Results.....	60
Discussion.....	76
References.....	81

CHAPTER 3: Investigation of novel antitumor agent anthracenyl isoxazole amide (AIM) 1 as a mitochondrial modulator of apoptosis

Abstract.....	84
Introduction.....	85
Materials and Methods.....	90
Results.....	94
Discussion.....	108
References.....	113

CHAPTER 4: A novel series of 4-isoxazolyl-1,4-dihydropyridines (IDHPs) P-gp inhibitors enhance the cytotoxicity of anthracenyl isoxazole amide (AIM) antitumor compounds when co-dosed together *in vitro*

Abstract.....	117
Introduction.....	118
Materials and Methods.....	121
Results.....	124
Discussion.....	140
References.....	145

CHAPTER 5: Synthesis of new quinolinequinone derivatives and preliminary exploration of their cytotoxic properties

Abstract.....	148
Introduction.....	150
Materials and Methods.....	153
Results.....	155
Discussion.....	163
References.....	166

CHAPTER 6: Conclusions

Conclusions.....	168
References.....	175

APPENDIX

Appendix I.....	177
Appendix II.....	227

LIST OF FIGURES

Chapter 1

1.1. Extrinsic apoptotic pathway.....	8
1.2. G-quadruplex structure.....	15
1.3. Structure and biological roles of telomeres.....	20
1.4. Efflux transporters.....	29
1.5. Selected antitumor quinone structures.....	37

Chapter 2

2.1. AIM structures.....	62
2.2. AIMs toxicity testing.....	63
2.3. Confocal microscopy of AIM dimer vs double tail structure.....	65
2.4. LSC with PI counterstaining.....	66
2.5. AIM 1 bioavailability vs AIM 2.....	68
2.6. LSC of AIM 1.....	70
2.7. NMR spectra of AIM 1.....	72
2.8. AIM 1 induction of apoptosis.....	73
2.9. LSC of single tail AIMs.....	75

Chapter 3

3.1. Structure and toxicity of AIM 1.....	96
3.2. AIM localization in SNB-19 cells.....	97
3.3. AIM 1 short term exposure.....	98
3.4. AIM induction of mitochondrial superoxide.....	100
3.5. Assessment of mitochondrial dysfunction.....	102
3.6. Caspase-9 activation.....	104
3.7. hTERT staining.....	106
3.8. Shuttling of hTERT.....	107

Chapter 4

4.1. Double tail AIMs in ADR-RES cell lines.....	126
4.2. IDHPs and P-gp inhibition.....	128
4.3. IDHPs cytotoxicity vs known P-gp inhibitors.....	129
4.4. Doxorubicin cytotoxicity vs AIMs.....	131
4.5. Doxorubicin cytotoxicity after IDHP exposure.....	132
4.6. AIM 1 cytotoxicity after IDHP exposure.....	135
4.7. AIM 3 cytotoxicity after IDHP exposure.....	136
4.8. IDHPs and AIM 1 cytotoxicity in SNB-19 cells.....	137
4.9. IDHPs and AIM 3 cytotoxicity in SNB-19 cells.....	139

Chapter 5

5.1. Streptonigrin and lavendamycin structures.....	157
5.2. NMR spectra of 19 with Zn ²⁺	161
5.3. NMR spectra of 22 with Zn ²⁺	162

LIST OF TABLES

Chapter 5

5.1. Reduction rates and oxygen consumption.....	158
5.2. Cytotoxicity of quinolinequinones in MDA-468 cells.....	159

CHAPTER 1: INTRODUCTION

Brain Cancer

Overview

The National Cancer Institute estimates that approximately 23,000 people in the United States will be diagnosed with cancer of the brain and central nervous system in 2013 and of those diagnosed, it is predicted that over half will die from the disease. Primary brain tumors represent approximately 2% of adult cancers and 23% of childhood cancers (Marie and Shinjo, 2011). The most common and most aggressive primary brain tumor, glioblastoma multiforme, is particularly difficult to treat and patients diagnosed with this subset of brain cancer, have a median survival time of only 15 months (Bleeker and Molenaar, 2012). Despite poor prognoses, compared to other malignancies, there have been only small advancements made in the pharmacologic intervention and treatment of glioblastoma. The standard treatment has remained the same for many years—newly diagnosed cases of glioblastoma are managed with a combination of gross tumor removal or resection followed by radiation and the highly cytotoxic DNA methylating agent temozolomide (Westermarck, 2012). Treatment is most often ineffective due to failure to completely resect the tumor on account of poor cellular differentiation and invasiveness, drug resistance, and subsequent aggressive tumor metastasis to other areas of the body (Candolfi *et al.*, 2011).

Glioblastoma classification and development

Similar to other cancers, glioblastoma results from accumulated genetic and epigenetic alterations, characterized by genetic instability and complex alterations in both chromosome copy number and structure (Volgstein and Kinzler, 2004). Historically, glioblastoma treatment was based on histopathological classification of the tumor (cell type and morphology, presence of necrosis or microvascular proliferation), however, this type of diagnosis is quickly being supplemented with treatment strategies based on mutational and amplification characterization of the individual's tumor (Dunn *et al.*, 2012). Due largely to wide genomic studies of glioblastoma, common genetic alterations as well as molecular subclasses and commonly mutated biochemical and signaling pathways have been uncovered. To date, glioblastoma has been studied the most extensively under genomic profiling conditions and yet successful treatment options remain elusive.

Primary glioblastomas that arise *de novo* most often exhibit dysfunctions in the tumor suppressor proteins p53 and retinoblastoma protein (Rb), as well as abnormalities of the RTK/Ras/PI3K signaling pathway, allowing tumor growth to go cellularly unchecked and unregulated (Dunn *et al.*, 2012). Another commonly mutated protein, epidermal growth factor receptor (EGFR) has been widely studied for its role in the development of glioblastoma. EGFR, a cell surface receptor responsible for intrinsic intracellular protein-kinase activation and

downstream signaling resulting in eventual DNA synthesis and cellular proliferation, is overexpressed in over 50% of primary glioblastoma and is associated with particularly poor prognosis in those patients presenting with EGFR mutations (Hurt et al., 1999). Ligands associated with the platelet-derived growth factor (PDGF) receptor pathway are also commonly mutated, with over 30% of primary glioblastoma cases involving up-regulation of these proteins (Dunn et al., 2012). Alterations in the PDGF signaling pathway has been found to promote aggressive glioma growth and is attributed to tumor angiogenesis. Additionally the phosphatase and tensin homolog (PTEN) is one of the most frequently mutated genes in all cancers and is responsible for antagonizing PI3K signaling and the downstream effects responsible for halting cell division and driving cells into apoptosis. PTEN undergoes genomic loss, mutation or epigenetic inactivation in upwards of 50% of gliomas, resulting in increased cellular proliferation and reduced apoptosis (Koul, 2008). Although there are many biochemical alterations that occur and are yet to be discovered, the ability to describe and characterize glioblastoma tumors by their genetic makeup and molecular changes is a promising approach to the design of new therapeutic strategies. Induction of apoptosis is also an important factor in the targeting of glioblastoma and other tumors and is an effective means by which to eliminate cancer cells following administration of chemotherapeutic agents.

Apoptosis

Overview

The term apoptosis, or programmed cell death, first appeared in the literature in 1972 as a means of describing a mode of cellular death morphologically distinct from the inflammatory and non-signal transduction pathway of cell death—necrosis (Kerr *et al.*, 1972). Morphologic changes indicative of apoptosis include cell membrane blebbing, cell shrinkage, chromatin condensation and nucleosomal fragmentation (Ricci and Zong, 2006). Apoptosis is a vital and complex manner of cell death via programmed cell suicide and is the cornerstone in maintaining homeostasis during development. Apoptosis is also recognized as one of the major barriers that must be overcome by tumor cells that allow them to survive and thrive under hostile conditions.

There are two major modes of initiating the apoptosis cascade: the intrinsic pathway and the extrinsic pathway; both result from activation of a series of proteins and enzymes belonging to the family of 14 cysteine proteases termed caspases. The intrinsic pathway of apoptosis involves mitochondrial dysfunction while the extrinsic pathway is associated with stimulation of cell membrane death receptors—both pathways converge at caspases-3 and from there follow a common activation process of executioner caspases (Mita *et al.*, 2008). Intracellular stress, such as high levels of reactive oxygen species (ROS) or DNA damage, is a typical activator of the

intrinsic pathway of apoptosis. In contrast, the extrinsic pathway requires for activation the binding of extracellular ligands (such as TNF- α) to plasma membrane bound receptors (Figure 1.1).

Apoptosis is a tightly regulated process involving both pro-apoptotic and anti-apoptotic factors for homeostatic balance. Under normal conditions, apoptosis functions as a protective means to remove genetically or otherwise damaged cells to prevent uncontrolled proliferation or tumorigenesis following unregulated mitogenic stimuli. A failure of cells to undergo apoptosis through evasion or acquired mutations, combined with maintenance of self-sufficient growth signals, insensitivity to anti-growth signals, tissue invasion and metastasis, limitless replicative capacity, and sustained angiogenesis, represents key features in the development and progression of cancer.

The extrinsic apoptotic pathway

The extrinsic pathway of apoptosis is activated by two groups of proteins: the tumor necrosis factor family (TNF) and the receptors that bind them. Not all TNF ligands signal apoptosis—some proteins function solely to activate molecules associated with induction of proinflammatory signals. TNF ligands ultimately responsible for apoptosis include TNF- α , CD95L (or FasL), and TNF receptor apoptosis-inducing ligand (TRAIL, or Apo2L) (Peter and

Krammer, 2003). In the case of Fas or TNF, once ligand binds receptor, recruitment of the adaptor protein Fas-associated death domain-containing protein (FADD) occurs. Bound FADD in turn recruits initiator caspases (in this case pro-caspase-8) and this assembly of proteins becomes the death-inducing signaling complex, DISC (Ricci and Zong, 2006). Inhibitory anti-apoptotic proteins can also block this process.

The intrinsic apoptotic pathway: mitochondrial-mediated apoptosis

One of the key features of the intrinsic pathway of apoptosis is the release of cytochrome *c* from the mitochondrial intermembrane space into the cytosol. Cytosolic cytochrome *c* binds Apaf-1, a cytosolic protein containing a caspase-recruitment domain (CARD), creating oligomerization and formation of the apoptosome (Wang, 2001). The Apaf-1/cytochrome *c* complex subsequently recruits pro-caspases-9 (to be cleaved to its active form caspases-9) and downstream activation of the executioner pro-caspases-3 (to be cleaved to active caspases-3). Active caspases-3 (regardless of its activation via the external or intrinsic pathway of apoptosis) initiates end stages of the apoptotic cascade through the cleavage of substrates leading to the characteristic morphological cellular features of apoptosis, as well as externalization of phosphatidylserine, a classic feature of apoptosis. Important upstream regulators of cytochrome *c* include Bax, Bak, Bik, Bad, and Bid (inducers of cytochrome *c* release) and Bcl-2 and Bcl-xL,

(suppressors of cytochrome *c* release). These proteins make up the Bcl-2 family of proteins, important mediators of mitochondrial-mediated apoptosis. Tumor suppressor protein p53 directly interacts with members of the Bcl-2 family to regulate apoptosis (Hanahan and Weinberg, 2000). Although mitochondrial events of apoptosis commit a cell to die, as with the extrinsic pathway of apoptosis, these events can be blocked downstream by anti-apoptotic proteins that interfere with or inactivate caspases (Kasibhatla and Tseng, 2003).

Figure 1.1

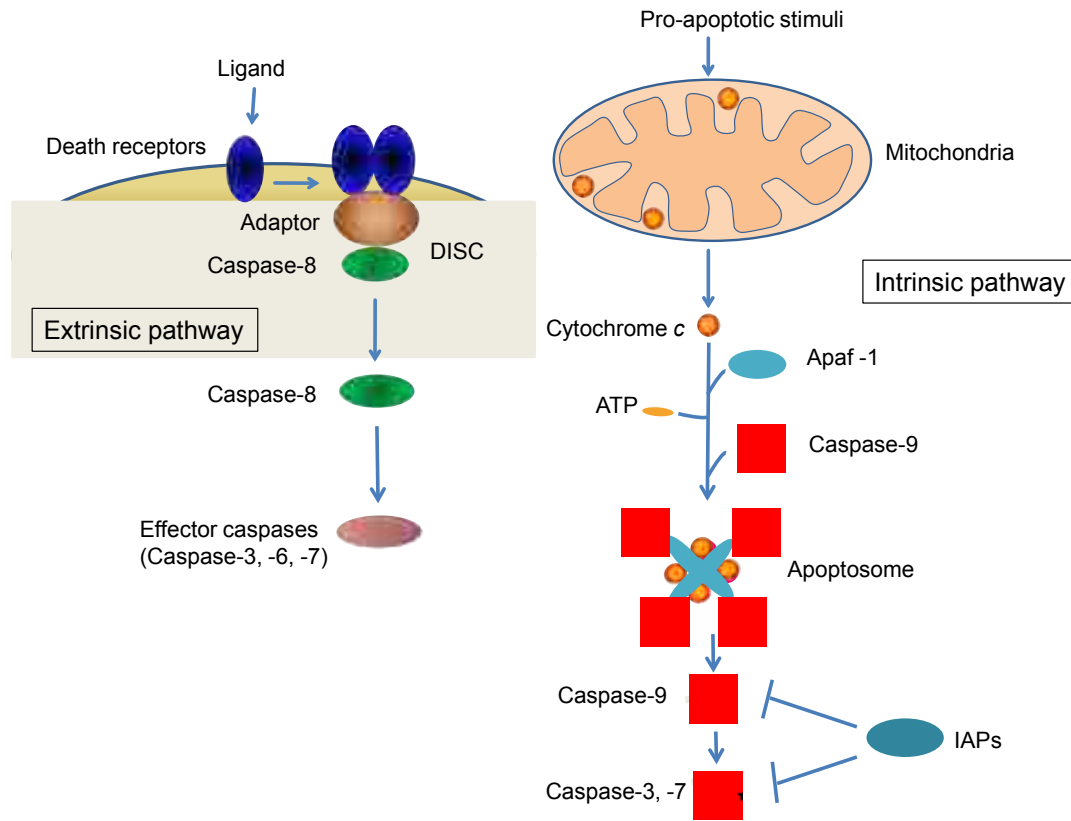


Figure 1.1. Extrinsic and intrinsic pathways of apoptosis. The two major apoptosis pathways. The extrinsic pathway is initiated by ligand binding to death receptors on the plasma membrane. The intrinsic pathway is activated by intracellular signals. Both pathways lead to activation of caspases (Li and Sheng, 2012).

Non-apoptotic methods of cell death

Although programmed cell death is vital to maintenance of normal cell functioning, non-apoptotic mechanisms also exist and can contribute to tumorigenesis when processes are disrupted. As previously mentioned, necrosis is a non-apoptotic and less controlled mode of cell death characterized morphologically by cytoplasmic vacuolization, loss of membrane integrity and cellular swelling (De Bruin and Medema, 2008). Necrosis results in the activation of inflammatory responses due to the release of cellular components into the microenvironment. An increase in localized inflammation also occurs following the necrosis of malignant cells. In contrast to necrosis, another non-apoptotic process, autophagy, is the degradation of proteins and organelles by lysosomal proteases. The major characteristic of autophagy is the fusion of autophagosomes (double membrane vesicles containing cytosolic organelles) with lysosomes, providing not only a means of cellular degradation but also an alternative source of nutrients for cells (De Bruin and Medema, 2008). In cancer, autophagy may prevent the malignancy of normal cells by degrading damaged organelles and reducing cellular stress, or by eliminating proteins that enhance tumor formation (Edinger and Thompson, 2003). Lastly, mitotic catastrophe is another means of cell death, distinctly different from those previously mentioned. Anomalous mitosis will cause mitotic catastrophe and results in deficient cell cycle checkpoints,

ultimately leading to enlarged and multinucleated cells, incomplete nuclear condensation, chromosome alignment defects, nondisjunction, or mitosis in the presence of DNA damage (Roninson *et al.*, 2001). In tumorigenesis, mitotic catastrophe can function to effectively eliminate cells entering mitosis with damaged DNA to reduce the likelihood that these defective cells will divide or acquire additional mutations that allow them to become tumorigenic.

Pharmacologic targeting of the apoptotic pathway as anticancer therapy

Resistance to apoptosis is closely linked to the development of cancer as a failure of damaged or malignant cells to undergo apoptosis allows them to expand into the interstitium. Preventing cancer cells from evading apoptosis has led to the development of small molecule drugs designed to target a wide range of pathways involved in cell death and apoptosis. The challenge in developing anticancer agents lies in identifying and exploiting the differences between normal non-cancerous cells versus cancerous cells and targeting of the various components of apoptosis (or other means of cell death) represents a viable method to do this. First generation chemotherapeutic agents rather indiscriminately cause cancer cell death by interfering with cell division or DNA synthesis and cell function. These drugs include: alkylating agents (such as cisplatin or cyclophosphamide), which cause DNA damage and ultimately cell death, anti-metabolites (mercaptopurine) that interfere with cell cycle and division, vinca

alkaloids (such as vincristine or vinblastine) that inhibit normal tubulin formation to disrupt cell cycle, taxanes (paclitaxel) that disrupt anaphase, topoisomerase inhibitors (such as topotecan or etoposide) causing inhibition of topoisomerase I or II leading to DNA damage, and anticancer antibiotics (such as doxorubicin or bleomycin) that can cause DNA damage through a variety of mechanisms including intercalation and formation of DNA crosslinks. Drugs developed to induce cancer cell apoptosis are designed to overcome the abnormal evasion of apoptosis and can target potentially any component of the apoptosis cascade. Common approaches include: the use of inhibitors against Bcl-2 proteins (fenretinide), drugs aimed at destabilizing or restoring mutant p53, caspases activators (which may be used in conjunction with more traditional chemotherapies to increase drug sensitivity), and small molecule antagonists of apoptosis-inhibitor proteins (Wong, 2011). While all of these methods have the potential to impact the viability of normal cells, the likelihood of inducing apoptosis in normal cells with therapy becomes less likely as more specific characteristics of cancer cells are identified and drugs are developed to only affect a specific component of the tumor cell. Although the targeting of apoptosis and apoptosis associated proteins represents a viable means of targeting cancer cells, there are other (and perhaps more specific) methods for anticancer drug therapies currently being investigated.

G-quadruplex

Overview

As mentioned previously, there are many chemotherapeutic agents currently being used to target DNA to damage and ultimately kill tumor cells. It is now recognized, however, that DNA structures exist outside of normal B-DNA that represent a feasible target for new anticancer drugs. Of particular interest are G-quadruplex (G4) DNA motifs, which adopt structures outside of normal Watson-Crick hydrogen bonding in duplex DNA formation. G-quadruplex structures are higher order DNA and RNA structures formed from guanine-rich sequences that can adopt a non-canonical, four-stranded topology. These guanine rich DNA sequences form quadruplex structures stabilized by guanine tetrads (G-G-G-G repeats), monovalent cations (notably Na^+ and K^+), and Hoogsteen hydrogen bonding (Burge *et al.*, 2006). Once a quadruplex is formed, it is very stable. Quadruplex can take on several different directionalities based on the arrangement of the backbone that constitutes the G-tetrad core (parallel versus antiparallel), by the syn or anti glycosidic bond arrangement of the guanines in the G-tetrad, the length and specifics of the G-G connecting loops, intra- or inter-molecular nature of the structure, and by the number of guanine tetrads (Sissi *et al.*, 2011) (Figure 1.2). G-quadruplex also function similarly to a molecular switch in that changes in the experimental

conditions or the introduction of G4 ligands into the environment can cause the quadruplex to fold or unfold. G-quadruplexes have been shown to form not only in humans, but other species as well, including yeast (Johnson *et al.*, 2008). The properties of quadruplex structure and function are even more intriguing considering their biologic significance—G-rich sequences have been found in specific regions of the genome and are over-represented in cells under certain physiologic conditions and disease states, including cancer.

In the context of cancer, it was first discovered that telomeres could form quadruplex and interfere with telomerase functioning, and more recently it has been found that there is disproportionately high expression of G-rich sequences in promoter regions of genes vital to cell signaling, especially proto-oncogenes (Balasubramanian *et al.*, 2011). These findings provide reasonable basis for the study and development of small molecule inhibitors that recognize and stabilize quadruplex in tumor cells.

Telomeric G-quadruplex

Telomeres are specialized and complex ribonucleoprotein structures that cap the ends of eukaryotic chromosomes. Since 1941, it has been known that telomeric structures are necessary for maintaining the integrity of chromosomes (McClintock, 1941). Telomeres function to protect internal chromosome sequences by preventing the improper activation of DNA damage-response

pathways (Lipps and Rhodes, 2009). In humans, telomeres consist of tandem repeats of G-rich sequences (TTAGGG) with a total length of up to 12 kb (Gunaratnam and Neidle, 2010).

Figure 1.2

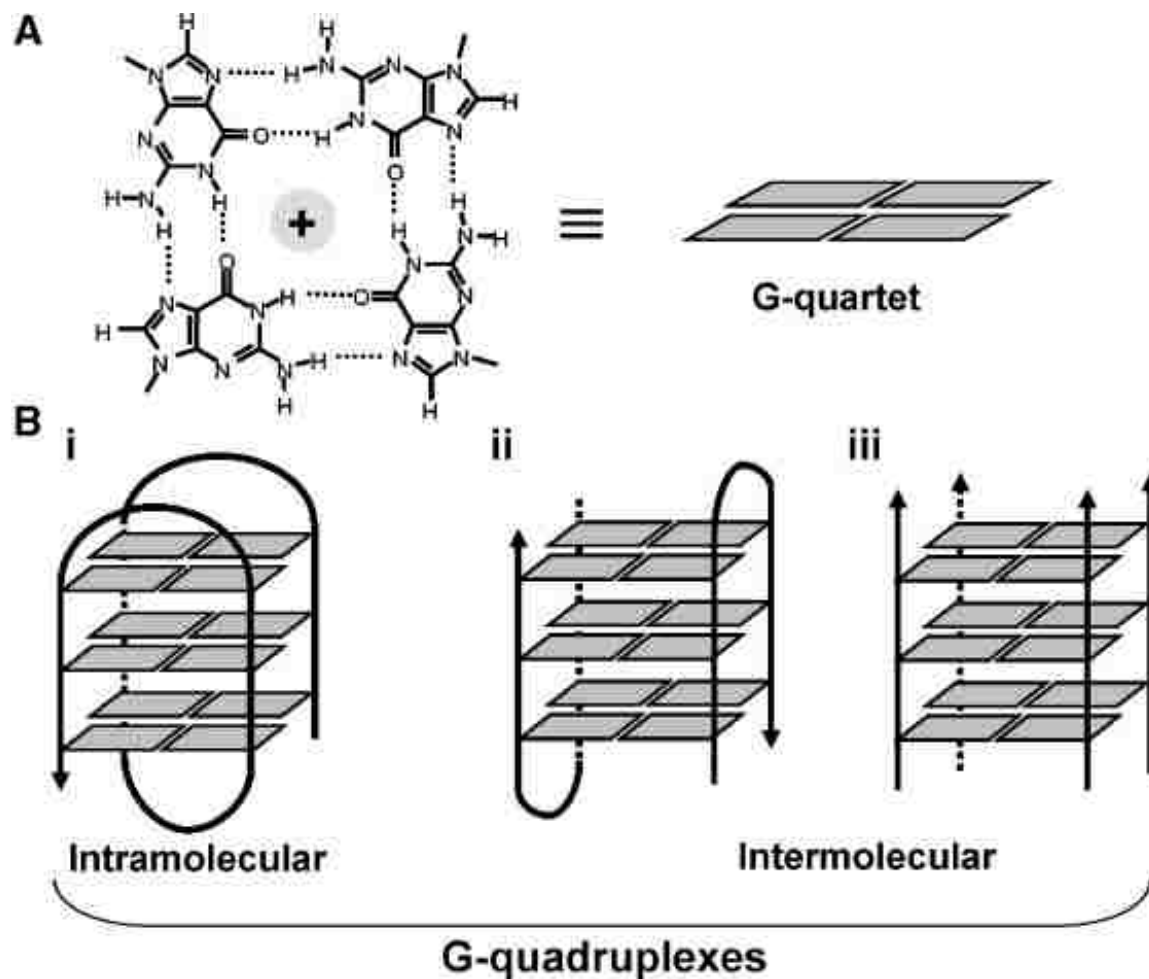


Figure 1.2 G-quadruplex structure. A Chemical structure of the G-quartet, the base unit of a G-quadruplex with a monovalent cation at its core. B Multiple layers of G-quartets stack on top of each other to form a G-quadruplex with various arrangements (adapted from Oganesian and Bryan, 2007).

Telomeric DNA is normal duplex DNA except for the final 100-200 3'-terminal residues, which are single stranded (Gunaratnam and Neidle, 2010). These single stranded overhangs, containing G-repeats, have been shown to fold intramolecularly upon themselves to form G-quadruplexes (Tang *et al.*, 2008). In normal somatic cells, telomeres progressively shorten at each round of cell division until reaching the Hayflick limit—the point at which cell division stops and cells can no longer replicate. Upon reaching the Hayflick limit, cells become senescent, a phase that under normal conditions precedes apoptosis. In over 80% of cancers, however, senescence is not achieved due to activation or up-regulation of the enzyme telomerase (Shay and Bacchetti, 1997).

Telomerase is a specialized reverse transcriptase enzyme that catalyzes the synthesis of TTAGGG repeats and adds these sequences to the end of chromosomes during replication to maintain telomeric DNA length. Telomerase is inactive in most somatic cells, but can be detected in germ cells and fetal tissue. In cancer cells, active telomerase prevents the progressive shortening of telomeres that would prime cells to enter apoptosis and instead enables these cells to replicate indefinitely. Because the single stranded overhang of telomeres is capable of forming G-quadruplex, small molecule inhibitors have been made to bind to and stabilize G-quadruplex in this region and prevent telomerase from extending or maintaining telomere length (Figure

1.3). The inhibition of telomerase by G-quadruplex inhibitors was first demonstrated *in vivo* using amidoanthraquinone analogues (Sun *et al.*, 1997). Since the first use of amidoanthraquinone molecules as G-quadruplex stabilizers, a large number of small molecules have since been developed and tested for their telomerase inhibition efficacy. Results of these studies and additional experimentation with porphyrins, perylenes, various acridine derivatives and others have consistently shown that G-quadruplex stabilization can lock telomeric DNA in a G-quadruplex conformation and lead to inhibition of telomerase, resulting in telomere shortening and senescence in cell based assays (Monchaud and Teulade-Fichou, 2008).

hTERT

In the mid 1990s, the genes encoding the two major components of human telomerase were cloned—the RNA hTERC subunit and the catalytic functional portion hTERT (Feng *et al.*, 1995; Nakamura *et al.*, 1997). Although the critical components of human telomerase are hTERC and hTERT, other subunits exist, including dyskerin and telomerase protein component I (Tep1). While the elements of telomerase such as dyskerin are important, only hTERT has been found to be essential in restoring telomerase activity in telomerase-negative normal cells, such as human fibroblasts (Artandi *et al.*, 2002). Although telomerase expression and more specifically hTERT is correlated with almost all cancers, recent evidence suggests a non-telomeric role for

hTERT in tumorigenesis; hTERT has been found to be involved in extra-telomeric functions such as regulation of gene expression, growth factors, and cellular proliferation (Smith *et al.*, 2003; Li *et al.*, 2005). Additionally, hTERT is capable of shuttling from the nucleus to the mitochondria upon exogenous stress (Santos *et al.*, 2006; Haendeler *et al.*, 2003). It appears as though hTERT translocation to the mitochondria is a protective mechanism—shuttling occurs following cellular stress (ROS generation, radiation) and confers resistance to apoptosis, although it may not be in and of itself the sole factor in determining entry into apoptosis.

Instead, hTERT shuttling to the mitochondria may reduce overall cellular stress by aiding in the reduction of nuclear DNA damage and by decreasing oxidative stress within the mitochondria (Singhapol *et al.*, 2013). In hTERT over-expressing cells (such as cancer cells), studies have shown that under conditions of stress, mitochondrial DNA (mtDNA) is protected, mitochondrial membrane potential is increased and mitochondrial superoxide production and cell peroxide levels are decreased, all indicating improved mitochondrial function in these cells (Ahmed *et al.*, 2008). Several oncogenes, including *c-Myc* and *c-Jun*, induce hTERT expression, while tumor suppressor proteins such as p53 reduce the expression of hTERT (Takakura *et al.*, 2005; Xu *et al.*, 2000). In this regard, hTERT mitochondrial translocation may be a factor in drug resistance, providing a means by which cancer cells evade apoptosis by protecting against nuclear DNA

damage and reducing mitochondrial stress following drug treatment (Singhapol *et al.*, 2013).

Figure 1.3

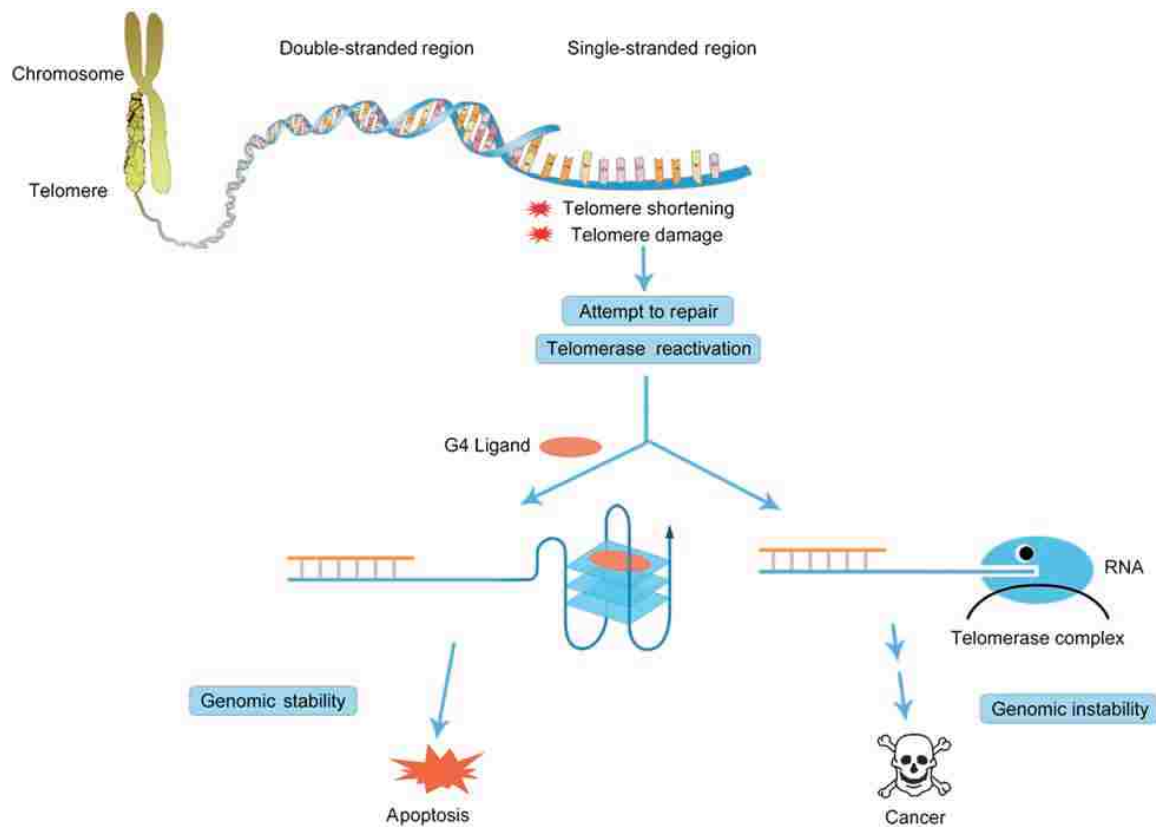


Figure 1.3. Structure and biological roles of telomeres. Repair mechanisms or telomerase reactivation is triggered by telomere shortening or damage. While repair or reactivation in excess would induce or trigger tumorigenesis, G4 ligands could induce or stabilize the G-quadruplex structure in this region and thus block telomerase from binding to the terminal single-stranded end of telomeres. (Ou *et al.*, 2008).

Although the extra-nuclear non-telomeric functions of hTERT in the mitochondria remain controversial, if hTERT expression is higher in cancer cells compared to normal counterparts, and expression of hTERT confers survival advantage to these cells, then the targeting of hTERT by small molecule inhibitors represents a feasible anticancer therapeutic target. Indeed, inhibition of telomerase and hTERT can selectively trigger apoptosis in cancer cells and can also facilitate apoptosis by sensitizing cells to more traditional chemotherapies such as cisplatin, etoposide and mitomycin C (Massard *et al.*, 2006). As previously mentioned, G-quadruplex ligands can be designed to inhibit telomerase through the stabilization of G-quadruplex within sections of the telomeres. Some telomeric directed G-quadruplex ligands, however, have been shown to induce cell senescence in the absence of telomere shortening, which suggests alternate mechanisms of actions in the presence of telomeric G-quadruplex stabilization (Pennarun *et al.*, 2005; Zhou *et al.*, 2009). In this regard, recent experimentation with two commercially available G-quadruplex ligands DODC and TMPyP4 induced hTERT translocation from the nucleus to the mitochondria, were capable of inhibiting telomerase and caused mitochondrial effects (reduced mitochondrial membrane potential, induction of apoptosis) consistent with disruption of mitochondrial function in cancer cell lines (Zhuang and Yao, 2013). Although these data are not necessarily G-quadruplex specific, they do support the

notion that hTERT functions in a more complex manner than just effecting telomerase in the nucleus, and also links G-quadruplex ligands to disruption of mitochondrial regulation as a mechanism of action. Additional research investigating G-quadruplex drug design should focus more broadly outside of just capacity for G-quadruplex stability and binding to include more finite molecular pathways leading to eventual apoptosis.

G-quadruplex in gene promoters

The most studied G-quadruplex forming region in a gene promoter is in that of the proto-oncogene *c-MYC*. Up to 80% of all solid tumors overexpress *c-MYC*, including brain tumors (Eilers and Eisman, 2008; Lutz *et al.*, 2002). Research has shown that transcriptional repression of *c-MYC* occurs by targeting a G-quadruplex in the nuclease hypersensitive element (NHE) within the promoter region (Siddiqui-Jain *et al.*, 2002). As discussed earlier, G-quadruplex can be formed from four separate strands of DNA into a tetramolecular arrangement. However, arrangements can also include two separate strands of DNA (bimolecular) or a single strand of DNA (unimolecular)—the most common formation in gene promoters is a continuous stretch of G-quadruplex sequences with four or more G-tracts that fold unimolecularly (Balasubramanian *et al.*, 2011). Of note structurally as well, in contrast to telomeric G-quadruplexes which can be formed from the single stranded overhang at the 3' end of telomeres, G-quadruplex in gene

promoter regions are constrained by duplex DNA structure (Balasubramanian *et al.*, 2011). Complexities in G-quadruplex structure and arrangement make modeling ligand/G-quadruplex binding a challenge, but also strengthen the hypothesis that many other G-quadruplex may exist in gene promoter regions. Indeed, in addition to *c-MYC*, proto-oncogene *KIT* has received attention for the discovery of regions within the gene that have been identified as forming G-quadruplex. *KIT* encodes a receptor tyrosine kinase that once activated stimulates cellular proliferation and differentiation and promotes cell survival (Yarden *et al.*, 1987). Because high activity of the protein KIT has been implicated in cancers, notably gastrointestinal stromal tumors, KIT has been the target of specific kinase inhibitors such as imatinib and sunitinib (Balasubramanian *et al.*, 2011). Upon discovery of G-quadruplex forming regions within promoter areas of *KIT*, research began to focus on the design of small molecule G-quadruplex stabilizers to target these regions. An advantage to the targeting of *KIT* in terms of G-quadruplex research is that *KIT* is already the focus of clinically relevant and established chemotherapy. Additional research in the area of *KIT* and other oncogenes is vital to understanding binding and stabilization of G-quadruplex in gene promoter regions and furthering drug design in this area.

G-quadruplex ligand features and druggability

As previously discussed, G-quadruplex can form varying structures depending on the

cellular location and features of the microenvironment, such as presence and type of cation within the central channel. Despite the vast array of conformations possible, there are common features among G-quadruplex structures that allow for specific design of ligands. A structural element that is conserved through all G-quadruplex is the large planar surface of the terminal G-quartet. This characteristic of G-quadruplex has led to the development of small molecules containing a heteroaromatic system that complements the G-quartet platform and encourages proper orientation upon binding (Balasubramanian *et al.*, 2011). The challenge in design of G-quadruplex ligands is the development of small molecule drugs that will specifically recognize discrete G-quadruplex structures and bind with high affinity. G-quadruplex ligands can be promiscuous in nature and if not specific enough for their target, can recognize single stranded or duplex DNA in addition to interacting with G-quadruplex DNA. However, structural selectivity for known G-quadruplexes can be achieved for example, by exploiting the steric hindrance imposed on ligands by loops (such as the T-loop formation that is found in telomeric G-quadruplex)—a result of ligand inaccessibility to the G-quartet platform. Identifying the location of grooves and loops within the G-quadruplex of interest provides an opportunity to model ligands to fit into specific binding pockets and increases the likelihood of specificity towards that G-quadruplex. Although creating specialized ligands is challenging, several drugs have recently

shown promise.

Telomestatin, a natural product analog isolated from *Streptomyces anulatus 3533-SV4*, is a promising G-quadruplex ligand that has shown good specificity towards telomeric G-quadruplex DNA (Shin-Ya *et al.*, 2001). In vitro, telomestatin is a potent telomerase inhibitor and has an EC₅₀ of 5nM. Additionally, telomestatin is a very specific ligand for the human intramolecular basket-type G-quadruplex conformation and has approximately a 70-fold greater affinity for G-quadruplex DNA over single stranded or duplex DNA (Rezler *et al.*, 2005). Another auspicious G-quadruplex ligand that has received scientific attention is quarfloxin. Quarfloxin reached Phase II clinical trials for the treatment of neuroendocrine carcinomas and is considered to be a relatively specific G-quadruplex ligand for *c-MYC*. Initial studies with quarfloxin demonstrated topoisomerase II interactions and consequently decreased specificity for G-quadruplex DNA. Cyclene Pharmaceuticals (San Diego, CA, USA) led the optimization of quarfloxin into the final drug design, which expanded a planar system to force better interactions with the tetrad in G-quadruplex DNA compared to duplex DNA. DNA groove binding arms were also added to the quarfloxin structure to decrease selectivity for topoisomerase II and increase specificity towards G-quadruplex within the promoter areas of *c-MYC*. Quarfloxin disrupts the interaction between the nucleolin protein and a G-quadruplex DNA structure located

within ribosomal DNA, causing inhibition of RNA polymerase I transcription leading to relocation of nucleolin to the nucleoplasm and subsequent inhibition of *c-MYC* through alterations in c-MYC expression. Tumor cells ultimately undergo apoptosis following treatment with quarfloxin (Balasubramanian *et al.*, 2011).

Barriers to effective drug treatment

Overview

All pharmacotherapy for treatment of brain and central nervous system cancers are limited by the blood-brain barrier (BBB). In glioblastoma for instance, in order for chemotherapeutic agents to gain access to the target tissue in the brain, the drug needs to be able to move across the BBB and overcome the physicality of the BBB in addition to export by transporters. The BBB serves to protect the brain from toxicants by providing a physical barrier between the brain and systemic circulation. The endothelial cells of the brain contain a wide array of transporters that regulate their movement across the BBB and into the brain. The ATP-binding cassette (ABC) superfamily of efflux transporters is the main class of multidomain integral membrane proteins that are responsible for the efflux of many drugs out of the brain (Figure 1.4). ABC transporters expressed at the level of the BBB include p-glycoprotein (ABCB1 or P-gp), MRP1 (ABCC1), MRP2 (ABCC2), MRP3 (ABCC3), MRP4 (ABCC4),

MRP5 (ABCC5), MRP6 (ABCC6), and BCRP (ABCG2). Although each transporter is capable of exporting any drug that is a substrate for it, one of the most studied and frequently implicated in cancer is P-gp.

P-glycoprotein

P-gp was first discovered in the 1970s and studied as the prototypical transporter involved in multidrug resistance in cancer cells (Juliano and Ling, 1976). There are two types of human P-gp: Type I (MDR 1 P-gp, herein denoted as P-gp) encoded by the *MDR1* gene, that confers the drug resistance phenotype at the BBB and Type II, encoded by the *MDR2* gene, that is present not at the BBB, but in the canalicular membrane of hepatocytes and that functions as a phosphatidylcholine translocase (Demeule *et al.*, 2002). P-gp, like other members of the ABC transporter family, uses the energy of ATP hydrolysis to translocate solutes across the cellular membrane. The molecular structure of P-gp includes four domains: two nucleotide-binding domains and two transmembrane domains. The cytosolic nucleotide-binding domains bind to and hydrolyze ATP, whereas each of the transmembrane domains consist of six transmembrane helices that together form the substrate or drug binding sites (Sauna and Ambudkar, 2007).

It has been suggested that the following are the minimum events that occur in regards to P-gp function: initial binding of ATP and/or substrate, conformational changes at the nucleotide-

binding domains following ATP binding and/or hydrolysis, transmission of the conformational changes at the nucleotide-binding domains to the transmembrane domains to effect an affinity switch (low or high) at the drug binding site, and then the subsequent resetting of the transporter back to the original conformation (Sauna and Ambudkar, 2007). At the subcellular level, P-gp is expressed at the apical membrane of brain capillary endothelial cells in humans—drugs that are substrates for P-gp enter the endothelial cells from circulation and are immediately pumped back into the blood, preventing them from reaching their site of action in the brain.

Figure 1.4

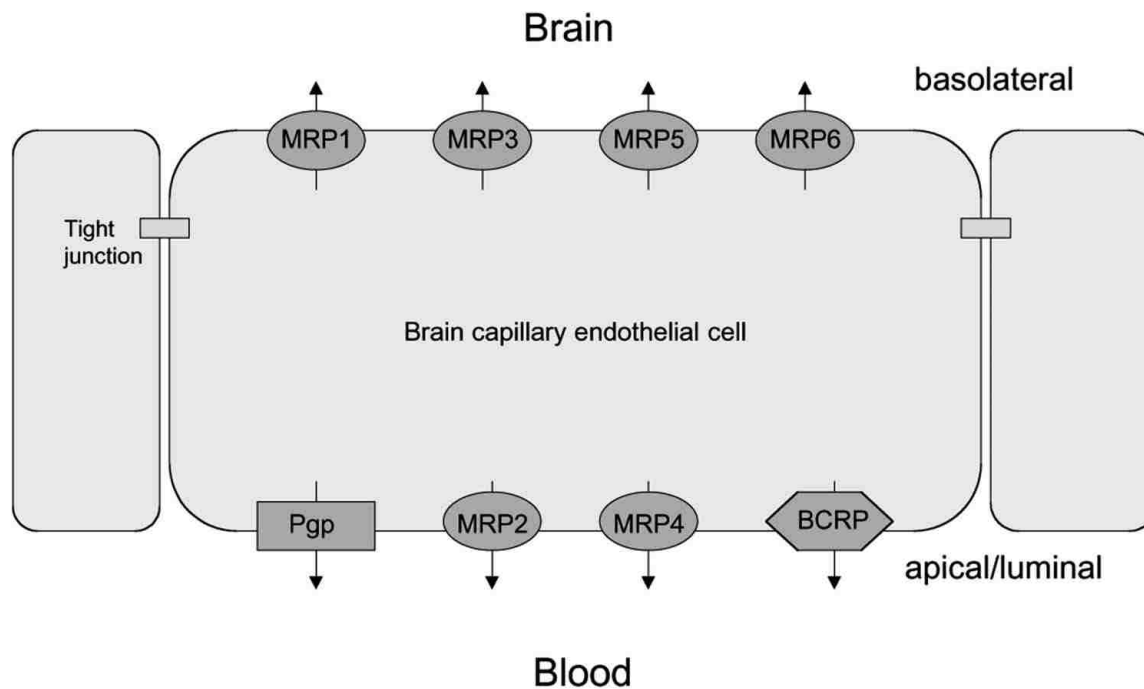


Figure 1.4. Efflux transporters. Localization of selected drug efflux proteins on brain capillary endothelial cells that form the blood-brain barrier. Only transporters that are localized on the apical (luminal) side of the brain capillary endothelium would be in a position to restrict brain uptake of xenobiotics (adapted from Loscher and Potschka, 2005).

There are many anticancer drugs that are P-gp substrates, notably doxorubicin, paclitaxel, methotrexate, vincristine, and etoposide (Loscher and Potschka, 2005). Therefore, using these drugs in clinical practice can be problematic because the efflux properties of P-gp at the BBB for P-gp Type II dramatically reduces the net penetration of these drugs at their site of action. Also, aside from their normal functioning as efflux transporters under physiologic conditions, ABC transporters, especially P-gp, have been found to be overexpressed in a variety of human diseases, including cancer (Leonard *et al.*, 2003). This overexpression can lead to the drug resistance encountered upon treatment with anticancer agents and leads to ineffective chemotherapy treatment. P-gp inhibitors are now being designed to prevent drug resistance and increase drug absorption at the designated site of action.

P-glycoprotein inhibitors

The development of P-gp inhibitors (or multidrug resistance, MDR, modulators) is a viable means to block the function of P-gp and encourage drug accumulation at the drug target sites of action. First generation P-gp inhibitors were found to have inhibition activity after already being used clinically for other conditions and include the calcium ionic channel blockers verapamil and diltiazem, the immunosuppressive agent cyclosporine, and tamoxifen, an estrogen receptor antagonist. When these drugs were examined *in vitro* for their inhibitory properties,

some produced almost complete P-gp inhibition and reversed the multidrug resistant effects, however, all of the first generation P-gp inhibitors were deemed minimally effective, non-specific and toxic when used *in vivo*. The issues of promiscuous binding and toxicity have plagued the progression of the field of P-gp inhibitors to be used clinically, but several pharmacophore models have provided insight into properties required for drug resistance reversal and complete P-gp inhibition. These include: liposolubility with hydrophobic centers, cationic species or a basic center in the physiologic range for pH, at least two coplanar aromatic rings and hydrophobic substituted aromatic rings to increase activity, and appropriate hydrogen bond acceptors (oxygen or nitrogen) and/or hydrogen bond donors (OH or NH groups) with appropriate spacial separation (Yang *et al.*, 2008). The development of P-gp inhibitors for concomitant use with anticancer agents is an important field of study with potential to create comprehensive cancer treatment that is effective and minimally toxic systemically.

Alternative anticancer drug targets

As mentioned previously, anticancer drugs are designed to be cytotoxic only to cancer cells, while exerting minimally toxic effects to normal healthy tissue. In order to develop effective anticancer therapies, it is necessary to identify differences between normal cells and cancer cells to target these metabolic or biologic alterations and exploit them for therapeutic

purposes. In regards to the design of new drugs, if the crystal structure of a potential drug target has been elucidated then structure-based ligand design is an effective approach to drug development.

NQO1

Overview

NAD(P)H:quinone oxidoreductase 1 (NQO1 or previously DT-diaphorase) is an enzyme responsible for the detoxification of toxicants or quinone-based compounds that are substrates for the enzyme. Early research suggested that NQO1 enzymatic activity is protective upon carcinogen exposure—NQO1 expression was induced following carcinogen treatments and reduced accumulated harmful effects following repeat exposure (Huggins, 1979). It is also known however, that some quinone substrates are inactive until they are reduced by NQO1 and then become toxic. This effect—in which an inactive or essentially nontoxic compound functions as a prodrug that gains activity only upon enzymatic reduction—is an important feature in the field of enzyme-directed bioreductive drug design. In the 1970s, bioreductive activation was hypothesized to occur because of the location of hypoxic cells proximal to necrotic cores of solid tumors that would potentiate reductive metabolism based drug activation in these cells selectively over normal aerobic cells (Lin *et al.*, 1972). Agents that undergo bioreductive activation can generate ROS through redox cycling or be reduced by one and two-electron

reductases to alkylating agents capable of cross-linking DNA (bioreductive alkylation). The other important component to bioreductive activation is the identification of enzymes that are overexpressed in tumor tissue (and not in normal tissue) and can thus drive the design of substrates that can be bioactivated by these enzymes and used as anticancer therapies. NQO1 has been widely studied as an enzyme capable of bioreductive activation due to its marked overexpression in tumor tissue (Ross *et al.*, 1994; Workman, 1994).

NQO1 structure and function

NQO1 is a two-electron reductase that is characterized by its utilization of either NADH or NADPH as reducing cofactors and by its inhibition by dicoumarol (Ernster, 1979). NQO1 is a homodimer containing one molecule of cofactor FAD for each monomer, that is required for catalytic activity (Danson, 2004; Lind, 1990). Found almost exclusively in the cytosol, NQO1 is responsible for the reduction of many quinone-based compounds. Quinone reduction occurs via an obligatory single-step two-electron reduction, which bypasses the reactive and toxic formation of semiquinone intermediates (Dinkova-Kostova and Talalay, 2000). The enzymatic functions of NQO1 are described as ping pong kinetics whereby NAD(P)H binds to the active site of NQO1, reduces FAD cofactor to FADH₂, and is then released prior to substrate binding and complete reduction by hydride transfer (Li *et al.*, 1995). Under conditions of oxidative stress, *NQO1*

expression is induced to protect the microenvironment; this upregulation is also accompanied by an increase in antioxidant enzymes (Nioi and Hayes, 2004). NQO1 functions to metabolize endogenous ubiquinone, which can lead to the scavenging of free radicals and the more traditional route of detoxification for which it was first implicated. It has also been suggested that NQO1 can stabilize p53 either by inhibiting its degradation or by a direct protein-protein interaction, leading to increased tumor suppression response (Ross and Siegel, 2004). In humans, NQO1 is also overexpressed in a variety of solid tumors, including those of the adrenal gland, bladder, breast, colon, liver, lung, ovaries and thyroid (Schlager and Powis, 1990; Malkinson *et al.*, 1992; Siegel and Ross, 2000). Aside from normal detoxification function, the overexpression of NQO1 in tumor tissue combined with properties of bioreductive activation make NQO1 a selective drug target in the treatment of solid tumors.

Quinones as NQO1 substrates

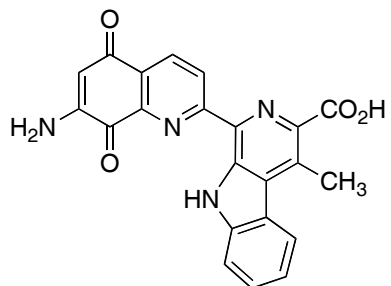
Quinones are a large group of natural products that are substrates for NQO1. Many quinones, such as doxorubicin and mitomycin c, have anticancer properties as well and are therefore good candidates to examine for their ability to be reduced to more active cytotoxic agents. One of the first NQO1 substrates to be studied was streptonigrin (SN), a natural product isolated from *Streptomyces flocculus* (Rao and Cullen, 1959). SN has shown to have broad-

spectrum antitumor activity and is cytotoxic against tumors of the lung, breast, head and neck, as well as lymphomas and melanoma; however, SN is toxic when used as treatment *in vivo* and has never been approved for use in the clinic (Bolzan and Bianchi, 2001).

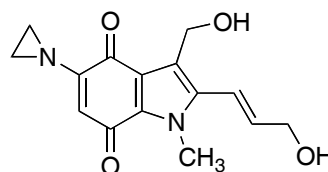
Other NQO1 substrates that have reached clinical trials or have been in use therapeutically include mitomycin c, EO9, and diaziquone (AZQ) (Beall and Winski, 2000) (Figure 1.5). Mitomycin c is considered the prototypical bio-reductive drug and has antitumor activity against tumors of the stomach, pancreas, colon and breast; it was also the first quinone-containing alkylating agent to be used successfully in the clinic alone and in combination therapy (Teicher, 1997). Mitomycin c, like SN, is potent and toxic and is limited by causative myelosuppression, which is directly related to cumulative administration of the drug. Mitomycin c is a relatively weak NQO1 substrate—newer analogues have been designed to increase enzyme specificity with limited bone marrow suppression. EO9 was designed as a mitomycin c analog and is a synthetic indolequinone. EO9 reached clinical trials for use in tumors of the breast, colon, pancreas and stomach, but was withdrawn, presumably due to poor pharmacokinetics (Phillips, 1998; Dirix *et al.*, 1996). AZQ, an aziridinybenzoquinone designed for tumors of the central nervous system, has shown effectiveness towards primary brain tumors, but similar to other quinones, is also a potent bone marrow suppressive agent (Teicher, 1997; Chou *et al.*,

1976). In an effort to probe for the minimum structural components needed for NQO1 substrate activity, lavendamycin analogues have been developed for examination of antitumor potential. Lavendamycin was isolated from *Streptomyces lavendulae* and is structurally and biosynthetically similar to SN (Balitz *et al.*, 1982; Doyle *et al.*, 1981). Lavendamycin activity is comparable and less potent than SN and investigation into structural properties explaining the activities have been important in continuing the research into the development of lavendamycin analogues (Boger *et al.*, 1987). Lavendamycin contains a pentacyclic ring structure, whereby any of the ring constituents may be modified to improve cytotoxicity and affinity for NQO1 (Fang *et al.*, 2003). Further investigation into the structure of lavendamycin has shown that although lavendamycin may be limited clinically due to toxicity and poor pharmacokinetics, structurally similar indolequinones and quinolinequinones are good NQO1 substrates. Structural modification of these compounds has the potential to lead to structure-activity relationship (SAR) studies and better substrates with increased specificity and tumor cytotoxicity (Hassani *et al.*, 2005; Fryatt *et al.*, 2004; Beall *et al.*, 1998; Swann, 2001; Hassani *et al.*, 2008; Cai *et al.*, 2008). Continued experimentation in the field of NQO1-directed antitumor quinones will provide important information on the structural components needed for NQO1 activity and has the potential to lead to the discovery of more specific antitumor agents.

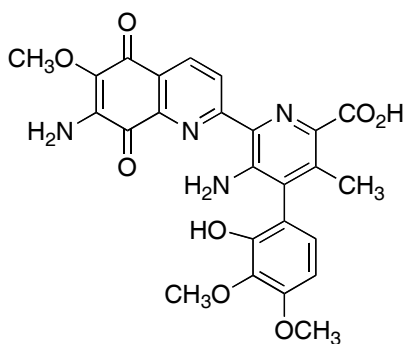
Figure 1.5



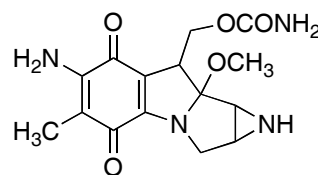
Lavendamycin



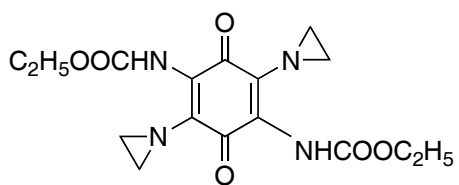
EO9



Streptonigrin



Mitomycin C



Diaziquone

Figure 1.5. Selected antitumor quinone structures.

Conclusions

Cancer is a common and often fatal disease. It is important to continue to research the mechanisms of tumor development and identify the characteristics of cancer cells that make them cellularly distinct from normal cells, in an effort to exploit these differences with new anticancer therapies. The goal of the proposed studies is to examine the cytotoxicity and therapeutic potential of new anticancer agents in an effort to better understand the mechanisms of cancer development. The results of this project will aid in the development of new and alternative approaches to selectively target and eliminate tumor cells.

Cytotoxicity and therapeutic potential of novel anticancer agents:

Hypothesis and Specific Aims:

- (1) We hypothesize that small molecule anthracenyl isoxazole amides (AIMs) selectively bind within mitochondria in cancer cells and induce apoptosis via the mitochondrial pathway of apoptosis.*
- (2) We hypothesize that small substituents at the R¹ position and small heterocyclic substitutions at the R² position of our lavendamycin quinolinequinone derivatives will be preferentially cytotoxic to NQO1-expressing human breast cancer cells.*

Specific Aim 1: Assess degree of AIM toxicity to human glioblastoma cell line SNB-19.

Determine whether compounds are cytotoxic to SNB-19 human glioblastoma cells and to what degree, using IC₅₀ values as a measure of toxicity.

Specific Aim 2: Evaluate the AIMs effects on the mitochondria of SNB-19 human glioblastoma cells

Using an in vitro cell culture model, examine AIMs potential to interact with mitochondria and induce apoptosis via the mitochondrial-regulated pathway of apoptosis

Specific Aim 3: Determine if AIMs have increased selective toxicity to P-gp expressing and non-P-gp expressing MDCK canine kidney cells when used in conjunction with novel P-gp inhibitors

Using an in vitro cell culture model, examine selective toxicity of AIMS used in conjunction with novel dihydropyridine compounds at the level of export protein interactions in brain tumor cells.

Specific Aim 4: Investigate the effect of aryl-substitutions on quinolinequinone analogues of lavendamycin derivatives

Using an in vitro cell culture model of NQO1 expressing and non-expressing human breast cancer cells, determine the NQO1 substrate efficiency and selective toxicity of structurally modified quinolinequinones.

References

- Ahmed, S., Passos, J. F., Birket, M. J., Beckman, T., Brings, S., Peters, H., Birch-Machin, M. A., Von Zglinicki, T., Saretzki, G. (2008). Telomerase does not counteract telomere shortening but protects mitochondrial function under oxidative stress. *J Cell Sci* **7**, 1046-1053.
- Artandi, S. E., Alson, S., M. K., Sharpless, N. E., Ye, S., Greenberg, R.A., Castrillon, D. H., Horner, J. W., Weiler, S. R., Carrasco, R. D., and DePinho, R. A. (2002). Constitutive telomerase expression promotes mammary carcinomas in aging mice. *Proc Natl Acad Sci* **12**, 8191-8196.
- Balasubramanian, S., Hurley, L. H., and Neidle, S. (2011). Targeting G-quadruplex in gene promoters: a novel anticancer strategy?. *Nat Rev* **10**, 261-275.
- Balitz, D. M., Bush, J. A., Bradner, W. T., Doyle, T. W., O'Herron, F. A., and Nettleton, D. E. (1982). Lavendamycin isolation and antimicrobial and antitumor testing. *J Antibiot* **35**, 259-265.
- Beall, H. D., and Winski, S. L. (2000). Mechanisms of action of quinone-containing alkylating agents:NQO1-directed drug development. *Front Biosci* **5**, 639-648.
- Beall, H. D., Winski, S., Swann, E., Hudnott, A. R., Cotterill, A. S., O'Sullivan, N., Green, S. J., Bien, R., Siegel, D., Ross, D., and Moody, C. J. (1998). Indolequinone antitumor agents: Correlation between quinone structure, rate of metabolism by recombinant human NAD(P)-H:quinone oxidoreductase, and in vitro cytotoxicity. *J Med Chem* **41**, 4755-4766.
- Bleeker, F. E., and Molenaar, R. J. (2012). Recent advances in the molecular understanding of glioblastoma. *J Neurooncol* **108**, 11-27.
- Boger, D. L., Yasuda, M., Mitscher, L. A., Drake, S. D., and Kitos, P. A. (1987). Streptonigrin and lavendamycin partial structures. Probe for the minimum, potent pharmacophore of streptonigrin, lavendamycin, and synthetic quinolone-5,8-diones. *J Med Chem* **30**, 1918-1928.
- Bolzan, A. D., and Bianchi, M. S. (2001). Genotoxicity of streptonigrin: A review. *Mutat Res* **488**, 25-37.
- Burge, S., Parkinson, G. N., Hazel, P., Todd, A. K., and Neidle, S. (2006). Quadruplex DNA: sequence, topology and structure. *Nucleic Acids Res* **34**, 5403-5415.
- Cai, W., Hassani, M., Karki, R., Walter, E. D., Koelsch, K. H., Seradj, H., Lineswala, J., P., Mirzaei, H., York, J. S., Olang, F., Sedighi, M., Lucas, J. S., Eads, T. J., Rose, A. S., Charkharrin, S., Hermann, N. G., Beall, H. D., and Behforouz, M. (2010). Synthesis,

- metabolism and in vitro cytotoxicity studies on novel lavendamycin antitumor agents. *Bioorg Med Chem* **18**, 1899–1909.
- Candolfi, M., Kroeger, K. M., Xiong, W., Liu, C., Puntel, M., Muhammad, A. G., Mineharu, Y., Foulad, Y., Wibowo, M., Assi, H., Baker, G. J., Lowenstein, P. R., and Castro, M. G. (2011). Targeting toxins for glioblastoma multiforme: pre-clinical studies and clinical implementation. *Anticancer Agents for Med Chem* **8**, 729-738.
- Chou, F., Khan, A. H., and Driscoll, J. S. (1976). Potential central nervous system antitumor agents. Aziridinylbenzoquinones. *J Med Chem* **19**, 1302-1308.
- Danson, S., Ward, T. H., Butler, J., and Ranson, M. (2004). DT-diaphorase: A target for new anticancer drugs. *Cancer Treat Rev* **30**, 437-449.
- De Bruin, E. C., and Medema, J. P. (2008). Apoptosis and non-apoptotic deaths in cancer development and treatment response. *Cancer Treat Rev*, **34**, 737– 749.
- Demeule, M., Regina, A., Jodoin, J., Laplante, A., Dagenais, C., Berthelet, F., Moghrabi, A., and Beliveau, R. Drug transport to the brain: key roles for the efflux pump P-glycoprotein in the blood-brain barrier. *Vascul Pharmacol* **38**, 339-348.
- Dinkova-Kostova, A. T., and Talalay, T. (2000). Persuasive evidence that quinone reductases type I (DT diaphorase) protects cells against the toxicity of electrophiles and reactive forms of oxygen. *Free Rad Biol Med* **29**, 231-240.
- Dirix, L. Y., Tonnesen, F., Cassidy, J., Epelbaum, R., ten Bokkel Huinink, W. W., Pavlidis, N., Sorio, R., Gamucci, T., Wolff, I., te Velde, A., Lan, J., and Verweij, J. (1996). EO9 phase II study in advanced breast, gastric pancreatic and colorectal carcinoma by the EORTC Early Clinical Studies Group. *Eur J Cancer* **32**, 2019-2022.
- Doyle, T. W., Balitz, D. M., Grulich, R. E., and Nettleton, D. E. (1981). Lavendamycin structure determination. *Tetrahedron Lett* **22** 4595-4598.
- Dunn, G. P., Rinne, M. L., Wykosky, J., Genovese, G., Quayle, S. N., Dunn, I. F., Agarwalla, P. K., Chheda, M. G., Campos, B., Wang, A., Brennan, C., Ligon, K. L., Furnari, F., Cavenee, W. K., Depinho, R. A., Chin, L., and Hahn, W. C. (2012). Emerging insights into the molecular and cellular basis of glioblastoma. *Genes Dev* **26**, 756-784.
- Edinger, A. L., and Thompson, C. B. (2003). Defective autophagy leads to cancer. *Cancer Cell* **4**,422–424.
- Eilers, M., and Eisman, R. N. (2008). Myc's broad reach. *Genes Dev* **22**, 2755-2766.
- Ernster, L. (1967). DT-diaphorase. *Methods Enzymol* **10**, 309-317.
- Fang, Y., Linardic, C. M., Richardson, D. A., Cai, W., Behforouz, M., and Abraham, R.

- T. (2003). Characterization of the cytotoxic activities of novel analogues of the antitumor agent, lavendamycin. *Mol Cancer Ther* **2**, 517-526.
- Feng, J., Funk, W. D., Wang, S. S., Weinrich, S. L., Avillon, A. A., Chiu, C. P., Adams, R. R., Chang, E., Allsopp, R. C., Yu, J., Le, S.m West, M. D., Harley, C. B., Andrews, W. H., Greider, C. W., and Villeponteau, B. (1995). The RNA component of human telomerase. *Science* **269**, 1236-1240.
- Fryatt, T., Pettersson, H. I., Gardipee, W. T., Bray, K. C., Green, S. J., Slawin, A. M. Z., Beall, H. D., and Moody, C. J. (2004). Novel quinolinequinone antitumor agents: structure-metabolism studies with NAD(P)-H:quinone oxidoreductase (NQO1). *Bioorg Med Chem* **12**, 1667–1687.
- Gunaratnam, M., and Neidle, S. (2010). An evaluation cascade for G-quadruplex telomere targeting agents in human cancer cells. *Methods Mol Biol* **613**, 303-313.
- Haendeler, J., Hoffman, J., Brandes, R. P., Zeiher, A. M., and Dimmerler, S. (2003). Hydrogen peroxide triggers nuclear export of telomerase reverse transcriptase via Src kinase family-dependent phosphorylation of tyrosine 707. *Mol Cell Biol* **23**, 4598-4610.
- Hanahan, D., and Weinberg, R. A. (2000). The hallmarks of cancer. *Cell* **100**, 57-70.
- Hassani, M., Cai, W., Holley, D. C., Lineswala, J. P., Maharjan, B. R., Ebrahimian, G. R., Seradj, H., Stocksdales, M. G., Mohammadi, F., Marvin, C. C., Gerdes, J. M., Beall, H. D., and Behforouz, M. (2005). Novel lavendamycin analogues as antitumor agents: Synthesis, in vitro cytotoxicity, structure–metabolism, and computational molecular modeling studies with NAD(P)H:quinone oxidoreductase 1. *J Med Chem* **48**, 7733–7749.
- Hassani, M., Cai, W., Koelsch, K. H., Holley, D. C., Rose, A. S., Olang, F., Lineswala, J. P., Holloway, W. G., Gerdes, J. M., Behforouz, M., and Beall, H. D. (2008). Lavendamycin antitumor agents: Structure-based design, synthesis, and NAD(P)H:quinone oxidoreductase 1 (NQO1) model validation with molecular docking and biological studies. *J Med Chem* **51**, 3104–3115.
- Huggins, C. B. (1979). Experimental leukemia and mammary cancer. Induction, prevention, cure. *Univ Chicago Press Chicago*.
- Hurt, M. R., Moossy, J., Donovan-Peluso, M., and Locker, J. (1992). Amplification of epidermal growth factor receptor gene in gliomas: Histopathology and prognosis. *J Neuropathol Exp Neurol* **51**, 84-90.
- Johnson, J. E., Smith, J.S., Kozak, M. L., and Johnson, F. B. (2008). In vivo veritas: using yeast to probe the biological functions of G-quadruplexes. *Biochimie* **90**, 1140-1148.

- Juliano, R. L. and Ling, V. (1976). A surface glycoprotein modulating drug permeability in Chinese hamster ovary cell mutants. *Biochim Biophys Acta* **455**, 152-162.
- Kasibhatla, S., and Tseng, B. (2003). Why target apoptosis in cancer treatment?. *Mol Cancer Ther* **2**, 573-580.
- Kerr, J., Wyllie, A., and Currie, A. (1972). Apoptosis: a basic biological phenomenon with wide-ranging implications in tissue kinetics. *Br J Cancer* **26**, 239-257.
- Koul, D. (2008). PTEN signaling pathways in glioblastoma. *Cancer Biol Ther* **7**, 1321-1325.
- Leonard, G. D., Fojo, T., and Bates, S. E. (2003). The role of ABC transporters in clinical practice. *The Oncologist* **8**, 411-424.
- Li, R., Bianchet, M. A., Talalay, T., and Amzel, L. M. (1995). The three-dimensional structure of NAD(P)H:quinone reductases, a flavoprotein involved in cancer chemoprotection and chemotherapy: mechanism of the two-electron reduction. *Proc Natl Acad Sci* **92**, 8846-8850.
- Li, S., Crothers, J., Haqq, C. M., and Blackburn, E. H. (2005). Cellular and gene expression responses involved in the rapid growth inhibition of human cancer cells by RNA interference-mediated depletion of telomerase RNA. *J Biol Chem* **280**, 23709-23717.
- Li, Z., and Sheng, M. (2012). Caspases in synaptic plasticity. *Mol Brain* **5**, 15.
- Lin, A. J., Cosby, L. A., Shansky, C. W., and Sartorelli, A. C. (1972). Potential bioreductive alkylating agents. 1. Benzoquinone derivatives. *J Med Chem* **15**, 1247-1252.
- Lind, C., Cadenas, E., Hochstein, P., and Ernster, L. (1990). DT-diaphorase: Purification, properties, and function. *Methods Enzymol* **186**, 287-301.
- Lipps, H. J., and Rhodes, D. (2009). G-quadruplex structures: *in vivo* evidence and function. *Trends in Cell Biol* **19**, 414-422.
- Loscher, W., and Potschka, H. (2005). Blood-brain barrier active efflux transporters: ATP-binding cassette gene family. *NeuroRx* **1**, 86-98.
- Lutz, W., Leon, J., and Eilers, M. (2002). Contributions of Myc to tumorigenesis. *Biochim Biophys Acta* **1602**, 61-71.
- Malkinson, A. M., Siegel, D., Forrest, G. L., Gazdar, A. F., Oie, H. K., Chan, D. C., Bunn, P. A., Mabry, M., Dykes, D. J., Harrison, S. D., and Ross, D. (1992). Elevated DT-diaphorase activity and messenger RNA content in human non-small cell lung carcinoma: relationship to the response of lung tumor xenografts to mitomycin C. *Cancer Res* **52**, 4752-4757.
- Marie, S. K. N., and Shinjo, S. M. O. (2011). Metabolism and brain cancer.

- Clinics* **66**, 33-43.
- Massard, C., Zermati, Y., Pauleau, A. L., Larochette, N., Metivier, D., Sabatier, L., Kroemer, G., and Soria, J. C. (2006). hTERT: a novel endogenous inhibitor of the mitochondrial cell death pathway. *Oncogene* **25**, 4505-4514.
- McClintock, B. (1941). The stability of broken ends of chromosomes in *Zea mays*. *Genetics* **41**, 234-282.
- Mita, A. C., Mita, M. M., Nawrocki, S. T., and Giles, F. J. (2008). Survivin: Key Regulator of mitosis and apoptosis and novel target for cancer therapeutics. *Clin Cancer Res* **14**, 5000-5005.
- Monchaud, D., and Teulade-Fichou, M. P. (2008). A hitchhiker's guide to G-quadruplex ligands. *Org Biomol Chem* **6**, 627-636.
- Nakamura, T. M., Morin, G. B., Chapman, K. B., Weinrich, S. L., Andrews, W. H., Lingner, J., Harley, C. B., and Cech, T. R. (1997). Telomerase catalytic subunit homologs from fission yeast and human. *Science* **277**, 955-959.
- Nioi, P., and Hayes, J. D. (2004). Contribution of NAD(P)H:quinone oxidoreductase 1 to protection against carcinogenesis, and regulation of its gene by the Nrf2 basic-region leucine zipper and the arylhydrocarbon receptor basic helix-loop-helix transcription factors. *Mutat Res* **555**, 149-171.
- Oganesian, L., and Bryan, T. M. (2007). Physiological relevance of telomeric G-quadruplex formation: a potential drug target. *BioEssays* **29**, 155-165.
- Ou, T-M., Lu, Y-J., Tan, J-H., Huang, Z-S., Wong, K-Y., and Gu, L-Q. (2008). G-quadruplexes: Targets in anticancer drug design. *Chem Med Chem* **3**, 690-713.
- Pennarun, G., Granotier, C., Gauthier, L. R., Gomez, D., Hoffschir, F., Mandine, E., Riou, J-F., Mergny, J-L., Mailliet, P., and Boussin, F. (2005). Apoptosis related to telomere instability and cell cycle alterations in human glioma cells treated by new highly selective G-quadruplex ligands. *Oncogene* **24**, 2917-2928.
- Peter, M. E., and Krammer, P. H. (2003). The CD95(APO-1/Fas) DISC and beyond. *Cell Death Differ* **10**, 26-35.
- Phillips, R. M. (1998). Prospects for bioreductive drug development. *Exp Opin Invest Drugs* **7**, 905-928.
- Rao, K. V., and Cullen, W. P. (1959). Streptonigrin an antitumor substance. I. Isolation and characterization. *Antibiot Annu* **7**, 950-953.
- Rezler, E. M., Seenisamy, J., Bashyam, S., Kim, M. Y., White, E., Wilson, W. D., and Hurley, L. H. (2005). Telomestatin and diseleno saphyrin bind selectively to two different forms of the human telomeric G-quadruplex structure. *J Am Chem Soc* **127**,

- 9439-9447.
- Ricci, M. S., and Zong, W. X. (2006). Chemotherapeutic approaches for targeting cell death pathways. *The Oncologist* **11**, 342-357.
- Roninson, I. B., Broude, E. V., and Chang, B. D. (2001). If not apoptosis, then what? Treatment-induced senescence and mitotic catastrophe in tumor cells. *Drug Resist Updat* **4**, 303–313.
- Ross, D., and Siegel, D. (2004). NAD(P)H:quinone oxidoreductase 1 (NQO1, DT-diaphorase), functions and pharmacogenetics. *Methods Enzymol* **382**, 115-144.
- Ross, D., Beall, H., Traver, R. D., Seigel, D., Phillips, R. M., and Gibson, N. W. (1994). Bioactivation of quinones by DT-diaphorase. Molecular, biochemical and chemical studies. *Oncol Res* **6**, 493-500.
- Santos, J. H., Meyer, J. N., Van Houten, B. (2006) Mitochondrial localization of telomerase as a determinant for hydrogen peroxide-induced mitochondrial DNA damage and apoptosis. *Hum Mol Genet* **15**, 1757-1768.
- Sauna, Z. E., and Ambudkar, S. V. (2007). About a switch: how P-glycoprotein (ABCB1) harnesses the energy of ATP binding and hydrolysis to do mechanical work. *Mol Cancer Ther* **6**, 13-23.
- Schlager, J. J., and Powis, G. (1990). Cytosolic NAD(P)H (quinone acceptor) oxidoreductase in human normal and tumor tissue: effects of cigarette smoking and alcohol. *Int J Cancer* **52**, 403-409.
- Shay, J. W., and Bacchetti, S. (1997). A survey of telomerase activity in human cancer. *Eur J Cancer* **33**, 787-791.
- Shin-Ya, K., Wierzba, K., Ohtani, T., Yamada, Y., Furihata, K., Hayakawa, Y., and Seto, H. (2001). Telomestatin, a novel telomerase inhibitor from *Streptomyces anulatus*. *J Am Chem Soc* **123**, 1262-1263.
- Siddiqui-Jain, A., Grand, C. L., Bearss, D. L., and Hurley, L. H. (2002). Direct evidence for a G-quadruplex in a promoter region and its targeting with a small molecule to repress *c-MYC* transcription. *Proc Natl Acad Sci* **99**, 11593-11598.
- Siegel, D., and Ross, D. (2000). Immunodetection of NAD(P):quinone oxidoreductase 1(NQO1) in human tissues. *Free Rad Biol Med* **29**, 246-253.
- Singhapol, C., Pal, D., Czapiewski, R. Porika, M., Nelson, G., and Saretzki, G. C. (2013). Mitochondrial telomerase protects cancer cells from nuclear DNA damage and apoptosis. *PLOS One* **8**, 1-11.
- Sissi, C., Gatto, B., and Palumbo, M. (2011). The evolving world of protein-G-quadruplex recognition: A medicinal chemist's perspective. *Biochimie* **93**, 1219-1230.

- Smith, L. L., Collier, H.A., and Roberts, J. M. (2003). Telomerase modulates expression of growth-controlling genes and enhances cell proliferation. *Nat Cell Biol* **5**, 474-479.
- Sun, D., Thompson, B., Cathers, B. E., Salazar, M., Kerwin, S. M., Trent, J. O., Jenkins, T. C., Neidle, S., and Hurley, L. H. (1997). Inhibition of human telomerase by a G-quadruplex-interactive compound. *J Med Chem* **40**, 2113-2116.
- Swann, E., Barraja, P., Oberlander, A. M., Gardipee, W. T., Hudnott, A. R., Beall, H. D., and Moody, C. J. (2001). Indolequinone antitumor agents: Correlation between quinone structure and rate of metabolism by recombinant human NAD(P)H:quinone oxidoreductase. Part 2. *J Med Chem* **44**, 3311–3319.
- Takakura, M., Kyo, S., Inoue, M., Wright, W. E., and Shay, W. E. (2005). Function of AP-1 in transcription of the telomerase reverse transcriptase gene (TERT) in human and mouse cells. *Mol Cell Biol* **25**, 8037-8043.
- Tang, J., Kan, Z. Y., Yao, Y., Wang, Q., Hao, Y. H., and Tan, Z. (2008). G-quadruplex preferentially forms at the very 3' end of vertebrate telomeric DNA. *Nucleic Acids Res* **36**, 1200-1208.
- Teicher, B. A. (1997). Antitumor alkylating agents. *Cancer Prin and Prac Oncol* **5**, 405-418.
- Wang, X. (2001) The expanding role of mitochondria in apoptosis. *Genes Dev* **15**, 2922-2933.
- Westermarck, B. (2012). Glioblastoma—a moving target. *Upsala J of Med Sci* **117**, 251-256.
- Wong, R. S. Y. (2011). Apoptosis in cancer: pathogenesis to treatment. *J Exp Clin Cancer Res*, **30**, 1-14.
- Workman, P. (1994). Enzyme directed bioreductive drug development revisited: A commentary on recent progress and future prospects with emphasis on quinone anticancer agents and quinone metabolizing enzymes, particularly DT-diaphorase. *Oncol Res* **6**, 461-475.
- Xu, D., Wang, Q., Gruber, A., Bjorkholm, M., Chen, Z., Zaid, A., Selivanova, G., Peterson, C., Wiman, K. G., and PISA, P. (2000). Downregulation of telomerase reverse transcriptase mRNA expression by wild type p53 in human tumor cells. *Oncogene* **19**, 5123-5133.
- Yang, K., Wu, J., and Li, X. (2008). Recent advances in research on P-glycoprotein Inhibitors. *BioSci Trends* **2**, 136-146.
- Yarden, Y., Kuang, W-J., Yang-Feng, T., Coussens, L., Munemitsu, S., Dull, T. J., Chen, E., Schlessinger, J., Francke, U., and Ullrich, A. (1987). Human proto-oncogen *c-kit*: a

- new cell surface receptor kinase for an unidentified ligand. *EMBO J* **6**, 3341-3351.
- Zhou, W. J., Deng, R., Zhang, X-Y., Feng, G-K., Gu, L-Q., and Zhu, X-F. (2009). G-quadruplex ligand SYUIQ-5 induces autophagy by telomere damage and TRF2 delocalization in cancer cells. *Mol Cancer Ther* **8**, 3203-3213.
- Zhuang, X-Y., and Yao, Y-G. (2013). Mitochondrial dysfunction and nuclear-mitochondrial shuttling of TERT are involved in cell proliferation arrest induced by G-quadruplex ligands. *FEBS Lett* **11**, 1656-1662.

CHAPTER 2

Cytotoxicity and mechanisms of antitumor anthracenyl isoxazole amides (AIMs) as G- quadruplex ligands

Authors

Alison K. Kearns and Howard D. Beall

Corresponding Author

Dr. Howard D. Beall

Address: University of Montana

Department of Biomedical and Pharmaceutical Sciences

32 Campus Drive, Skaggs

Missoula, MT 59812

Telephone: 406-243-5112

Fax: 406-243-2807

Email: Howard.Beall@umontana.edu

ABSTRACT

The design and synthesis of G-quadruplex ligands as selective anticancer agents is a rapidly emerging scientific field of study. Recently, we have developed a series of anthracenyl isoxazole amides (AIMs) that function as G-quadruplex ligands and possess unique fluorescent and intracellular characteristics. In this study, we evaluate several AIM analogues for their cytotoxic potential, fluorescent properties, and preliminary mechanism of action. In contrast to published studies, we show that our AIMs preferentially localize to cellular structures outside of the nucleus—the generally accepted site of action of G-quadruplex ligands. Our results demonstrate an intriguing extra-nuclear mechanism of action and implicate a mitochondrial role in the function of our compounds. Due to this unexpected finding, further investigation into the mechanisms of action of our AIMs is warranted.

INTRODUCTION

Classic chemotherapy used in the treatment of solid tumors includes the administration of small molecule drugs that target DNA. While these agents are effective, there is an inherent lack of selectivity in targeting DNA, as well as issues with toxicity to normal tissue when these drugs are used clinically. New anticancer agents have been developed that are more specifically designed to interrupt abnormal cell signaling and interfere with cellular processes that are implicated in the development and progression of cancer. Recently, the discovery of higher order secondary DNA structures, G-quadruplexes, has led to investigation into new anticancer agents that bind to and stabilize G-quadruplex DNA and selectively induce apoptosis in cancer cells that overexpress G-quadruplex structures. This approach to drug design is a viable option in creating selective anticancer agents because of the features of G-quadruplex within cells, and within cancer cells more specifically. Although G-quadruplex structures exist in normal non-cancerous cells, G-quadruplex structures have been found to be overexpressed in cancer cells within the promoter region of oncogenes (Siddiqui-Jain *et al.*, 2002). G-quadruplexes also exist in telomeres, a finding that has sparked interest in investigating methods of G-quadruplex stabilization that prevent the elongation and maintenance of telomeres that is characteristic of

cancer cells (Sen and Gilbert, 1988). The ability to maintain telomere length and continue cellular replication and avoid reaching the Hayflick limit is advantageous to cancer cells in that it promotes excessive cell growth and can lead to cellular immortality, as cells are not instructed to die by normal apoptotic stimuli. One way by which cancer cells evade apoptosis in this regard is by overexpressing telomerase, the enzyme responsible for maintaining telomere length. By stabilizing G-quadruplex structures within the telomeres, G-quadruplex ligands function to inhibit the ability of telomerase to add the DNA sequence repeats TTAGGG to the 3' ends of chromosomes and maintain telomere length. When this process is interrupted, cells become senescent or enter apoptosis and are eventually eliminated. Telomerase inhibition by G-quadruplex stabilization is an important area of drug discovery research, however, as is the case with all new drugs, it is not without problems. One of the most prominent barriers to G-quadruplex ligand synthesis is the issue of binding promiscuity and problems with lack of selectivity for G-rich sequences. For example, Quarfloxin, a G-quadruplex ligand that reached clinical trials for use as anticancer therapy, issues with binding promiscuity led to interactions with single stranded or B-DNA and limited its use in the clinic (Drygin *et al.*, 2009; Bates *et al.*, 2009).

In this regard, we have developed a series of novel anthracenyl isoxazole amide compounds (AIMs) that exert toxic effects on a SNB-19 human glioblastoma cell line and preferentially interact with telomeric G-quadruplex DNA sequences. Our AIMs were originally developed for use as anti-HIV agents, but when evaluated showed no activity for this target. Surprisingly, follow up studies revealed antitumor potential. Data from the NCI-DTP 60 cell line screen indicated that the AIMs possess antitumor activity against central nervous system (CNS) SNB cell lines (Han *et al.*, 2009). Upon further investigation, several structural themes emerged that were consistent with G-quadruplex binding capability (Gajewski *et al.*, 2009; Han *et al.*, 2009). For example, the planar isoxazole component of the AIMs encourages proper perpendicular spatial orientation to allow G-quadruplex binding and the nitrogens at each tail increase solubility. The tails of the AIMs (single or double) presumably anchor to the phosphate backbone of the quadruplex and aid in binding as well. Additionally, one of the more experimentally useful properties of our AIMs comes from the aromatic anthracene moiety that leads to autofluorescence—that is, under appropriate excitation, our compounds emit fluorescence that allows for the careful examination of the AIMs without the use of additional fluorescent tags.

In this study we assess the cytotoxicity and antitumor potential, as well as perform preliminary experimentation into the mechanisms of action of our lead compound. In developing the AIMS, we had several hypotheses: first, we believe that the C10 position of the AIMS is the site of potential cationic interactions that are essential for proper G-quadruplex interaction; therefore, synthesis proceeded with modifying this site, with the goal being to add small substituents that would overall make the AIMS more cytotoxic (and presumably better G-quadruplex binders). Second, the AIMS were synthesized with either one or two tails bearing either two or three nitrogens, respectively. Based on initial molecular modeling, we believe that the tails serve to anchor the ligand to the phosphate backbone of the quadruplex. We hypothesize that the addition of two tails will allow for stronger binding and that this will be reflected in a more cytotoxic ligand. Taken together, we believe that customization of the AIMS with modifications to the tails and to the C10 position will increase their selectivity for G-quadruplex DNA and will result in enhanced toxicity to brain cancer cells.

MATERIALS AND METHODS

Chemicals. AIMs were obtained from the University of Montana (Missoula, MT). We are appreciative of the efforts Matthew J. Weaver and the Natale laboratory for contribution to the synthesis of the AIM compounds.

Cell Culture. SNB-19 human glioblastoma cells (American Type Cell Culture Cat No. CRL-2266) were grown in RPMI 1640 medium with L-glutamine and penicillin/streptomycin, supplemented with 10% fetal bovine serum (FBS). Cell culture medium and supplements were obtained from Invitrogen (Carlsbad, CA). The cells were incubated at 37 °C under a humidified atmosphere containing 5% CO₂ and allowed to achieve confluence prior to experimentation.

Cell Viability Assay. Cell survival was measured by the [3-(4,5-dimethylthiazol-2-yl)-2,5-diphenyltetrazolium bromide (MTT) colorimetric assay. MTT was obtained from Sigma-Aldrich (St. Louis, MO). As previously described, cells were plated in 96-well plates at a density of 10,000 cells/mL and allowed to attach overnight (16 h). AIM solutions were applied in medium for 24 h, removed, and replaced with fresh medium, and the plates were incubated at 37°C under a humidified atmosphere containing 5% CO₂ for 3–5 days. MTT (50 µg) was added

and the cells were incubated for another 4 h. Medium/MTT solutions were removed carefully by aspiration, the MTT formazan crystals were dissolved in 100 μ L of DMSO, and absorbance was recorded on a spectrophotometer at 560 nm. IC₅₀ values (concentration at which cell survival equals 50% of control) were determined from semilog plots of percent of control versus concentration. Each experiment was performed in triplicate. Average IC₅₀ values are reported from triplicate results.

Confocal Microscopy. SNB-19 cells were plated on cover slips in 6-well plates at a density of 1×10^3 /well, allowed to adhere, and incubated overnight at 37°C in 5% CO₂ to achieve adherence. AIM solutions (1 μ M) were added to cells and incubated overnight. After incubation, medium was aspirated, cells were washed twice with PBS and fixed in 4% paraformaldehyde/PBS (on ice; 10 min). Following three additional washes in PBS, cells were washed once with de-ionized water, and fluorescent images were taken with an Olympus FV1000 confocal laser scanning microscope using selective laser excitation at 405 nm (40X objective with an optical magnification lens of 10X and oil immersion objective of 40X [NA, 1.35]). Images were processed with Nuance 1.6.2.368 alpha software (Cambridge Research Institute).

Laser Scanning Cytometry with Propidium Iodide. SNB-19 cells were plated at a density of 2000 cells/mL on cover slips in medium. The cells were incubated at 37 °C under a humidified atmosphere containing 5% CO₂ and allowed to adhere. Media was aspirated and replaced with 1 μM AIM in medium. Drug was removed and cells were washed twice with phosphate buffered saline (PBS). Cells were fixed in 4% paraformaldehyde (10 minutes, RT) and washed once with PBS. To determine nuclear localization, samples were permeabilized with 0.2% Saponin and exposed to propidium iodide (Invitrogen, Carlsbad, CA). Following washes, cover slips were inverted to microscope slides and sealed using FluoroSave Reagent (Calbiochem). Light absorption was measured to produce a DIC-like image for cell morphology and each signal was given a pseudo-color.

Laser Scanning Cytometry with MitoTracker Red and HCS Nuclear Mask. As described, SNB-19 cells were plated at a density of 2000 cells/mL on cover slips in medium. The cells were incubated at 37 °C under a humidified atmosphere containing 5% CO₂ and allowed to adhere. Media was aspirated and replaced with 1 μM AIM in medium. Drug was removed and cells were washed twice with phosphate buffered saline (PBS). Cells were fixed in 4% paraformaldehyde (10 minutes, RT) and washed once with PBS. To determine cellular localization, HCS NuclearMask

Deep Red stain and MitoTracker Red stain (Invitrogen, Carlsbad, CA) were added directly to cells and incubated following manufacturer's directions. Following two additional washes, slides were inverted to microscope slides and sealed using FluorSave Reagent (Calbiochem). Images were generated from scans from a CompuCytex iCys Laser Scanning Cytometer (CompuCytex, Westwood, MA). Cells were scanned sequentially and light absorption was also measured to produce a DIC-like image for cell morphology as necessary. Each signal was given a pseudo-color and overlaid to produce images. Untreated samples were run as negative controls.

Bioavailability Estimates. Parameters relating to oral bioavailability were calculated using the Symyx Draw v3.1 program. The pentagonal plot takes into consideration: log P (the oil water partition coefficient), PSA (polar surface area), nRotb (number of rotatable bonds), MW (molecular weight) and WS (water solubility). The color of the pentagon corresponds to the best fit in relation to the Lipinski guidelines for oral bioavailability. Green = 0-1 violations, Yellow = 2 violations, Orange = 3-4 violations, Red = 5 violations. The Symyx Draw Log P calculation is based on Ghose's AlogP method (Ghose *et al.*, 1998). The Polar Surface area computation is based on Ertl's method (Ertl *et al.*, 2000).

NMR Spectroscopy. DNA oligonucleotides were purchased from Integrated DNA Technologies. For analysis, we followed the methods of Dai *et al.* (2011), as well as those of Wang and Patell (2003; with modifications). Briefly, NMR samples were prepared containing oligonucleotide (0.1-1.0 mM) in 90% H₂O/10% D₂O buffer at pH 6.0 with 100 mM or 200 mM K⁺ ions. Ion concentrations were obtained with KH₂PO₄ 25 mM/KCl 75 mM or 50 mM/150 mM. Samples were re-annealed prior to each round of data collection and those containing AIM 1 ligand (1 equivalent) were subjected to a subsequent round of re-annealing after the addition of ligand. Experiments were performed on a Varian 500 MHz spectrophotometer at 25°C. Following Watergate and Wet 1D water suppression techniques, data was transformed using the squared shifted sine bell function.

Flow Cytometry Annexin V Apoptosis. Apoptosis levels of SNB-19 cells treated with AIM solutions (1 μM, 2.5 μM, 5 μM) were determined by Annexin-V staining and propidium iodide (PI) exclusion using the FITC Annexin-V Apoptosis Detection Kit I (BD Pharmingen, San Diego, CA, USA) following manufacturer's instructions. Cells were treated with each concentration of AIM and plated in 6-well culture dishes for exposure period. Samples were carefully trypsinized and transferred to flow cytometry tubes for processing, following the

protocol for Annexin V for adherent cells indicated by the manufacturer. Untreated samples were run as negative control. Staurosporine treated samples were run as positive control.

Statistics. All statistical analyses were performed using GraphPad Prism 4.0 for Macintosh (GraphPad Software, San Diego, CA). Student's *t*-test was used to compare untreated and treated samples. Mean and standard deviation were used to calculate IC₅₀ values. Values $p \leq 0.05$ were determined to be significant.

RESULTS

AIMs are cytotoxic at single digit micromolar levels. Five AIMs were examined for this study (Figure 2.1). Results from MTT analysis showed that all AIMs produced growth inhibition in SNB-19 cells at doses no higher than 8 μ M for a 24 hour treatment period (Figure 2.2). The first AIM that was synthesized in this series, AIM 2, had good toxicity towards SNB-19 cells, which was somewhat surprising considering its large molecular weight that would presumably limit solubility. However, in the original development of the AIMs, AIM 2 was synthesized as a dimer due to the hypothesis that this structure would allow for multiple G-quadruplex binding at a time and result in more potent telomerase inhibition downstream. Overall, results indicate that AIMs

bearing double tails (AIM 1 and AIM 4) were more cytotoxic to SNB-19 cells compared to their single tail counterparts (AIM 3 and AIM 5).

Figure 2.1

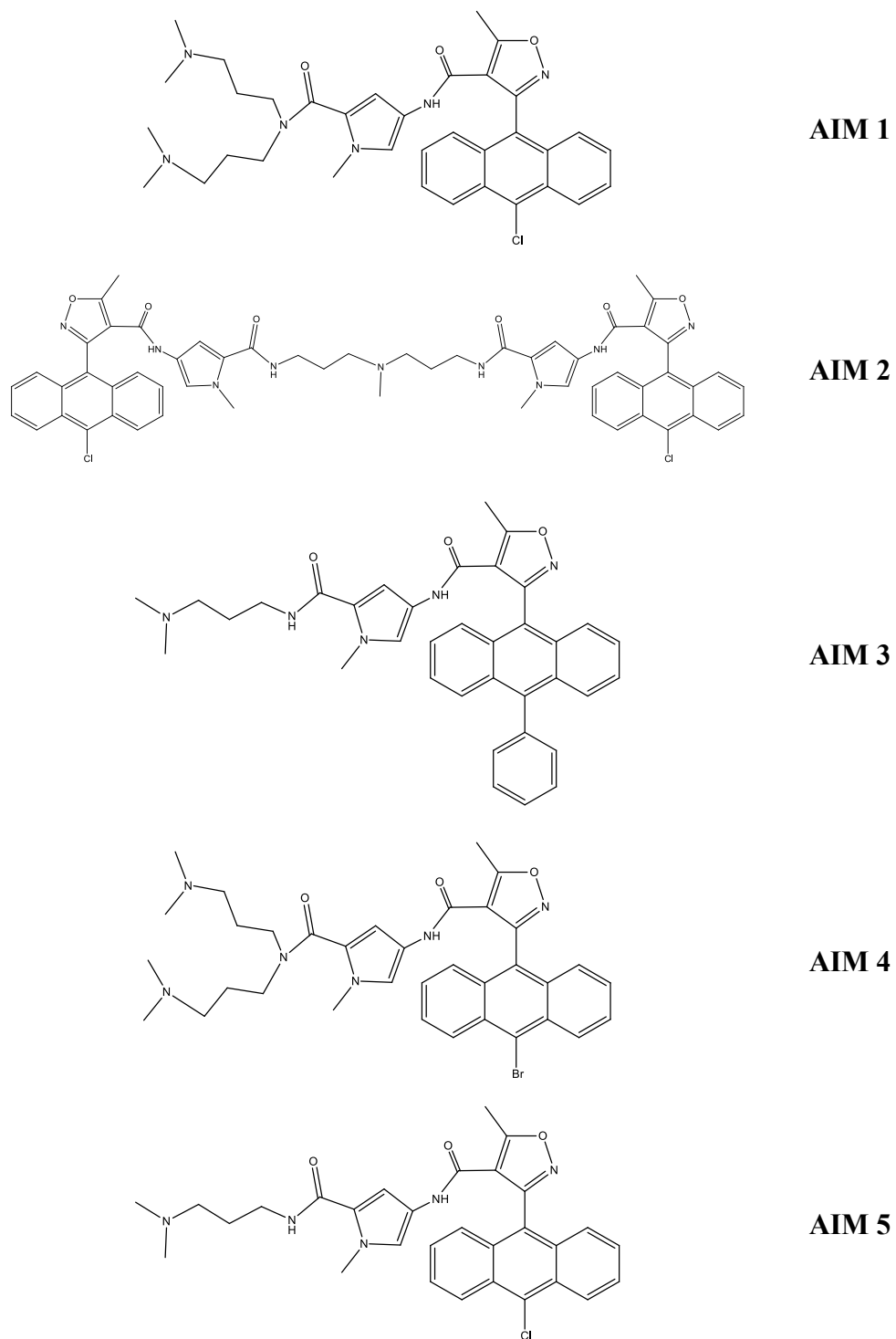
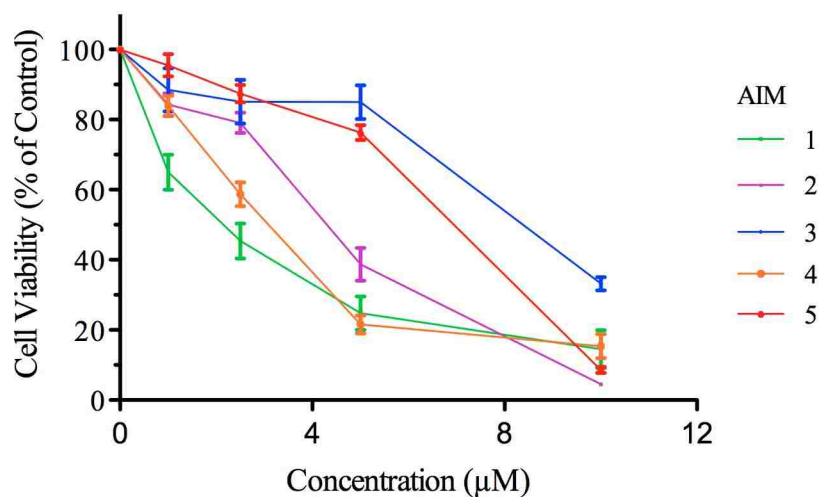


Figure 2.1. AIM structures. AIMS 1-5 and corresponding structures.

Figure 2.2

A.



B.

AIM	Molecular Weight (g/mol)	IC ₅₀ (µM)
1	629.19	3.13 ± 0.45
2	1028.97	4.75 ± 0.27
3	585.69	7.66 ± 0.73
4	673.64	3.16 ± 0.25
5	544.04	6.27 ± 0.23

Figure 2.2. AIMs toxicity testing. MTT viability assay results reveal all AIMs have single digit micromolar IC₅₀ values and are cytotoxic to a SNB-19 human glioblastoma cell line.

AIM 1 and AIM 2 penetrate cell membranes and can be observed fluorescently within the cell.

Initial fluorescent experimentation was performed to determine ability of AIMs to be visualized without additional fluorescent labeling. The effect of double tail structure versus dimer configuration on AIMs localization within cells was selected as the initial investigation (Figure 2.3). Confocal microscopy revealed that both AIM 1 and AIM 2 appeared to be localized outside the nucleus. These findings were surprising given that telomeres, the target of G-quadruplex ligands, are located within the nuclei of cells. To investigate the localization of AIM 1 and AIM 2 further, we performed LSC imaging with the nuclear indicator propidium iodide (PI) (Figure 2.4). These results seem to indicate that both AIMs were in fact inside the nucleus, as demonstrated by the overlapping fluorescence of both the AIMs and PI. Due to the conflicting microscopy showing first that the AIMs were extra-nuclear and then that with the addition of a counterstain appeared to be nuclear, we could not decisively confirm the location. This led us to modify our microscopy procedures and alter sample preparation to ensure the effects of the AIMs on SNB-19 cells were only due to inherent cytotoxicity and not due to the way in which we processed samples.

Figure 2.3

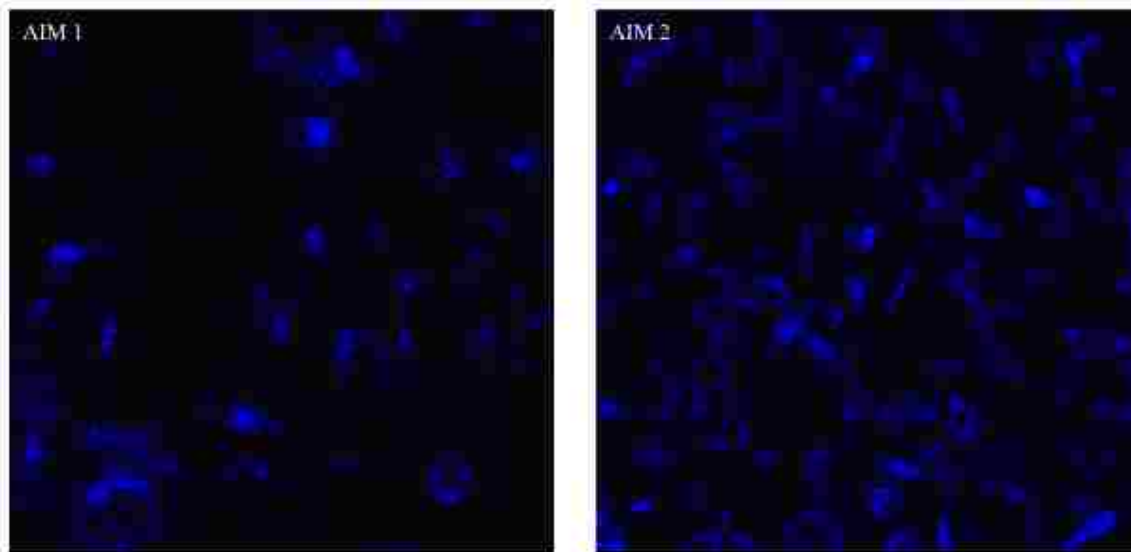


Figure 2.3. Confocal microscopy indicates differences in cellular distribution of AIM dimer vs. double tail structures. Fluorescent imaging of SNB-19 cells exposed to 1 μM of each AIM reveal that AIM 2, with a high molecular weight of 1028.97 g/mol appears to penetrate cells, but it is unclear as to what cellular structure it is localized. In contrast, AIM 1 (molecular weight 629.19 g/mol) appears to permeate the membrane of the human glioma cells, and punctate binding is observed.

Figure 2.4

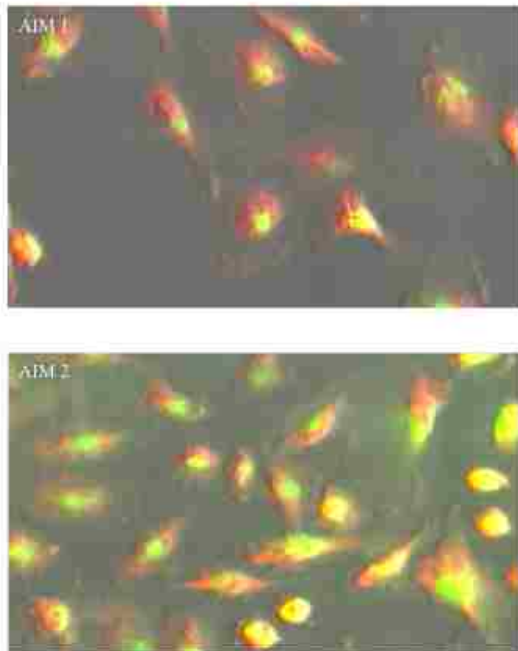


Figure 2.4. Laser Scanning Cytometry with PI counterstaining. DIC-like images were produced to allow for visualization of cell morphology. AIMS (shown in green) appear to localize within the nucleus of SNB-19 cells (nucleus stained in red). When the fluorescence overlaps substantially, areas of AIM in the nucleus appear yellow in color.

AIM 1 possesses a better bioavailability profile than AIM 2. Due to the fluorescent imaging results that showed both AIM 1 and AIM 2 enter SNB-19 cells, we performed analysis of bioavailability parameters to better understand the effect that double tail vs dimer structure has on solubility. Radar plots (Figure 2.5) indicate that based on all parameters assessed, AIM 1 is a more suitable drug for continued evaluation. Due in part to the large molecular weight of AIM 2, these results are not altogether surprising.

Figure 2.5

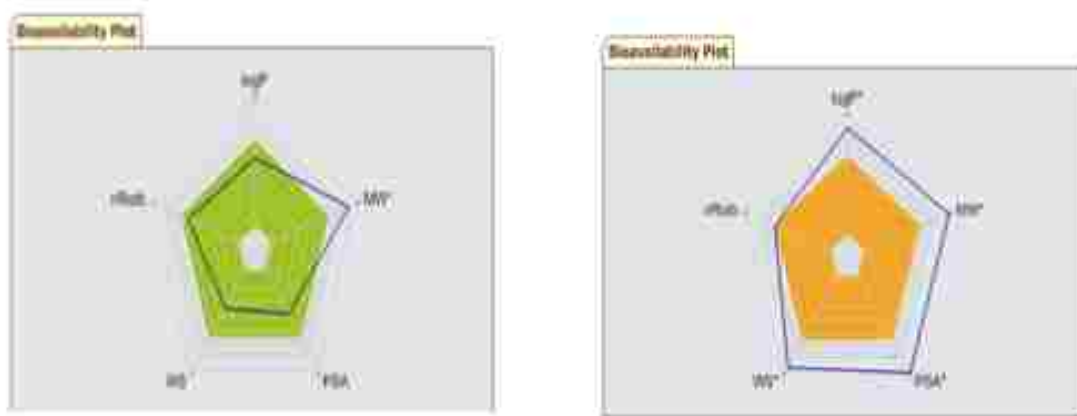


Figure. 2.5. AIM 1 possesses better bioavailability properties compared to AIM 2. Radar graphs summarizing properties of AIM 1 (green) and AIM 2 (orange). AIM 1 lies within the acceptable parameters for bioavailability with acceptable cLogP and AlogD values. AIM 2 lies outside of the optimum parameters for bioavailability in almost all respects.

Lead compound AIM 1 localizes to the mitochondria of cells. Due to the fluorescent imaging results, MTT viability assay and solubility properties, AIM 1 was selected as our lead compound for further investigation. Because results from our preliminary microscopy were conflicting in terms of the cellular location of AIM 1, we performed additional fluorescence experimentation. Initial confocal microscopy appeared to indicate AIM 1's location outside of the nucleus; however, LSC imaging demonstrated that AIM 1 was nuclear. To address this disparity, changes were made in the experimental protocol to omit the permeabilization step discussed previously with images shown in Figure 2.4. We hypothesized that the permeabilization required for propidium iodide counterstaining might be impacting the true cellular location of the AIMs; therefore, nuclear counterstaining was performed with HCS Nuclear Mask, which does not require permeabilization. Results revealed that as shown by confocal microscopy, AIM 1 localized outside of the nucleus (Figure 2.6a). Because of these results and the punctate staining profile observed both with confocal microscopy and LSC imaging with HCS Nuclear Mask, we believed AIM 1 may be localized in the mitochondria of SNB-19 cells. With the addition of a mitochondrial marker, AIM 1 was confirmed to be concentrated within the mitochondria of SNB-19 cells (Figure 2.6b).

Figure 2.6

A.



B.



Figure 2.6. Laser scanning cytometry of AIM 1 in SNB-19 cells with counterstaining. HCS nuclear mask (blue), a nuclear indicator, was used to confirm AIM 1 distribution (green) outside of the nucleus (A). Additional imaging with a mitochondrial marker, MitoTracker Red (red), revealed AIM 1 localized to the mitochondria (B).

AIM 1 binds the human telomeric G-quadruplex sequence as determined by NMR spectroscopy. In order to determine if AIM 1 functions as a G-quadruplex ligand, we performed NMR spectrophotometry using a commercially available human telomeric G-quadruplex sequence (Figure 2.7). Results indicated that AIM 1 binds G-quadruplex sequences within telomeres.

AIM 1 induces apoptosis. To investigate the mechanism of action for AIM 1, Annexin V flow cytometry was performed at three doses: 1 μ M, 2.5 μ M, 5 μ M for a 24 h exposure period (Figure 2.8). Annexin V analysis was performed using PI exclusion to determine the stages of apoptosis that occur at each dose: Annexin V+/PI- corresponds to early apoptosis, Annexin V+/PI+ indicates late stage apoptosis and Annexin V-/PI+ are those samples that are showing signs of necrosis. Results for AIM 1 show a significant induction of apoptosis at the highest concentration as compared to untreated control.

Figure 2.7

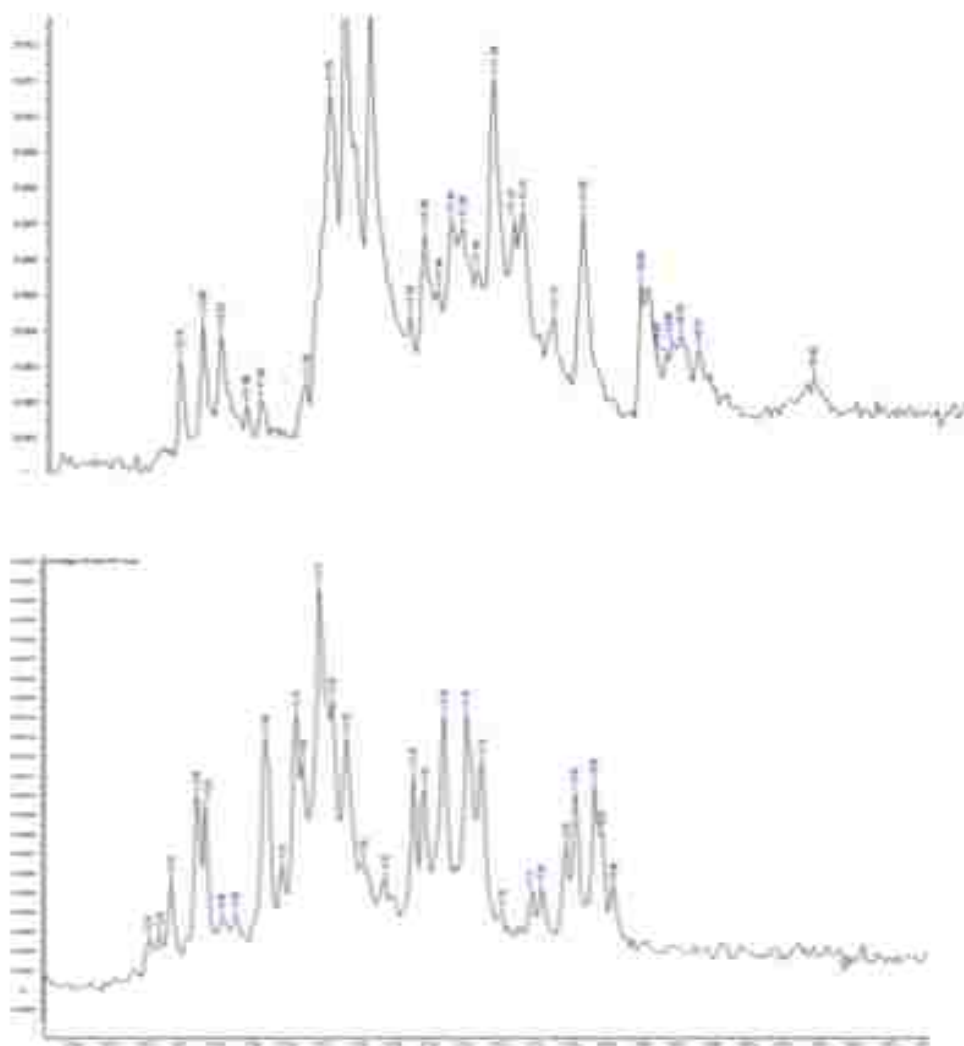
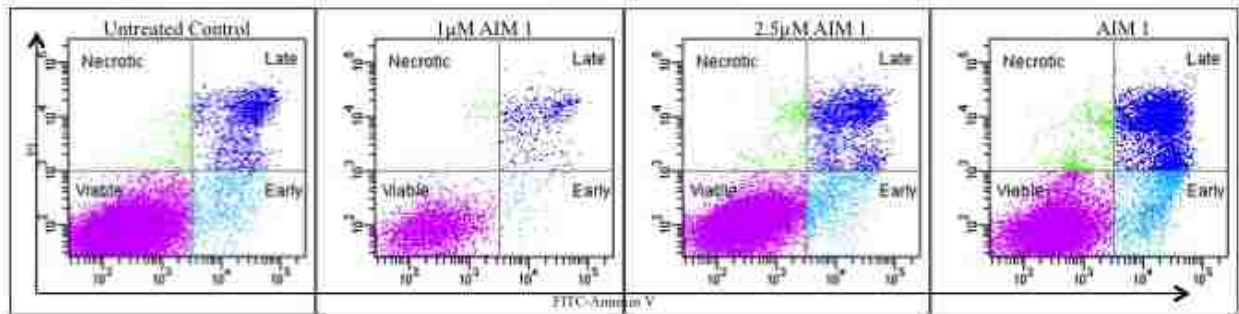


Figure 2.7. NMR spectra with AIM 1. NMR of oligonucleotide 5'-(T₂AG₃)₄-3' with 1 Eq of AIM 1 (top) and with DNA only (bottom) showing upfield shift of guanine imino protons. Chemical shift scale is from 9.7-12.4 ppm. Guanine imino proton signals are between 10.5 and 12.5 ppm; upfield shifts occur due to ligand binding to G4 DNA. (The authors wish to acknowledge the contributions of Dr. Nicholas R. Natale and Matthew J. Weaver for NMR spectroscopy).

Figure 2.8

A.



B.

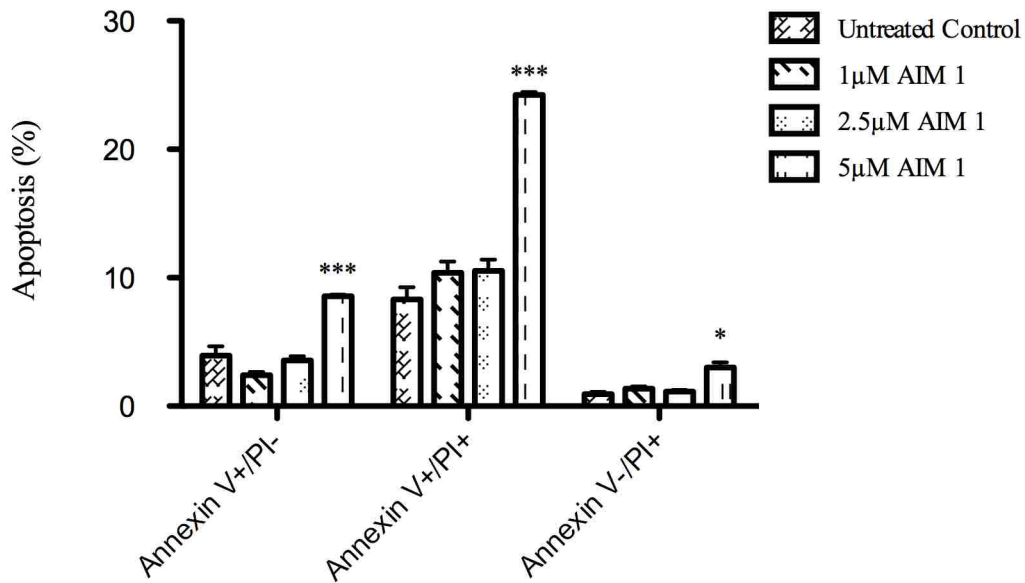


Figure 2.8. AIM 1 induces apoptosis in SNB-19 cells. Flow cytometry indicates AIM 1 induces apoptosis in a dose dependent trend (A). Analysis of Annexin V staining details the overall amount of apoptosis induction by AIM 1 at varying doses (B). *indicates significance of $p \leq 0.05$, and ***indicates significance of $p \leq 0.0001$.

Single tailed AIMS are able to penetrate cells and be visualized within the cells. To evaluate if small structural changes on single tail structures effect the localization and fluorescent properties of the AIMS, laser scanning cytometry was performed (Figure 2.9). Fluorescent microscopy of single tail structures revealed that while both AIMS are able to enter cells, they bear different fluorescent properties. That is, AIM 3, which contains a phenyl group at the C10 position, is more fluorescent compared to AIM 5, when both AIMS are excited at the same wavelength. These results are consistent with the notion that aromatic groups, such as phenyl groups, contribute structural fluorescence due to the ability to excite the electrons within the aromatic ring. Results from fluorescent microscopy demonstrated that single tail AIMS can be visualized within cells.

Figure 2.9



Figure 2.9. Laser scanning cytometry of single tail AIM structures. AIM 3 and 5 (highlighted in blue) visualized by laser scanning cytometry. AIMS are minimally punctate in nature and appear diffuse within SNB-19 cells. AIM 5 produces a dimmer fluorescent compared to other single tail structures; therefore DIC images were acquired to more clearly show cellular morphology and AIM location within cells (Mirzaei *et al.*, 2012).

DISCUSSION

The purpose of this study was to develop a library of potential G-quadruplex ligands, determine their cytotoxicity to SNB-19 human glioblastoma cells and identify lead compounds for additional experimentation. Overall, studies indicated that one of the most important structural features of the AIMs was the addition of a double tail that resulted in AIMs that were more cytotoxic than their single tailed counterparts. This supports our original hypothesis that the addition of a double tail can anchor more effectively than a single tail on to the phosphate backbone of the G-quadruplex and that this would make these compounds better drugs (and result in a more cytotoxic drug). In addition, AIMs synthesized with two tails bear three nitrogens that are ionizable at physiologic pH, giving these AIMs better solubility properties as well. In regards to substituents at the C10 position of the AIMs, it appears as though smaller groups (for example Cl vs Br in the double tail AIMs) lead to a more cytotoxic compound, however, the differences in IC_{50} values are subtle. Regardless, these effects are likely due to a smaller molecular weight—large groups at C10 will result in a larger compound that may not as efficiently enter cells to exert activity. Additionally, AIM 2, a structural dimer, was able to penetrate cell membranes despite its large size and poor bioavailability. Based on initial molecular modeling results performed during the genesis of this project, the C10 position of the

AIMs was believed to be the site of cationic interactions of ligands within the central channel of the G-quadruplex—an essential feature of G-quadruplex stabilization. While this hypothesis was not tested directly, we believe that if these interactions were occurring, the results would be more potent AIMs that are able to bind to G-quadruplex efficiently. The results of this study indicate modifications at the C10 position alters the fluorescence of the AIMs as well as changes the overall cytotoxicity (as indicated by IC_{50} values), although the results were subtle in this regard.

To summarize the results of investigation of lead compound AIM 1, NMR experiments indicated AIM 1 interacts with telomeric G-quadruplex DNA and MTT analysis demonstrated that AIM 1 had good cytotoxicity, but fluorescent microscopy was intriguing as results showed extra-nuclear localization—traditional G-quadruplex ligands are designed to target G-quadruplex structures within the nucleus (Casagrande *et al.*, 2011; Ou *et al.*, 2008). In this regard, contrary to what was expected, AIM 1 was highly concentrated in the mitochondria of cells. We believe that the original LSC experiments with AIM 1 and AIM 2 and the nuclear indicator PI were somewhat misleading. First, after repeating several experiments with PI, permeabilization was determined to be a factor leading to fluorescent quenching which may also explain why PI appears to not only stain the nucleus but also almost the entire SNB-19 cells. Second, in these early experiments sequential laser scanning was not performed—meaning that it is possible that

AIM 1 and AIM 2 in the nucleus were actually a result of excitation by the fluorescence of PI and were therefore falsely staining positive in the nucleus. Third, in respect to AIM 1 even when the HCS Nuclear Mask nuclear indicator was used, there is a small subset of cells (always <10% of the entire population sampled) that appear morphologically distinct from the majority and appear to stain positive for AIM 1 in the nucleus. Due to the fact that SNB-19 cells are heterogeneous at the time of sampling (at different stages of cell cycle), we believe this explains these somewhat varying microscopy results; some cells are naturally more apoptotic at the time of drug exposure and take up AIM 1 through damaged membranes, resulting in AIM 1 in the nucleus when these samples are visualized.

There are several points worth considering in regards to the data that indicate AIM 1 is localized in the mitochondria. First, the effect of telomeric G-quadruplex DNA stabilization by ligands has been experimentally shown to be caused by the inhibition of telomerase and the consequent interference with telomere length leading to apoptosis or senescence (Neidle and Parkinson, 2002). However, some unexpected research findings have also demonstrated that G-quadruplex ligands interact with telomeric G-quadruplex DNA but induce cell death in the absence of telomere shortening (Pennarun *et al.*, 2005; Zhou *et al.*, 2009). These results contradict the original theory that G-quadruplex ligands function only to interfere with telomere

length and support our research findings that another mechanism of action may exist outside of telomerase inhibition in the nucleus (Kelland, 2007). Research is also emerging that implicates the mitochondria in the role of G-quadruplex stabilization and indicates that some G-quadruplex ligands, once bound to quadruplex, cause mitochondrial dysfunction and mitochondrial-dependent apoptosis (Zhuang and Yao, 2013). While the research showing that G-quadruplex ligands affect the mitochondria do not include fluorescent studies indicating cellular localization of these G-quadruplex ligands within the mitochondria, we believe that collectively, our data with AIM 1 indicates that our AIMs may also possess properties leading to mitochondrial-specific effects. We propose that, based on our results that AIM 1 functions as a G-quadruplex DNA binder and is highly concentrated outside of the nucleus within the mitochondria of cells, that AIM 1 is causing mitochondrial-specific intracellular effects following or coinciding with the binding to and stabilization of telomeric G-quadruplex structures. Data showing AIM 1 in the mitochondria of cells supports the emerging hypothesis that the mitochondria may be implicated in ways that are yet undiscovered in the field of G-quadruplex.

This series of AIMs targeting G-quadruplex is the first of their kind to possess fluorescent properties that do not require additional labeling to be visualized while also being preferentially localized outside of the nucleus and in the mitochondria. We have demonstrated that lead

compound AIM 1 induces apoptosis at single digit micromolar doses in SNB-19 human glioblastoma cells and additionally, is concentrated in the mitochondria of these cells. The investigation into the role of the mitochondria in the functioning of the AIM compounds is imperative to determining to what extent G-quadruplex ligands might impact the mitochondria. Also, in light of recent findings that demonstrate a mitochondrial-based extra-telomeric mechanism of action of G-quadruplex ligands, a further detailed investigation into the cellular pathways involved in the stabilization of G-quadruplex structures is warranted. Additional studies examining the mechanisms of action of G-quadruplex ligands outside of solely testing for binding affinity is a crucial component in the design of more specific G-quadruplex ligands as anticancer agents.

ACKNOWLEDGEMENTS

The authors wish to thank Dr. Nick Natale and lab members for their contributions to the synthetic chemistry of the AIMS. Also, we would like to acknowledge Matthew J. Weaver for his work in regards to the NMR spectroscopy.

REFERENCES

- Ahmed, S., Passos, J. F., Birket, M. J., Beckman, T., Brings, S., Peters, H., Birch-Machin, M. A., Von Zglinicki, T., Saretzki, G. (2008). Telomerase does not counteract telomere shortening but protects mitochondrial function under oxidative stress. *J Cell Sci* **7**, 1046-1053.
- Bates, P. J., Laber, D. A., Miller, D. M., Thomas, S. D., and Trent, J. O. (2009). Discovery and development of the G-rich oligonucleotide AS1411 as a novel treatment for cancer. *Mol Pathol* **86**, 151-164.
- Casagrande, V., Salvati, E., Alvino, A., Bianco, A., Ciammaichella, A., D'Angelo, C., Ginnari-Satriani, L., Serrilli, A. M., Iachettini, S., Leonetti, C., Neidle, S., Ortaggi, G., Porru, M., Rizzo, A., Franceschin, M., and Biroccio, A. (2011). N-cyclic bay-substituted perylene G-quadruplex ligands have selective antiproliferative effects on cancer cells and induce telomere damage. *J med Chem* **54**, 1140-1156.
- Dai, J., Carver, M., Hurley, L. H, and Yang, D., (2011). Solution structure of a 2:1 quindoline c-MYC G-Quadruplex: Insights into G-Quadruplex-Interactive small molecule drug design. *J Am Chem Soc* **133**, 17673-17680.
- Drygin, D., Siddiqui-Jain, A., O'Brien, S., Schwaebe, M., Lin, A., Bliesath, J., Ho, C. B., Profitt, C., Trent, K., Whitten, J. P., Lim, J. K., Von Hoff, D., Anderes, K., and Rice, W. G. (2009). Anticancer activity of CX-3543: a direct inhibitor of rRNA biogenesis. *Cancer Res* **69**, 7653-7661.
- Ertl, P., Rohde, B., and Selzer, P. (2000). Fast calculation of molecular polar surface area as a sum of fragment-based contributions and its application to the prediction of drug transport properties. *J Med Chem* **43**, 3714–3717.
- Gajewski, M. P., Beall, H., Schnieder, M., Stranahan, S. M., Mosher, M. D., Rider, K. C., and Natale, N. R. (2009). Bis-anthracenyl isoxazolyl amides have enhanced anticancer activity. *Bioorg Med Chem Lett* **19**, 4067–4069.
- Ghose, A. K., Viswanadhan, V. N., and Wendoloski, J. J. (1998). Prediction of hydrophobic (lipophilic) properties of small organic molecules using fragmental methods: An analysis of ALOGP and CLOGP methods. *J Phys Che. A* **102**, 3762–3772.
- Haendeler, J., Drose, S., Buchner, N., Jakob, S., Altschmied, J., Goy, C., Spyridopoulos, I., Zeiher, A. M., Brandt, U., and Dimmeler, S. (2009). Mitochondrial telomerase reverse transcriptase binds to and protects mitochondrial DNA and function from damage.

- Arterioscler Thromb Vasc Biol* **29**, 929-935.
- Han, X., Li, C. L., Mosher, M. D., Rider, K. C., Zhou, P., Crawford, R. L., Fusco, W., Paszczynski, A., and Natale, N. R. (2009). Design, synthesis and biological evaluation of a novel class of anticancer agents: Anthracenylisoxazole lexitropsin conjugates. *Bioorg Med Chem* **17**, 1671-1680.
- Kelland, L. (2007). Targeting the limitless replicative potential of cancer: the telomerase/telomere pathway. *Clin Cancer Res* **13**, 4960-4963.
- Masutomi, K., Possemato, R., Wong, J. M. Y., Currier, J. L., Tothova, Z., Manola, J. B., Ganesan, S., Lansdorp, P. M., Collins, K., and Hahn, W. C. (2005). *Proc Natl Acad Sci* **102**, 8222-8227.
- Mirzaei, Y. R., Weaver, M. J., Steiger, S. A., Kearns, A. K., Gajewski, M. P., Rider, K. C., Beall, H. D., and Natale, N. R. (2012). Improved synthesis of 3-aryl isoxazole containing fused aromatic rings. *Tetrahedron* **68**, 10360-10364.
- Neidle, S., and Parkinson, G. (2002). Telomere maintenance as a target for anticancer drug discovery. *Nat Rev Drug Disc* **1**, 383-393.
- Ou, T-M., Lu, Y-J., Tan, J-H., Huang, Z-S., Wong, K-Y., and Gu, L-Q. (2008). G-quadruplexes: Targets in anticancer drug design. *Chem Med Chem* **3**, 690-713.
- Pennarun, G., Granotier, C., Gauthier, L. R., Gomez, D., Hoffschir, F., Mandine, E., Riou, J-F., Mergny, J-L., Mailliet, P., and Boussin, F. (2005). Apoptosis related to telomere instability and cell cycle alterations in human glioma cells treated by new highly selective G-quadruplex ligands. *Oncogene* **24**, 2917-2928.
- Sen, D., and Gilbert, W. (1988). Formation of parallel four stranded complexes by guanine rich motifs in DNA and its implications for meiosis. *Nature* **334**, 364-366.
- Siddiqui-Jain, A., Grand, C. L., Bearss, D. L., and Hurley, L. H. (2002). Direct evidence for a G-quadruplex in a promoter region and its targeting with a small molecule to repress *c-MYC* transcription. *Proc Natl Acad Sci* **99**, 11593-11598.
- Wang, Y., and Patell, D. (1993). Solution structure of the human telomeric repeat d[AG₃(T₂AG₃)₃] G tetraplex. *Structure* **1**, 4.
- Zhou, W. J., Deng, R., Zhang, X-Y., Feng, G-K., Gu, L-Q., and Zhu, X-F. (2009). G-quadruplex ligand SYUIQ-5 induces autophagy by telomere damage and TRF2 delocalization in cancer cells. *Mol Cancer Ther* **8**, 3203-3213.
- Zhuang, X-Y., and Yao, Y-G. (2013). Mitochondrial dysfunction and nuclear-mitochondrial shuttling of TERT are involved in cell proliferation arrest by G-quadruplex ligands. *FEBS Lett* **11**, 1656-1662.

CHAPTER 3

Investigation of novel antitumor agent anthracenyl isoxazole amide (AIM) 1 as a mitochondrial modulator of apoptosis

Authors

Alison K. Kearns and Howard D. Beall

Corresponding Author

Dr. Howard D. Beall

Address: University of Montana

Department of Biomedical and Pharmaceutical Sciences

32 Campus Drive, Skaggs

Missoula, MT 59812

Telephone: 406-243-5112

Fax: 406-243-2807

Email: Howard.Beall@umontana.edu

ABSTRACT

Development of G-quadruplex ligands for the treatment of solid tumors is an emerging field of research. The site of G-quadruplex structures within the nucleus of cells has been the target of these ligands, with the goal of inhibiting telomerase and causing replicative senescence or selective apoptosis of tumor cells. We have shown previously that an anthracenyl isoxazole amide, AIM 1, is a good candidate for further investigation into the mechanisms of G-quadruplex ligand functions due to its cytotoxicity and ability to induce apoptosis in a human glioblastoma cell line. Our initial research curiously showed that AIM 1 was localized within the mitochondria of cells—a finding that differs from the believed site of action of G-quadruplex ligands within the nucleus. Several parameters of mitochondrial function are assessed and detailed in this study. Our results indicate AIM 1 induces mitochondrial-specific apoptosis and that exposure results in mitochondrial dysfunction. Additionally, we were interested in investigating the potential of AIM 1 to actuate hTERT shuttling. hTERT nuclear export is an advancing field of telomerase research, that has potential to impact the way in which investigators view the site of action of G-quadruplex ligands and other telomerase inhibitors. Collectively, the results of our investigation into the mechanisms of AIM 1 demonstrate that G-quadruplex ligands may function in ways more complex than previously thought.

INTRODUCTION

Mitochondrial research is an active discipline in pharmaceutical research. Mitochondria have long been accepted as the ‘power house of the cell’, but it is the revelation that mitochondria also represent the ‘motor of cell death’, that is most intriguing in mitochondrial medicine (Brown *et al.*, 1999). The mitochondria are crucial regulators of the intrinsic pathway of apoptosis and control the activation of apoptosis by regulating the translocation of pro-apoptotic proteins from the mitochondrial intermembrane space to the cytosol (Fulda *et al.*, 2010). In this regard, mitochondrial-targeted anticancer agents represent a promising approach to the treatment of cancer for three reasons: mitochondria are key regulators of cell death, altered mitochondrial functions are a hallmark of cancer, and cancer cell mitochondria are structurally and functionally different from mitochondria in normal cells; the latter which allows for the selective targeting of cancer cell mitochondria (Gogvadze *et al.*, 2008; Modica-Napolitano and Singh, 2004). Additionally, an increasing number of xenobiotics and pharmaceuticals are being recognized as agents capable of manifesting toxicity through interference with mitochondrial functions (Wallace and Starkov, 2000). There are several means by which to target the mitochondria including the use of ROS regulators, modulators of BCL-2, metabolic inhibitors, and agents that deplete mitochondrial DNA (Fulda *et al.*, 2010). One of the advantages of

mitochondria-targeted drugs in the context of cancer is the potential to induce apoptosis in the absence of the apoptosis-resistance that often plagues traditional anticancer agents (Weissig *et al.*, 2004).

Aside from changes in the mitochondria, cancer cells are also distinct from normal cells due to telomerase activation. Telomerase, the enzyme responsible for adding the telomeric repeats TTAGGG on to the 3' ends of chromosomes, is overexpressed in >85% of all cancer and enzyme activation results in the maintenance of telomere length and enhanced replicative capacity (Shay and Bacchetti, 1997). The guanine-rich sequence in telomeres have been shown to form 4-stranded G-quadruplex DNA structures that can be stabilized with small molecules and effectively interfere with the functioning of telomerase, leading to telomere shortening, cellular senescence and apoptosis (Burge *et al.*, 2006; Neidle *et al.*, 2002). The development of telomerase inhibitors such as G-quadruplex ligands is a viable therapy to treat malignancy; however, new research is emerging in the field of telomeres that is changing the way researchers view telomerase targeted anticancer therapies.

The catalytic subunit of human telomerase, hTERT, is the major determinant and the rate-limiting factor of telomerase activity (Cong *et al.*, 2002; Poole *et al.*, 2001). The conventional oncogenic role of hTERT has been linked to cellular immortalization, but evidence

to support non-canonical activities of hTERT is emerging. In examining the extra-nuclear functions of hTERT, it is important to first consider the role of the mitochondria in cellular homeostasis. The mitochondria are an inherent source of reactive oxygen species (ROS) due in part to close proximity to the electron transport chain (ETC). In situations where the mitochondria or the anti-oxidant defense systems are impaired or inefficient, cells may become exposed to the damaging effects of ROS and accumulate mitochondrial DNA damage or amass excessive ROS within the mitochondria; damage to the mitochondria through extensive oxidative stress leads to eventual cell death and apoptosis. Similar to the way in which cellular outcomes are affected by redox states within the mitochondria, hTERT expression is also regulated by many redox-sensitive transcriptional factors (Akiyama *et al.*, 2003; Cong and Shay, 2008). In addition to ROS-mediated transcriptional consequences, ROS is also a determinant of hTERT intracellular location and therefore, cellular function.

Following periods of oxidative stress, hTERT shuttles from the nucleus to the mitochondria; however, once in the mitochondria, the role of hTERT is not fully understood (Ahmed *et al.*, 2008; Massard *et al.*, 2006; Passos *et al.*, 2006). At the cytosol, hTERT interacts with mitochondrial import proteins that facilitate transport into the mitochondria (Indran *et al.*, 2010). Following cellular stress, hTERT localization from the nucleus to the mitochondria is

correlated with increased mitochondrial DNA damage (Santos *et al.*, 2006). Conversely, under some experimental conditions after inducing cellular stress, hTERT in the mitochondria has also been associated with improved mitochondrial function, presumably due to reinforcement of cellular anti-oxidant systems following the initial period of cellular stress (Massard *et al.*, 2006). These contrasting effects may be drug and dose specific, but taken together, they highlight a role for hTERT as a toggle switch whereby the cellular balance can be tipped to favor either cell survival or cell death.

In the past, it has been generally accepted that G-quadruplex ligands interfere with telomerase functioning in the nucleus of cancer cells (Biffi *et al.*, 2013). Our recent data with a new G-quadruplex ligand anthracenyl isoxazole amide 1 (referred to hereon as AIM 1) demonstrated an alternate site of functioning as fluorescent microscopy consistently revealed AIM 1 localization to the mitochondria of human glioblastoma cells (described in Chapter 2). While performing studies investigating the mechanism of action of AIM 1, reports emerged regarding the role of two commercially available G-quadruplex ligands on the mitochondria of cells (Zhuang and Yao, 2013). These data were the first of its kind to show alternate activities for G-quadruplex ligands that include effects on the mitochondria and examine the functions of hTERT shuttling. Although our results are consistent with the findings from these experiments,

the advantage to our studies is the use of a novel G-quadruplex ligand created in conjunction with our laboratory, as well as the additional benefit of inherent fluorescence of compound AIM 1—both of which are lacking from the results published from this group. The results detailed in this study indicate AIM 1 is preferentially located in the mitochondria of cells, induces mitochondrial apoptosis and mitochondrial dysfunction, and leads to shuttling of hTERT out of the nucleus. These data provide essential insight into the specific mechanisms of action of small molecule G-quadruplex inhibitors.

MATERIALS AND METHODS

Chemicals. AIM 1 was obtained from the University of Montana (Missoula, MT). We are appreciative of the efforts Matthew J. Weaver and the Natale laboratory for contribution to the synthesis of the AIM compounds.

Cell Culture. SNB-19 human glioblastoma cells (American Type Cell Culture Cat No. CRL-2266) were grown in RPMI 1640 medium with L-glutamine and penicillin/streptomycin, supplemented with 10% fetal bovine serum (FBS). Cell culture medium and supplements were obtained from Invitrogen (Carlsbad, CA). The cells were incubated at 37 °C under a humidified atmosphere containing 5% CO₂ and allowed to achieve confluence prior to experimentation.

AIM Localization Studies. SNB-19 cells were plated on cover slips in 6-well plates at a density of 1×10^3 /well, allowed to adhere, and incubated overnight at 37°C in 5% CO₂ to achieve adherence. AIM solutions (1 μM) were added to cells and incubated overnight. After incubation, medium was aspirated, cells were washed twice with phosphate buffered saline (PBS) and fixed in 4% paraformaldehyde/PBS (on ice; 10 min). To determine mitochondrial co-localization

MitoTracker Red stain at a concentration of 250 nM (Invitrogen, Carlsbad, CA) was added directly to cells and incubated following manufacturer's directions. Following washes in PBS, cells were washed once with de-ionized water, and fluorescent images were taken with an Olympus FV1000 confocal laser scanning microscope using selective laser excitation at 405 nm. Images were processed with Nuance 1.6.2.368 alpha software (Cambridge Research Institute).

Mitochondrial Superoxide Determination. MitoSox Red selectively and rapidly targets the mitochondria of live cells and allows for the visualization of mitochondrial superoxide. SNB-19 cells were plated on sterile coverslips in 6-well culture dishes and treated with 1 μ M AIM 1 overnight and 5 μ M MitoSox Red (Invitrogen, Carlsbad, CA) for 10 min at 37 °C immediately prior to imaging, following manufacturer's directions for use. For this experiment, modifications to manufacturer's protocol included a fixation step immediately before analysis (4% paraformaldehyde for 10 minutes, RT). Hydrogen peroxide was used as a positive control. After exposure to MitoSox Red, samples were washed with PBS and inverted to microscope slides and sealed using FluorSave Reagent (Calbiochem, Billerica, MA, USA). Images and histograms were generated from scans from a CompuCyte iCys Laser Scanning Cytometer (CompuCyte, Westwood, MA).

Mitochondrial Membrane Potential Analysis. Mitochondrial membrane potential was determined using a JC-1 for flow cytometry kit (Invitrogen, Carlsbad, CA). JC-1 has advantages over other cationic dyes in that it can selectively enter into mitochondria and reversibly change color from red to green as the membrane potential decreases. For these experiments, manufacturer's protocol was followed and 2 μ M JC-1 was added to SNB-19 as described in the protocol. Samples with CCCP (m-chlorophenylhydrazine) served as a positive control. CCCP was included in the JC-1 for flow cytometry kit and causes rapid mitochondrial dysfunction and mitochondrial membrane depolarization. SNB-19 cells were treated with AIM 1 for a 24 h exposure period at concentrations of 1 μ M, 2.5 μ M, 5 μ M and fluorescent data from cells were acquired using a BD FACSAria flow cytometer and analyzed using BD FACSDiva 4.0 Software (BD Biosciences San Jose, CA).

FLICA Caspase-9 Detection. Green FLICA for Caspase 9 kit (ImmunoChemistry Technologies, Bloomington, MN) was used to probe for active caspase-9. FLICA assays allow for whole cell detection of caspase activity in apoptotic or caspase-positive cells. FLICA is advantageous because it is membrane-permeant and the dye forms covalent bonds with activated caspase

enzymes and is retained only in cells with active caspases. FLICA caspase probes are not retained in non-apoptotic cells following a simple wash process. For this experiment, SNB-19 cells were plated in 6 well tissue culture dishes and treated with AIM 1 for 24 h at doses of 1 μ M, 2.5 μ M, 5 μ M. After exposure, the staining protocol for adherent cells was followed for the FLICA kit. Propidium Iodide (PI) exclusion was also performed, as suggested by manufacturer. Hydrogen peroxide was used as a positive control to ensure kit accuracy and samples were acquired using BD FACSAria flow cytometer and analyzed using BD FACSDiva 4.0 Software.

hTERT Shuttling. To determine the effects of AIM exposure on hTERT shuttling out of the nucleus the methods of Wu, *et al.*, were followed with modifications. Briefly, fixed SNB-19 cells incubated with 1 μ M AIM 1 (16 h) were permeabilized with 0.1% Triton X, blocked with normal goat serum supplemented with PBS, bovine serum albumin (BSA), and sodium azide, and incubated with a 1:2000 dilution of rabbit anti-hTERT antibody (Rockland Immunochemicals, Gilbertsville, PA). Following several washes, AlexaFluor 594 anti-rabbit 2^o antibody (Invitrogen, Carlsbad, CA) diluted to 1:1000 was added for 1 h and samples were washed thoroughly. HCS NuclearMask Deep Red stain (Invitrogen, Carlsbad, CA) was added following manufacturer instructions to counterstain organelles. Untreated samples were also included in

this experiment to visualize baseline hTERT expression in SNB-19 cells. Samples were acquired with an Olympus FV1000 confocal laser scanning microscope at 60X objective. Images were additionally magnified for optimal visualization and processed with Nuance 1.6.2.368 alpha software (Cambridge Research Institute).

Statistics. All statistical analyses were performed using GraphPad Prism 4.0 for Macintosh (GraphPad Software, San Diego, CA). Student's *t*-test was used to compare untreated and treated samples. Values $p \leq 0.05$ were determined to be significant.

RESULTS

AIM 1 is localized in the mitochondria of SNB-19 human glioblastoma cells. We have shown previously using iCys Laser Scanning Cytometry that AIM 1 (Figure 3.1) appears to distribute outside of the nucleus, within the mitochondria of cells. To confirm our finding, we performed confocal imaging. Samples were counterstained using the dye MitoTracker Red to visualize the mitochondria (Figure 3.2). A time course evaluation was also performed to determine the staining profile of AIM 1 following short-term exposure (Figure 3.3A). SNB-19 cells treated only with MitoTracker Red are shown for comparison. (Figure 3.3B) This experiment revealed

AIM 1 staining profile consistent with all other microscopy and with our previous findings from Laser Scanning Cytometry (detailed in Chapter 2).

Figure 3.1

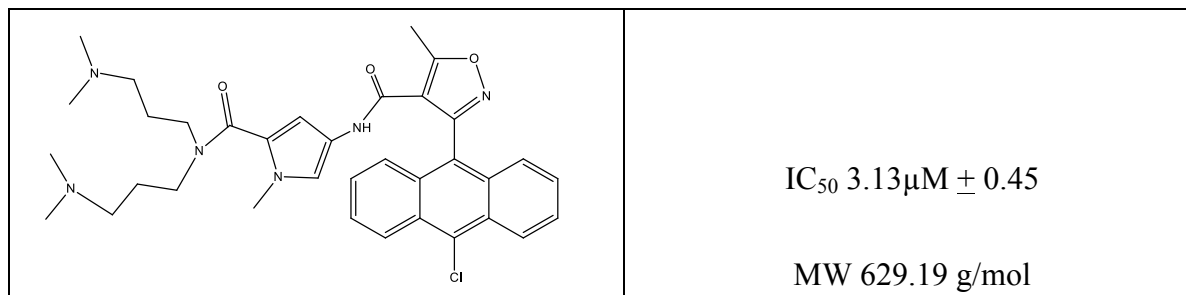


Figure 3.1. Structure and corresponding toxicity data of AIM 1 in SNB-19 human glioblastoma cells. AIM 1 is cytotoxic to SNB-19 cells at the single digit micromolar level.

Figure 3.2

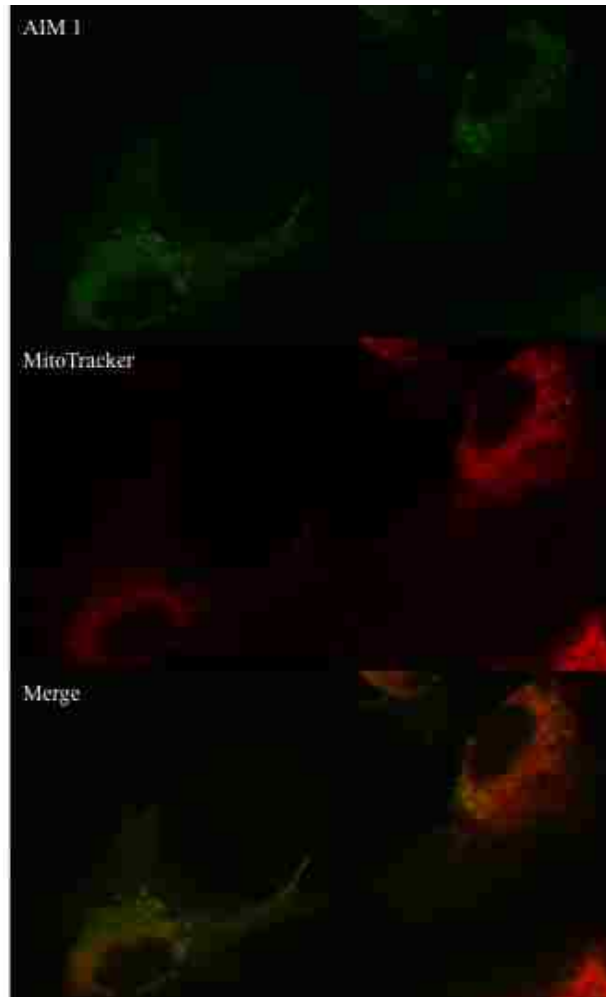
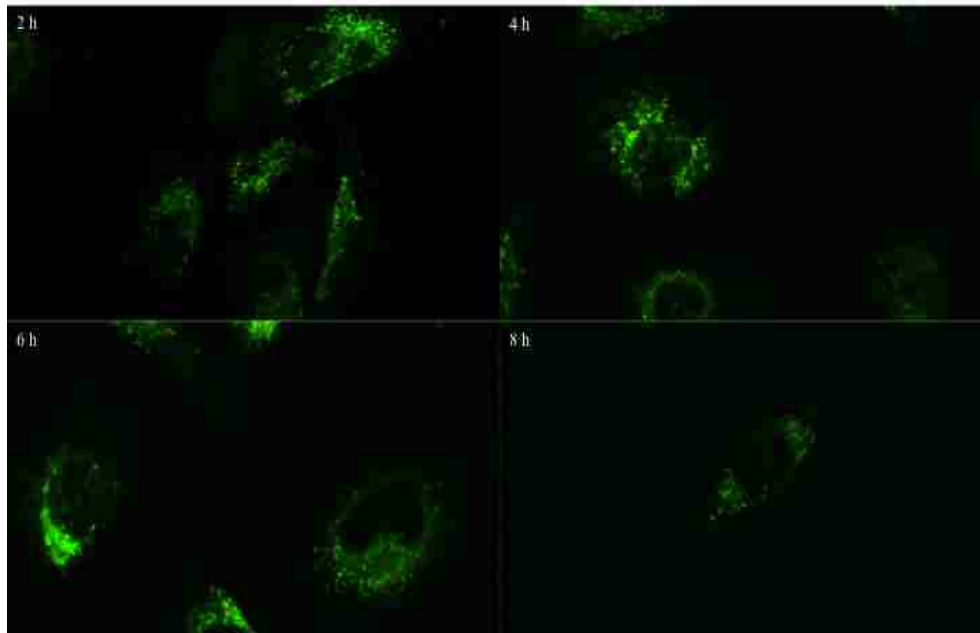


Figure 3.2. AIM 1 location within SNB-19 cells. Confocal microscopy (60X, additionally magnified images) allow for visualization of AIM 1 (top, shown in green) with the addition of MitoTracker Red mitochondrial indicator in SNB-19 cells (bottom, images overlaid). Center images indicate MitoTracker localization within the mitochondria of AIM 1 treated cells. Overlay images clearly show AIM within mitochondria of cells.

Figure 3.3

A.



B.

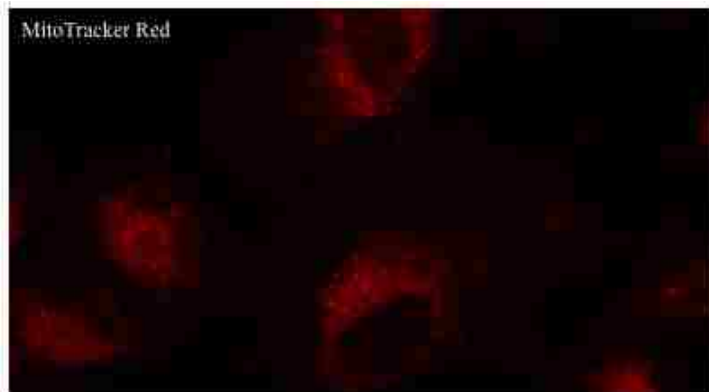


Figure 3.3. AIM 1 short-term exposure shows immediate localization to the mitochondria.

Confocal microscopy shows staining of AIM 1 (green) in SNB-19 cells at various time points.

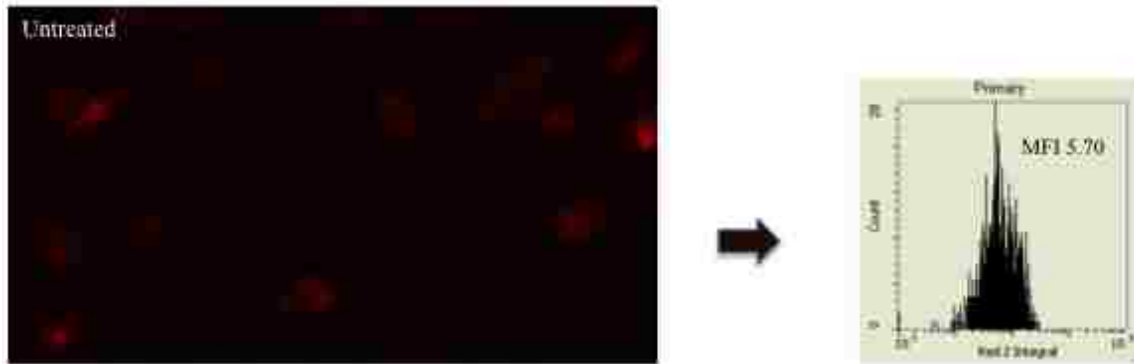
For comparison, MitoTracker Red stained untreated SNB-19 cells (red) were examined. Results

indicate AIM 1 is located in mitochondria at all exposures.

AIM 1 induces mitochondrial reactive oxygen species generation. Following results indicating that AIM 1 is preferentially located in the mitochondria of SNB-19 cells and that AIM 1 induces apoptosis, we hypothesized that AIM 1 was also causing mitochondrial dysfunction and stress. To test this theory, the mitochondrial superoxide indicator MitoSox Red was used. MitoSox Red will only be observed when mitochondrial ROS is present within the cell and will fluoresce brighter when there is a greater amount of superoxide. Results from these experiments demonstrated a visual and quantitative change in the amount of mitochondrial superoxide in samples treated with AIM 1 as compared to untreated groups (Figure 3.4). Histograms indicating the mean fluorescence intensity (MFI) of MitoSox Red in both untreated and AIM 1 treated groups are also shown. Fluorescence intensity is proportional to superoxide concentrations.

Figure 3.4

A.



B.

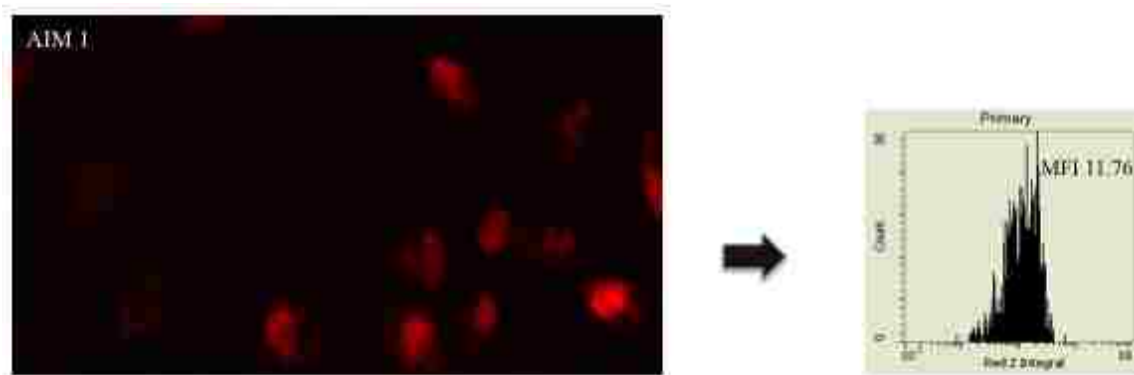


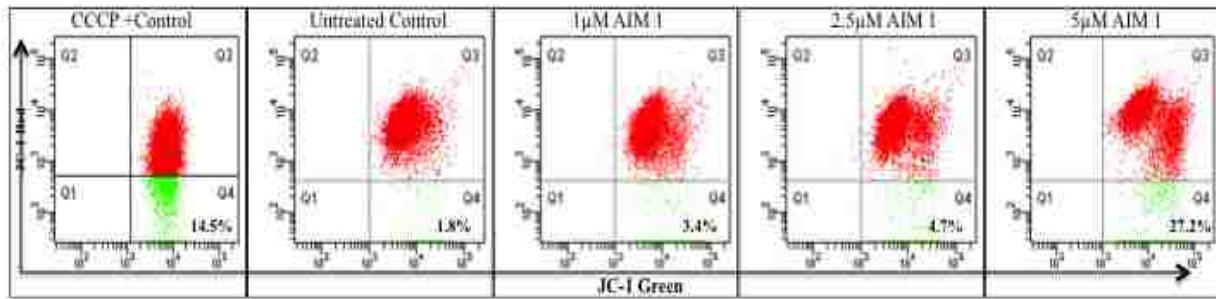
Figure 3.4. AIM 1 induces mitochondrial superoxide production. Laser Scanning Cytometry shows MitoSox Red staining (shown in red), an indicator of mitochondrial ROS. SNB-19 untreated samples (A) show positive MitoSox Red staining as expected of cancer cells, however, mean fluorescence intensity (MFI) values for this sample were determined to be less than half that of treated samples. SNB-19 cells treated with only 1 μ M of AIM 1 (B) show much brighter

MitoSox Red fluorescence. This is also reflected in a MFI for MitoSox Red that was two-fold higher than untreated samples.

AIM 1 exposure results in a reduction in mitochondrial membrane potential. Following results from mitochondrial superoxide analysis, we sought to examine in more detail AIM 1 induced effects on the mitochondria. Apoptosis and ROS experiments led us to speculate that AIM 1 exposure to SNB-19 cells was disrupting the mitochondrial membrane potential leading to the excessive ROS accumulation observed in MitoSox Red mitochondrial superoxide experiments. To evaluate this hypotheses, experiments to assess the mitochondrial membrane potential using JC-1 staining for flow cytometry were performed. As shown in Figure 3.5 (A and B), results indicate a significant reduction in the mitochondrial membrane potential following a 24 h exposure to 5 μ M AIM 1. A dose dependent trend towards mitochondrial membrane depolarization above untreated control at each increasing dose of 1 μ M, 2.5 μ M, 5 μ M of AIM 1 was also observed. Additionally, it should be noted that exposure to the highest dose of AIM 1 produced mitochondrial depolarizing effects that were even greater than the positive control using the protonophore m-chlorophenylhydrazine, CCCP.

Figure 3.5

A.



B.

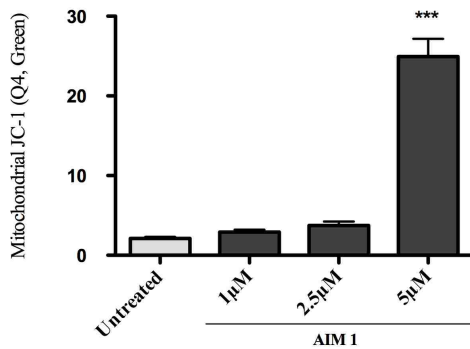


Figure 3.5. Assessment of mitochondrial dysfunction. Flow cytometry was performed using JC-1 staining to highlight the effects of AIM 1 on mitochondrial membrane potential (A). Green fluorescence indicates mitochondrial membrane depolarization. Statistical analysis demonstrated a dose dependent trend in mitochondrial membrane depolarization with increasing doses of AIM 1 (B). ***indicates significance of $p \leq 0.0001$.

AIM 1 exposure results in activation of caspase-9. Following AIM 1 exposure, mitochondrial dysfunction observed in JC-1 experiments was speculated to coincide with activation of caspases—specifically caspases-9, which is responsible for mitochondrial-mediated apoptosis. Flow cytometry was performed to assess induction of apoptosis and caspases-9 activation by application of FLICA. As demonstrated in Figure 3.6, SNB-19 cells exposed to 5 μ M AIM 1 for 24 h resulted in a statistically significant increase in induction of activated caspase as compared to untreated control. It is of importance to note also that these results are consistent with previous Annexin V apoptosis analysis that showed similar values for each stage of apoptosis (Chapter 2).

Figure 3.6

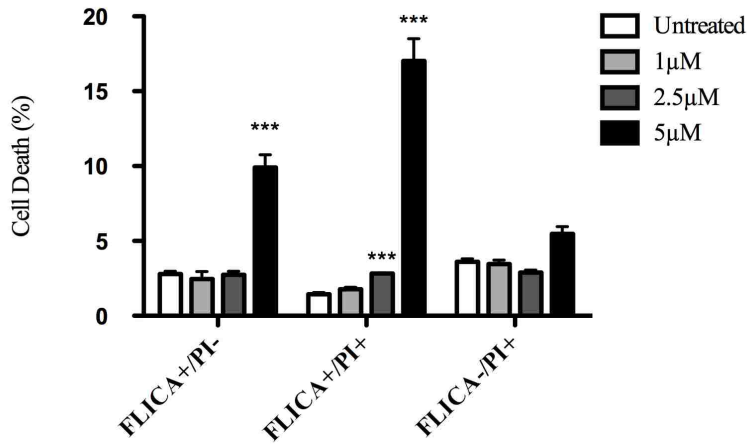


Figure 3.6. AIM 1 exposure leads to activated caspase-9. FLICA binding indicates an induction of activated caspase 9 following exposure to AIM 1. FLICA⁺ groups indicate positive staining for active caspases-9. PI exclusion was used to identify the various stages of apoptosis coinciding with caspases-9 activation: early (FLICA⁺/PI⁻), late (FLICA⁺/PI⁺) and necrotic (FLICA⁻/PI⁺). ***indicates significance of $p \leq 0.0001$.

hTERT shuttles out of the nucleus following AIM 1 exposure. We tested whether overnight treatment (16 h) at 1 μ M AIM 1 was a sufficient exposure period to cause hTERT shuttling from the nucleus to the mitochondria. For these experiments, we treated SNB-19 cells with the nuclear indicator HCS Nuclear Mask to visualize the nucleus, shown in Figure 3.7. As expected, in untreated cells, hTERT is primarily nuclear. However, following exposure to AIM 1, it is clear that hTERT moves out of the nucleus (Figure 3.8). Once again, in these images we are also able to visualize AIM 1 cellular location. Although it is clear that hTERT has shuttled out of the nucleus upon AIM 1 treatment, we are unable to determine if the location following exposure is mitochondrial or cytoplasmic. However, both extra-nuclear cellular locations have been observed in the literature following cellular stress (Chung *et al.*, 2012; Zhuang and Yao, 2013).

Figure 3.7

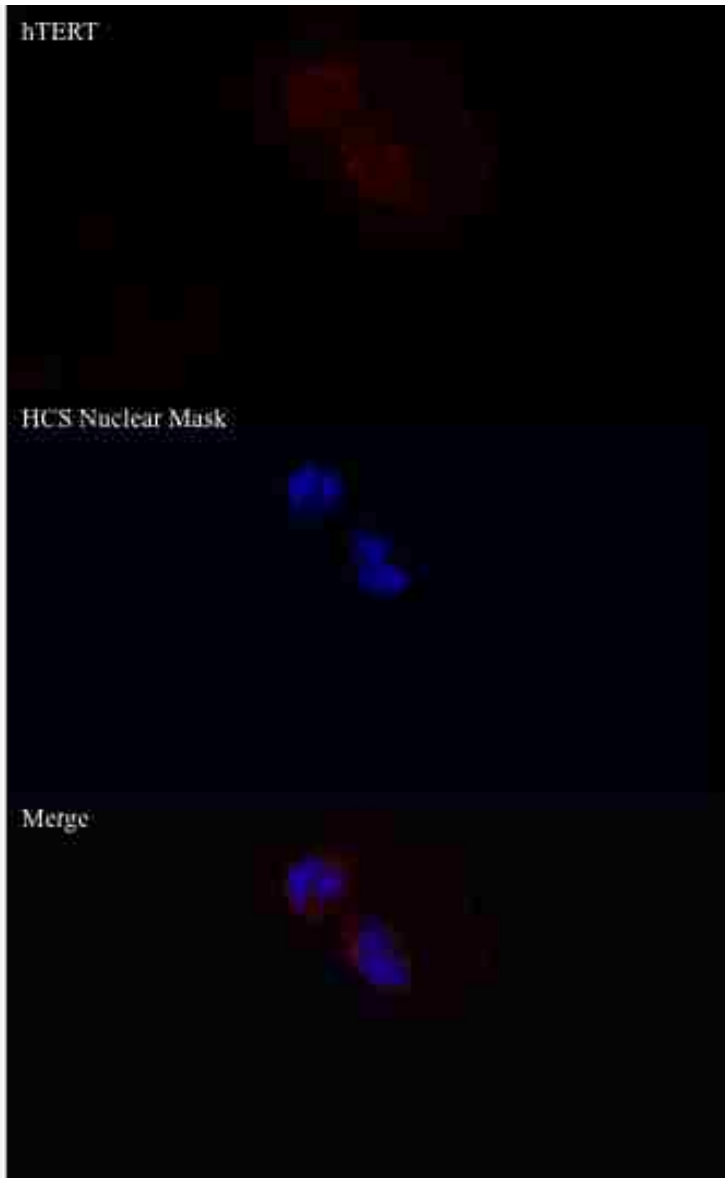


Figure 3.7. hTERT staining in untreated cells. Confocal microscopy (60X, magnified) shows untreated SNB-19 cells with hTERT (red). Nuclear counterstaining is highlighted in blue. Overlaid images are also indicated.

Figure 3.8

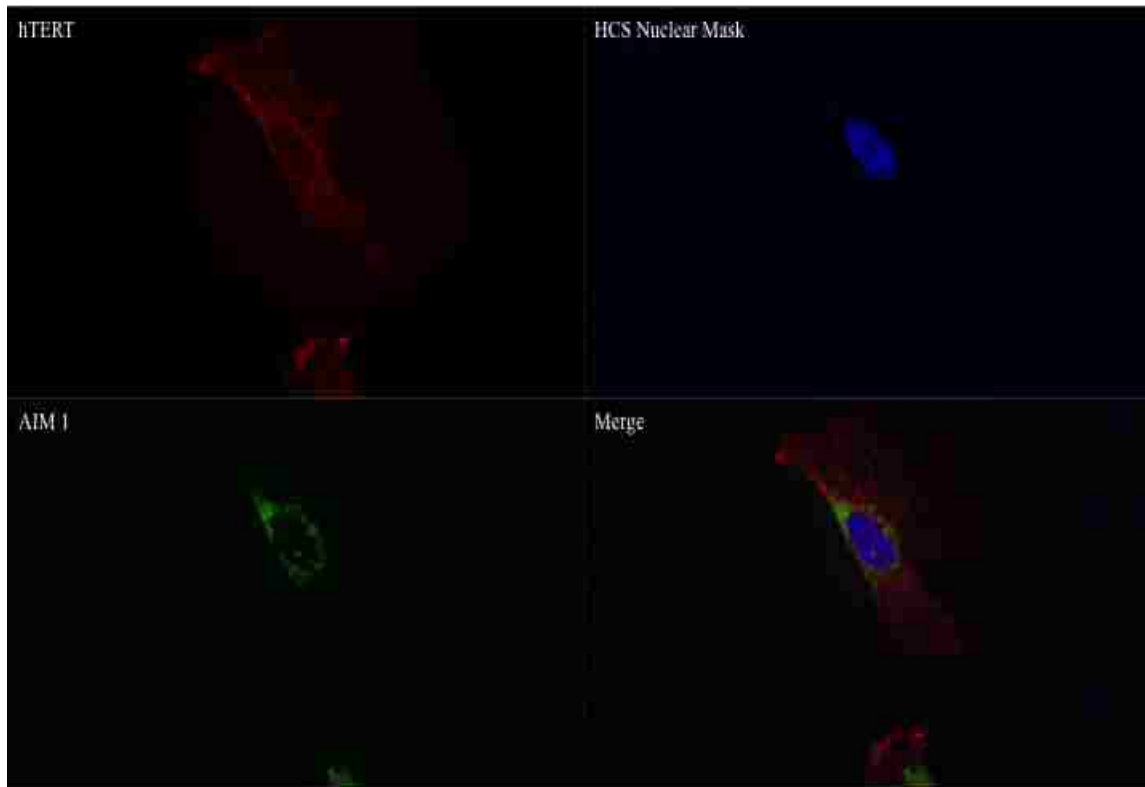


Figure 3.8. Shuttling of hTERT following AIM 1 treatment. Confocal images (60X, magnified) show hTERT (red), AIM 1 (green) and nuclear counterstain (blue). Each frame is shown independently with overlaid images indicated (merge).

DISCUSSION

Conventional chemotherapy for advanced malignant tumors is many times ineffective and there remains a need for new drugs that specifically target cancers and possess minimal toxicity to other tissues in the body. G-quadruplex ligands are promising anticancer agents that have potential to enhance current therapies and improve patient outcomes. We have examined here some of the characteristics of the apoptotic pathway induced by AIM 1 and conclude that the AIM 1 G-quadruplex ligand exerts effects beyond what was traditionally believed to be limited to telomere specific roles within the nucleus of cells. Indeed, studies are beginning to investigate the detailed mechanisms of toxicity of G-quadruplex ligands and evidence is emerging that the effects of stabilizing G-quadruplex structures are much more complex than originally thought (Tatuchi *et al.*, 2003; Doure *et al.*, 2005; Li *et al.*, 2004; Zhuang and Yao 2013).

The traditional approach to studying potential G-quadruplex ligands included experimental design that, once G-quadruplex interaction was confirmed, focused on basic toxicity testing and general apoptotic analysis. It is only recently becoming more common to include detailed microscopy highlighting the cellular localization of G-quadruplex ligands, as demonstrated by the comprehensive article in *Nature Chemistry*, which includes not only

visualization using fluorescent microscopy, but quantification of their G-quadruplex ligand within chromosomes as well (Biffi *et al.*, 2013). In this regard, our research is a vital component in the progression of G-quadruplex study and moreover, the use of AIM 1 that already possesses inherent fluorescent properties, is incredibly advantageous to detailed microscopy experimentation.

To ensure that the localization of AIM 1 was indeed a true event and not an artifact of a downstream site of action, a time course experiment was performed that demonstrated AIM 1 in the same cellular location during all short time periods of exposure. A mitochondrial counterstain was not included in these AIM 1-treated SNB-19 cells to rule out the possibility that the localization of AIM 1 to the mitochondria was being induced or being caused by the addition of a marker. To this end, untreated SNB-19 cells stained with a mitochondrial dye MitoTracker dye was included as a separate experiment to highlight the similar staining profiles between MitoTracker Red and AIM 1. What is clear is that the staining profile of AIM 1 is identical to all other experiments, including those performed with the additional MitoTracker dye in AIM 1-treated cells. These conclusive results support the analysis that AIM 1 is binding somewhere within the mitochondria, immediately following exposure.

At this time, the effects of hTERT shuttling from the nucleus are unknown. Based on

fluorescence staining of hTERT following AIM 1 exposure, it appears as though hTERT has moved out of the nucleus, as evidenced by the lack of red fluorescence in the nuclear region. Additionally, the exterior outline of untreated cells is visible in confocal microscopy (likely due to nonspecific staining) and highlights the stark contrast between the nuclear concentrated hTERT in untreated cells versus the very obvious increase in both hTERT fluorescence and location in AIM 1 exposed cells out of the nucleus. Due to fluorescence overlap and constraints relating to the available dyes, we were unable to confirm hTERT localization to the mitochondria and cytoplasm with counterstains. It has been reported that hTERT contains a mitochondrial targeting signal (MTS) and that hTERT import to the mitochondrial matrix is driven by changes in the mitochondrial membrane potential (Sharma *et al.*, 2012). It is plausible that following AIM 1 binding to G-quadruplex and the subsequent mitochondrial membrane depolarization reported in this study, hTERT shuttling out of the nucleus observed in confocal microscopy experiments is a consequence of intracellular stress. hTERT shuttling to the mitochondria is also speculated to occur to protect the mitochondria from DNA damage and apoptosis (Haendeler *et al.*, 2009). Apoptosis and caspase activation are occurring in AIM 1 treated SNB-19 cells, which can explain extra-nuclear hTERT shuttling as an effect of cellular damaged caused by AIM 1.

While the mitochondrial effects of AIM 1 are detailed in this study, what still remains

under investigation is the actual binding site of AIM 1 within the mitochondria. Initial NMR experiments showed an interaction with AIM 1 and a commercially available telomeric G-quadruplex sequence (detailed in Chapter 2), but research suggests that G-quadruplex ligands do have some promiscuity for G-rich sequences in general, for which there are many. AIM 1 is not located within the nucleus, where telomeres are located; this suggests that AIM 1 is binding to a similar guanine-rich sequence and G-quadruplex structure in another cellular organelle. Currently, the data on G-quadruplex formation within mitochondrial DNA is not definitive, however, several groups suggest the presence of G-quadruplex structures within the mitochondria (Wanrooij *et al.*, 2012; Capra *et al.*, 2010; Ngo *et al.*, 2013). If AIM 1 is binding to G-quadruplex in mitochondrial DNA, this may also explain the hTERT shuttling effects. Both mitochondrial DNA and mitochondrial hTERT are located within the mitochondrial matrix; the very presence of AIM 1 in the matrix could be enough to induce the export of hTERT out of the nucleus. Based on the fact that AIM 1 was designed as a G-quadruplex ligand, shows specificity for G-quadruplex structures (as demonstrated by NMR), the effects are not associated with any other known mechanism as detailed by COMPARE analysis (Han *et al.*, 2009), and is localized in the mitochondria associated with the mitochondrial effects detailed in this study, we believe the likely binding of AIM 1 is to G-quadruplex within mitochondrial DNA. However, since this

is not definitive at this time, further investigation into the sub-mitochondrial location of AIM 1 needs to be performed to determine if binding occurs in the mitochondrial matrix, where mitochondrial DNA is located, or somewhere along the membrane. Furthermore, it would be relevant to examine mitochondrial DNA following AIM 1 treatment in SNB-19 cells to determine the effects of exposure.

Collectively, results of this study support an intriguing and alternate mechanism of action for the function of G-quadruplex ligands. Fluorescent microscopy and flow cytometric analyses support our hypothesis that AIM 1 acts as a mitochondrial modulator in addition to its role as a G-quadruplex stabilizer. Additionally, our data definitively demonstrating the mitochondrial location of AIM 1, combined with our NMR results indicating the G-quadruplex interaction potential of AIM 1, is supportive of the theory that G-quadruplex structures do exist within the mitochondria. Future work carefully examining the effects of AIM 1 on structures within the mitochondria as well as the mitochondrial DNA will be an exciting and necessary addition to the field of G-quadruplex.

REFERENCES

- Ahmed, S., Passos, J. F., Birket, M. J., Beckmann, T., Brings, S., Peters, H., Birch-Machin, M. A., von Zglinicki, T., and Saretzki, G. (2008). Telomerase does not counteract telomere shortening but protects mitochondrial function under oxidative stress. *J Cell Sci* **121**, 1046-1053.
- Akiyama, M., Hideshima, T., Hayashi, T., Tai, Y. T., Mitsiades, C. S., Mitsiades, N., Chauhan, D., Richardson, P., Munshi, N. C., and Anderson, K. C. (2003). Nuclear factor-kappaB p65 mediates tumor necrosis factor alpha-induced nuclear translocation of telomerase reverse transcriptase protein. *Cancer Res* **63**, 18-21.
- Biffi, G., Tannahill, D., McCafferty, J., and Balasubramanian, S. (2013). Quantitative visualization of DNA G-quadruplex structures in human cells. *Nat Chem* **5**, 182-186.
- Brown, G. C., Nicholls, D. G., and Cooper, C. E. (1999). Mitochondria and cell death. Princeton University Press, Princeton, NJ. Vii-viii.
- Burge, S., Parkinson, G. N., Hazel, P., Todd, A. K., and Neidle, S. (2006). Quadruplex DNA: sequence, topology and structure. *Nucleic Acids Res* **34**, 5402-5415.
- Capra, J. A., Paeschke, K., Singh, M., and Zakian, V. A. (2010). G-quadruplex DNA sequences are evolutionarily conserved and associated with distinct genomic features in *Saccharomyces cerevisiae*. *PLOS Comput Biol* **6**, 1-13.
- Chung, J., Khadka, P., and Chung, I. K. (2012). Nuclear import of hTERT requires a bipartite nuclear localization signal and Akt-mediated phosphorylation. *J Cell Sci* **25**, 2684-2697.
- Cong, Y. S., Wright, W. E., and Shay, J. W. (2002). Human telomerase and its regulation. *Microbiol Mol Biol Rev* **66**, 407-425.
- Cong, Y., and Shay, J. W. (2008). Actions of human telomerase beyond telomeres. *Cell Res* **18**, 725-732.
- Douarre, C., Gomez, D., Morjani, H., Zahm, J-M., O'Donohue, M-F., Eddabra, L., Mailliet, P., Riou, J-F., and Trentesaux, C. (2005). Overexpression of Bcl-2 is associated with apoptotic resistance to the G-quadruplex ligand 12459 but is not sufficient to confer resistance to long-term senescence. *Nucleic Acids Res* **33**, 2192-2203.
- Fulda, S., Galluzzi, L., and Kroemer, G. (2010). Targeting mitochondria for cancer therapy. *Nat Rev Drug Disc* **9**, 447-464.
- Gogvadze, V., Orrenius, S., and Zhivotovsky, B. (2008). Mitochondria in cancer cells, what is so special about them? *Trends Cell Biol* **18**, 165-173.
- Haendeler, J., Drose, S., Buchner, N., Jakob, S., Altschmied, J., Goy, C., Spyridopoulos,

- I., Zeiher, A. M., Brundt, U., and Dimmeler, S. (2009). Mitochondrial telomerase reverse transcriptase binds to and protects mitochondrial DNA and function from damage. *Arterioscler Thromb Vasc Biol* **6**, 929-935.
- Han, X., Li, C. L., Mosher, M. D., Rider, K. C., Zhou, P., Crawford, R. L., Fusco, W., Paszczynski, A., and Natale, N. R. (2009). Design, synthesis and biological evaluation of a novel class of anticancer agents: Anthracenylisoxazole lexitropsin conjugates. *Bioorg Med Chem* **17**, 1671-1680.
- Indran, I. R., Hande, M. P., and Pervaiz, S. (2010). Tumor cell redox state and mitochondria at the center of the non-canonical activity of telomerase reverse transcriptase. *Mol Aspects Med* **31**, 21-28.
- Li, C-P., Huang, J-H., Chang, A-C., Hung, Y-M., Lin, C-H., Chao, Y., Lee, S-D., Whang-Peng, J., and Huang, T-S. (2004). A G-quadruplex ligand 3,3'-diethyloxadicyanone iodide induces mitochondrion-mediated apoptosis but not decrease of telomerase activity in nasopharyngeal carcinoma NPC-TW01 cells. *Pharm Res* **21**, 94-100.
- Massard, C., Zermati, Y., Pauleau, A. L., Larochette, N., Metivier, D., Sabatier, L., Kroemer, G., Soria, J. C. (2006). HTERT: a novel endogenous inhibitor of the mitochondrial cell death pathway. *Oncogene* **25**, 4505-4515.
- Modica-Napolitano, J. S. and Singh, K. K. (2004). Mitochondrial dysfunction in cancer. *Mitochondrion* **4**, 755-762.
- Neidle, S., and Parkinson, G. (2002). Telomere maintenance as a target for anticancer drug discovery. *Nat Rev Drug Disc* **1**, 383-393.
- Ngo, J. K., Pomatto, L. C. D., and Davies, K. J. A. (2013). Upregulation of the mitochondrial Lon protease allows adaptation to acute oxidative stress but dysregulation is associated with stress, disease, and aging. *Redox Biol* **1**, 258-264.
- Passos, J. F., von Zglinicki, T., and Saretzki, G. (2006). Activity, function, and gene regulation of the catalytic subunit of telomerase (hTERT). *Gene* **269**, 1-12.
- Poole, J. C., Andrews, L. G., and Tollefsbol, T. O. (2001). Activity, function, and gene regulation of the catalytic subunit of telomerase (hTERT). *Gene* **269**, 1-12.
- Santos, J. H., Meyer, J. N., and Van Houten, B. (2006). Mitochondrial localization of telomerase as a determinant for hydrogen peroxide-induced mitochondrial DNA damage and apoptosis. *Hum Mol Genet* **15**, 1757-1768.
- Sharma, N. K., Reyes, A., Green, P., Caron, M. J., Bonini, M. G., Gordon, D. M., Holt, I. J., and Santos, J. H. (2012). Human telomerase acts as a hTR-independent reverse transcriptase in mitochondria. *Nucleic Acids Res* **2**, 712-724.

- Shay, J. W., and Bacchetti, S. (1997). A survey of telomerase activity in human cancer. *Eur J Cancer* **33**, 787-791.
- Tatuchi, T., Shin-ya, K., Sashida, G., Sumi, M., Nakajima, A., Shimamoto, T., Ohyashiki, J. H., Ohyashiki, K. (2003). Activity of novel G-quadruplex-interactive telomerase inhibitor, telomestatin (SOT-095), against human leukemia cells: involvement of ATM-dependent DNA damage response pathways. *Oncogene* **22**, 5338-5347.
- Wallace, K. B. and Starkov, A. A. (2000). Mitochondrial targets of drug toxicity. *Annu Rev Pharmacol Toxicol* **40**, 353-388.
- Wanrooij, P. H., Uhler, J. P., Westerlund, F., Falkenberg, M., and Gustaffson, C. M.(2012). A hybrid G-quadruplex structure formed between RNA and DNA explains the extraordinary stability of the mitochondrial R-loop. *Nucleic Acids Res* **20**, 10334-10344.
- Weissig, V., Cheng, S-M., and D'Souza, G. G. M. (2004). Mitochondrial pharmaceuticals. *Mitochondrion* **3**, 229-244.
- Wu, Y-L., Dudogon, C., Nguyen, E., Hillion, J., Pendino, F., Tarkanyi, I., Aradi, J., Lanotte, M., Tong, J-H., Chen, G-Q., and Segal-Bendirdjian, E. (2006). Immunodetection of human telomerase reverse-transcriptase (hTERT) re-appraised: nucleolin and telomerase cross paths. *J Cell Sci* **13**, 2797-2806.
- Zhuang, X-Y., and Yao, Y-G. (2013). Mitochondrial dysfunction and nuclear-mitochondrial shuttling of TERT are involved in cell proliferation arrest by G-quadruplex ligands. *FEBS Lett* **11**, 1656-1662.

CHAPTER 4

A novel series of 4-isoxazolyl-1,4-dihydropyridines (IDHPs) P-gp inhibitors enhance the cytotoxicity of anthracenyl isoxazole amide (AIM) antitumor compounds when co-dosed together *in vitro*

Authors

Alison K. Kearns and Howard D. Beall

Corresponding Author

Dr. Howard D. Beall

Address: University of Montana

Department of Biomedical and Pharmaceutical Sciences

32 Campus Drive, Skaggs

Missoula, MT 59812

Telephone: 406-243-5112

Fax: 406-243-2807

Email: Howard.Beall@umontana.edu

ABSTRACT

The P-glycoprotein efflux pump is a major contributor to the failure of many anticancer agents that are substrates for the transporter. P-gp overexpression is also an important mechanism that is responsible for the multidrug resistance phenotype observed in many different types of cancers, including brain cancer. To this end, the development of inhibitors that function to block the efflux of anticancer agents out of the brain and promote their entry into target tissues is an important area of research. The purpose of this study is to evaluate the effects of a newly synthesized series of 4-isoxazoly-1,4-dihydropyridines (IDHPs) that function as P-gp inhibitors and enhance the cytotoxicity of anthracenyl isoxazole amide (AIM) antitumor compounds when co-dosed together *in vitro*. 12 IDHPs were evaluated for their inhibition of P-gp. Two of these IDHPs 1A and 1K produced substantial P-gp inhibition and were selected for further investigation into their ability to increase the cytotoxicity of both known and novel anticancer agents. For the purposes of this study, a new modified MTT assay was developed to determine the change in cytotoxicity to P-gp expressing MDCK-MDR1⁺ cells and non-P-gp expressing MDCK-MDR1⁻ cells before and after IDHP exposure. Results of this study indicate that some IDHPs compounds in our series produce substantial P-gp inhibition and can be used *in vitro* to increase the cytotoxicity of a new series of AIM antitumor agents.

INTRODUCTION

Brain cancer, and more specifically glioblastoma, is a devastating and fatal disease and despite extensive research, patient prognosis is overwhelmingly poor and treatment remains largely ineffective. One of the major challenges in the treatment of brain cancer is the development and delivery of effective anticancer agents that are capable of reaching their target within tumor cells of the brain and central nervous system (CNS). The first obstacle that needs to be overcome is gaining access to tumor cells in the brain by bypassing the blood-brain barrier (BBB). The BBB is comprised of endothelial cells that are joined together to form tight junctions; they create a physical barrier that separates the blood from the brain and protects the brain from toxins and exposure to other harmful chemicals (Hawkins and Davis, 2005). In regard to brain tumors, this barrier also limits entry of drugs and prevents these therapeutic agents from reaching the brain, drastically decreasing the effectiveness of these anticancer agents. Additionally, cells of the BBB also contain efflux transporters that further limit the entry of xenobiotics, environmental contaminants and anticancer therapeutic agents into the brain (Pardridge, 1999). One particular transporter, P-glycoprotein (P-gp, also commonly known as MDR1 and ABCB1), is highly expressed at the level of the BBB and has been widely studied as a contributing factor to multidrug resistance. Drug resistance attributed to P-gp limits the

effectiveness of many clinical anticancer agents, including taxanes, etoposide, anthracyclines, vinca-alkaloids, and topotecan (Tsuji, 1998). Because so many anticancer agents are substrates for P-gp and because P-gp so effectively exports these drugs before they can reach tumor cells in the brain, developing P-gp inhibitors to be used clinically to block this transporter is an important area of research.

The first P-gp inhibitor studied was verapamil—a calcium channel blocker used to treat hypertension that was found to also possess P-gp inhibition properties (Tsuruo *et al.*, 1981). Since this discovery, many P-gp inhibitors have been developed and tested; however, aside from their ability to block the efflux functions of P-gp, few of these drugs have been examined for their ability to enhance drug delivery to the brain when dosed together with conventional chemotherapies (Avendano and Menendez, 2002; Pleban and Ecker, 2005; Agarwal *et al.*, 2011). To this end, we have developed a series of 4-isoxazolyl-1,4-dihydropyridines (IDHPs) that function as P-gp inhibitors and enhance the cytotoxicity of a select anthracenyl isoxazole amide (AIM) antitumor compound when co-dosed together *in vitro*. The series of IDHPs were synthesized after the discovery that many 4-aryl-1,4-dihydropyridines (DHPs) that bind the L-type voltage gated calcium channel are also P-gp inhibitors (Yusa and Tsuruo, 1989; Vilpo *et al.*, 2000; Boer *et al.*, 1994; Zhou *et al.*, 2005a). While the IDHPs do exhibit calcium channel

binding, we found that replacement of the 4-aryl substituent with an isoxazole in this series of IDHPs resulted in good selectivity for P-gp beyond the selectivity for calcium channels that traditional DHPs exhibit (Hulubei *et al.*, 2012). In this regard, our most active P-gp inhibitor (1K) contains a branched aryl group that is likely the structural feature leading to preferential binding to P-gp instead of adopting a conformation that would overwhelmingly favor calcium channel binding (Hulubei *et al.*, 2012).

In this study, a series of IDHPs were examined to determine their ability to inhibit P-gp. Several parameters were assessed including IDHP cytotoxicity to P-gp expressing and non-P-gp expressing cells as well as to a SNB-19 human glioblastoma cell line. Once P-gp inhibition was determined, lead IDHPs were selected for further investigation into their ability to enhance the cytotoxicity of AIMs when the two agents were dosed together *in vitro*. The results of this study suggest that IDHPs produce potent P-gp inhibition and are minimally cytotoxic. In addition, IDHPs have the potential to be useful drugs to administer with anticancer therapies to increase the overall cytotoxicity and aid in the ability of these chemotherapeutic agents to better reach their targets within the brain.

MATERIALS AND METHODS

Chemicals. IDHPs and AIM 1 were obtained from the University of Montana (Missoula, MT). IDHP and AIM 1 synthesis was performed by the Natale laboratory at the University of Montana. We are appreciative of the efforts of Scott A. Steiger and Matthew J. Weaver for their respective contributions to the synthesis of the IDHPs and AIM compounds.

MDCK Cell Culture. MDR1 transfected MDCK MDR1⁺ (P-gp expressing) and parent MDCK MDR1⁻ (non P-gp expressing) canine kidney epithelial cells were obtained from the National Cancer Institute (Bethesda, MD). Cells were grown in Dulbecco's Modified Eagle's Medium (DMEM) supplemented with 10% fetal bovine serum (FBS), glucose, L-glutamine, sodium pyruvate and penicillin/streptomycin (VWR International). MDCK MDR1⁺ cells were additionally supplemented with 80 µg/mL colchicine to maintain integrity of the cell line. Cells were grown to confluence prior to inhibition assays and maintained at 37 °C under a humidified atmosphere containing 5% CO₂.

SNB-19 Cell Culture. SNB-19 human glioblastoma cells (American Type Cell Culture Cat No. CRL-2266) were grown in RPMI 1640 medium with L-glutamine and penicillin/streptomycin,

supplemented with 10% fetal bovine serum (FBS). Cell culture medium and supplements were obtained from Invitrogen (Carlsbad, CA). The cells were incubated at 37 °C under a humidified atmosphere containing 5% CO₂ and allowed to achieve confluence prior to experimentation.

Cell Viability Assay. Cell survival was measured by the [3-(4,5-dimethylthiazol-2-yl)-2,5-diphenyltetrazolium bromide (MTT) colorimetric assay. MTT was obtained from Sigma-Aldrich (St. Louis, MO). As previously described, cells were plated in 96-well plates at a density of 10,000 cells/mL and allowed to attach overnight (16 h). P-gp inhibitor or substrate solutions were applied in medium for 24 h, removed, and replaced with fresh medium, and the plates were incubated at 37°C under a humidified atmosphere containing 5% CO₂ for 2–4 days. MTT (50 µg) was added and the cells were incubated for another 4 h. Medium/MTT solutions were removed carefully by aspiration, the MTT formazan crystals were dissolved in 100 µL of DMSO, and absorbance was recorded on a spectrophotometer at 560 nm. IC₅₀ values (concentration at which cell survival equals 50% of control) were determined from semilog plots of percent of control versus concentration. Average IC₅₀ values are reported from triplicate results.

Cytotoxicity Following P-gp Inhibition Assay. MDCK MDR1⁺ cells were plated at a density of 10,000 cells/mL in 96 well plates and allowed to adhere overnight (16 h). As previously mentioned, colchicine was added to the MDCK-MDR1⁺ medium immediately before cells were plated. On the day of IDHP treatment, medium was aspirated from plates and replaced with medium containing 10-50 μ M IDHP for a 1-h initial exposure. Following IDHP pre-treatment, AIM solutions containing IDHPs (to reach the desired final concentration of IDHP) were applied in medium for 24 h. Medium was then aspirated and fresh medium was applied and plates were incubated at 37 °C under a humidified atmosphere containing 5% CO₂ for 24-48 hours. MTT (50 μ g) was added and the cells were incubated for another 4 h. Medium/MTT solutions were removed carefully by aspiration, the MTT formazan crystals were dissolved in 100 μ L DMSO, and absorbance was determined on a plate reader at 560 nm. IC₅₀ values (concentration at which cell survival equals 50% of control) were determined from semi-log plots of percent of control vs. concentration. Data were analyzed as changes in AIMs IC₅₀ before and after IDHP exposure in MDCK-MDR1⁻ vs. MDCK-MDR1⁺ cells to determine the effect of IDHP pre-treatment on AIMs selective toxicity to MDCK-MDR1⁺ cells.

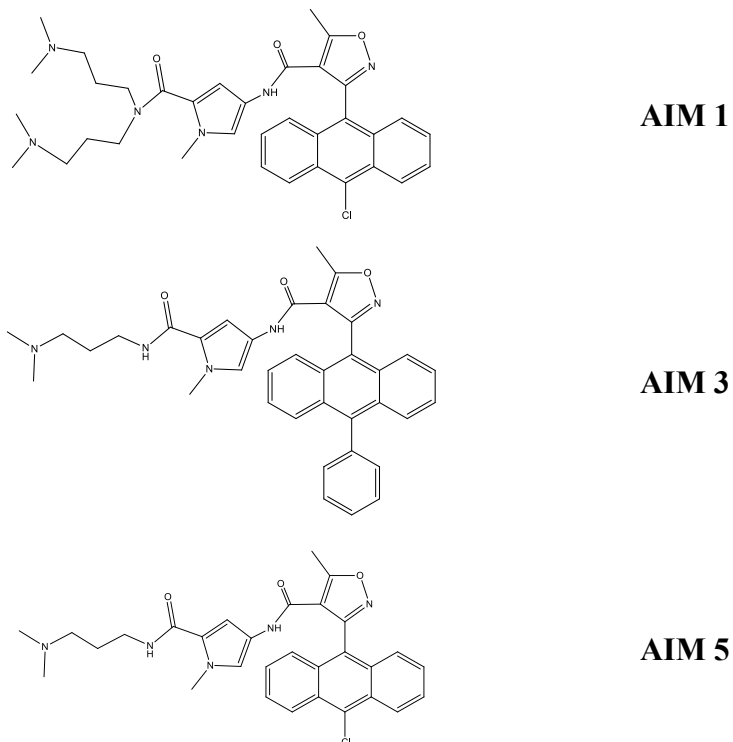
Statistics. All statistical analyses were performed using GraphPad Prism 4.0 for Macintosh (GraphPad Software, San Diego, CA). Student's *t*-test was used to compare change in IC₅₀ values of each compound in MDCK-MDR1⁻ vs MDCK-MDR1⁺ cell lines. ANOVA with *post hoc* Bonferroni test was used to compare effect of IDHP exposure on antitumor compound cytotoxicity across all groups. IC₅₀ values were expressed as the mean +/- standard deviation (SD). Values $p \leq 0.05$ were determined to be significant.

RESULTS

AIM 1 is less cytotoxic to high P-gp expressing ADR-RES cell line compared to cell lines not expressing significant P-gp. Results from NCI-DTP 60 cell line screen (NCI data courtesy of Dr. Nicholas Natale, University of Montana) demonstrate AIM 1 was approximately 7-fold more toxic in non-resistant cell lines tested (Figure 4.1). Compared to double tailed AIMS, there was no difference in growth inhibition across all cell lines tested as compared to the ADR-RES (adriamycin-resistant) cell line for single tail AIMS (AIM 3 and AIM 5). Other double tail and single tail AIMS were examined and results were consistent with double tail AIMS showing substantial toxicity to cell lines that were not resistant compared to the ADR-RES cell line (data not shown). Data from NCI-DTP 60 cell line screen suggest double tail AIMS, including AIM 1,

are substrates for P-gp and are effluxed out of cells, resulting in the minimal cytotoxicity observed in ADR-RES cells compared to other cell lines tested.

Figure 4.1



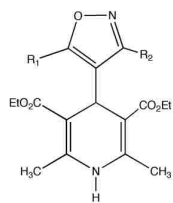
AIM	Mean GI ₅₀ (μM)	ADR-RES GI ₅₀ (μM)
1	2.0	14
3	1.4	1.6
5	1.8	1.9

Figure 4.1. Double tail AIMS are less cytotoxic in ADR-RES cell line. NCI-DTP 60 cell line screen indicating GI₅₀ values (concentration of drug that results in 50% growth inhibition) is reported. A larger GI₅₀ value in ADR-RES cells compared to the mean GI₅₀ value indicates AIM is sensitive to drug resistance and potentially a P-gp substrate.

IDHPs 1A and 1K produce substantial P-gp (MDR1) inhibition. Screening of IDHPs was performed by the Psychoactive Drug Screening Program (PDSP) of the National Institute of Mental Health (NIMH). Results from this screening demonstrated that all IDHPs produced P-gp inhibition of at least 10% (Figure 4.2). Of the IDHPs tested, two produced substantial P-gp inhibition; 1A produced 49% P-gp inhibition and 1K produced 61% P-gp inhibition. 1A and 1K were selected for further investigation.

1A has cytotoxicity profile comparable to nifedipine. The DHP calcium channel antagonist nifedipine was selected as a control for these experiments. MTT results demonstrate that IDHP 1A is similarly non-toxic to nifedipine with mean IC_{50} values >100 μ M for a 24 hour exposure (Figure 4.3). IDHP 1K showed some cytotoxicity to both cell lines tested: mean IC_{50} value 25.48 μ M in MDCK-MDR1⁻ cells and 20.98 μ M in MDCK-MDR1⁺ cells. Due to concerns over the cytotoxicity of 1K, for co-dosing experiments evaluating the change in AIM cytotoxicity following IDHP exposure, cells were exposed to a non-toxic dose of IDHP 1K compared to 1A.

Figure 4.2



IDHP	R ₁	R ₂	MDR-1 (% inhibition)
1a	CH ₃	C ₆ H ₅	49
1b	CH ₃	o-MeO-C ₆ H ₄	33
1c	CH ₃	2-MeO-5-Cl-C ₆ H ₃	15
1d	CH ₃	o-Cl-C ₆ H ₄	11
1e	CH ₃	m-Cl-C ₆ H ₄	27
1f	CH ₃	p-Cl-C ₆ H ₄	12
1g	i-Pr	C ₆ H ₅	38
1h	C ₆ H ₅ CH ₂ CH ₂	C ₆ H ₅	28
1i	p-Biphenyl-CH ₂ CH ₂	CH ₃	19
1j	1-naphthyl-CH ₂ CH ₂	CH ₃	19
1k	m-Br- C ₆ H ₅ CH ₂ (CH ₃)CH	CH ₃	61
1l	1-naphthyl-CH ₂ (CH ₃)CH	CH ₃	38

Figure 4.2. IDHPs produce P-gp (MDR-1) inhibition. All IDHPs in this series showed P-gp inhibition of at least 10%. Structure and percent MDR1 are indicated (adapted from Hulubei *et al.*, 2012).

Figure 4.3

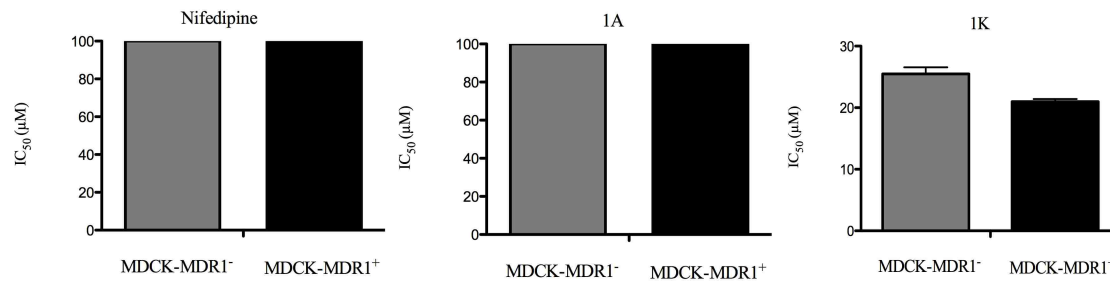


Figure 4.3. Assessment of cytotoxicity of IDHPs against known P-gp inhibitor. Nifedipine, a well documented P-gp inhibitor, shows no measurable cytotoxicity to both MDCK-MDR1⁻ and MDCK-MDR1⁺ cell lines. 1A also shows no measurable cytotoxicity. 1K is more cytotoxic to MDCK-MDR1⁺ cells but the difference is not statistically significant.

Doxorubicin, AIM 1, and AIM 3 are cytotoxic to MDCK-MDR1⁻ non-P-gp expressing cells.

Doxorubicin is a known P-gp substrate and was selected for viability assays as a comparison against the AIMS (Teodori *et al.*, 2002). Doxorubicin was more cytotoxic in cells not expressing P-gp compared to cells that do express P-gp (Figure 4.4). When AIM 1 was evaluated by MTT, similar results were observed. AIM 1 mean IC₅₀ value in MDCK-MDR1⁻ cells was 3.46 μM. and in MDCK-MDR1⁺ cells the mean IC₅₀ value increased significantly to 22.90 μM. AIM 3 mean IC₅₀ value was also significantly higher in MDCK-MDR1⁺ cells.

Exposure to IDHPs 1A and 1K significantly increases doxorubicin cytotoxicity in P-gp

expressing cells. For these experiments, a modified MTT assay was developed to examine the effects of co-treatment with IDHPs on the cytotoxicity of P-gp substrates (Figure 4.5). Doxorubicin, a known P-gp substrate was once again used as a control. Exposure to 50 μM IDHP 1A significantly increased the cytotoxicity of doxorubicin in MDCK-MDR1⁺ cells. For evaluation of 1K, a lower dose was used due to the concerns over cytotoxicity. Exposure to 10 μM IDHP 1K also significantly increased the cytotoxicity of doxorubicin in MDCK-MDR1⁺ cells.

Figure 4.4

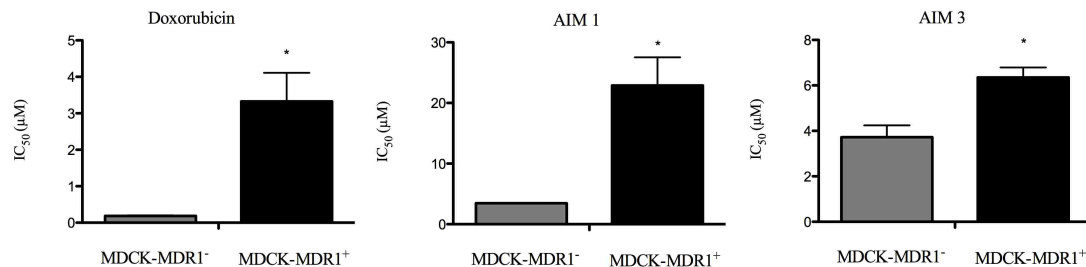


Figure 4.4. Assessment of P-gp substrate doxorubicin cytotoxicity compared to AIMS.

Histograms reveal results from MTT viability assays. Differences in IC₅₀ values between MDCK-MDR1⁻ cells (grey) compared to P-gp expressing MDCK-MDR1⁺ cells (black) are shown. * p≤0.05 compared to IC₅₀ values from non-P-gp expressing MDCK-MDR1⁻ cells.

Figure 4.5

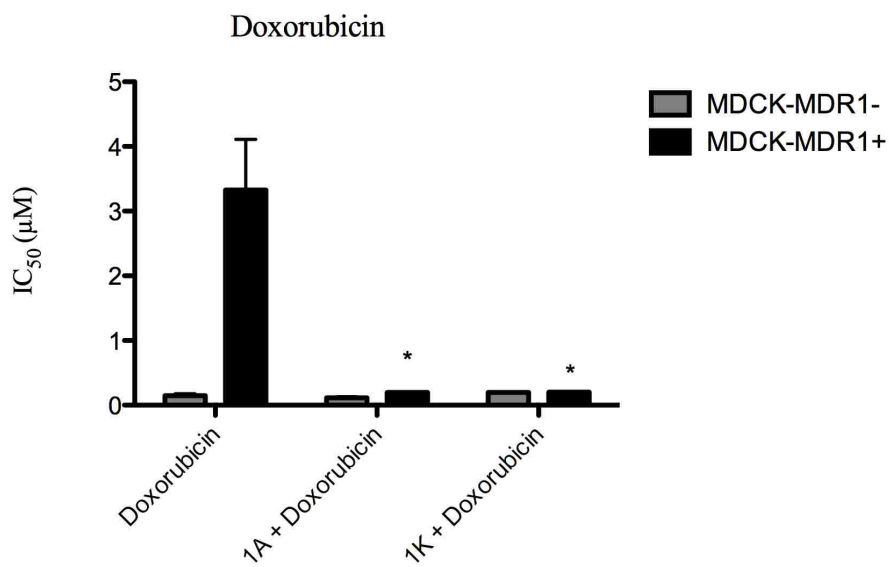


Figure 4.5. Doxorubicin cytotoxicity after addition of IDHP P-gp inhibitors. Histograms reveal results from modified MTT viability assays following co-dosing with IDHP. IDHP effect on doxorubicin cytotoxicity is indicated. IC₅₀ values in MDCK-MDR1⁻ cells (grey) compared to P-gp expressing MDCK-MDR1⁺ cells (black) are shown. * p ≤ 0.05 from doxorubicin before IDHP pre-treatment.

Cytotoxicity of AIM 1 is increased following pre-treatment with IDHPs. Following exposure to 50 μM IDHP 1A the cytotoxicity of AIM 1 in MDCK-MDR1⁺ cells significantly increased from a mean IC_{50} of 22.90 μM to 2.80 μM (Figure 4.6). In both cell lines, following exposure to 10 μM 1K, AIM 1 became significantly more cytotoxic.

Cytotoxicity of AIM 3 was not increased following IDHP pre-treatment. In MDCK-MDR1⁺ cells, AIM 3 mean IC_{50} value is 6.35 μM . Following exposure to 50 μM IDHP 1A, AIM 3 mean IC_{50} value was reduced to 5.94 μM (Figure 4.7). This change is not statistically significant. When MDCK-MDR1⁺ cells were exposed to 10 μM IDHP 1K, the cytotoxicity of AIM 3 decreased. Surprisingly, AIM 3 became significantly less toxic following pre-treatment with 1K in MDCK-MDR1⁺ cells.

IDHPs increased cytotoxicity of AIM 1 in SNB-19 cells. Due to the extensive data collected in relation to AIM 1 in SNB-19 human glioblastoma cells (Chapters 2 and 3), modified MTT assays were performed to examine the effects of IDHP pre-treatment on AIM 1 cytotoxicity (Figure 4.8). Following exposure to IDHPs 1A and 1K, AIM 1 became more cytotoxic in SNB-19 cells. Pre-treatment of 10 μM of IDHP 1K resulted in a statistically significant increase in AIM 1

cytotoxicity to SNB-19 cells. This effect is likely due to the inherent toxicity of 1K.

Figure 4.6

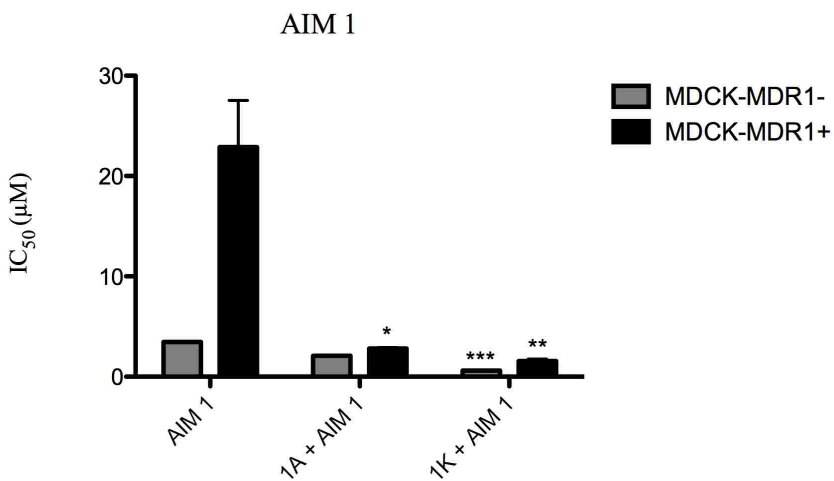


Figure 4.6. AIM 1 cytotoxicity after addition of IDHP P-gp inhibitors. Histograms reveal results from modified MTT viability assays following co-dosing with IDHP. IDHP effect on AIM 1 cytotoxicity is indicated. IC₅₀ values in MDCK-MDR1⁻ cells (grey) compared to P-gp expressing MDCK-MDR1⁺ cells (black) are shown. * p ≤ 0.05, ** p ≤ 0.001, *** p ≤ 0.0001.

Figure 4.7

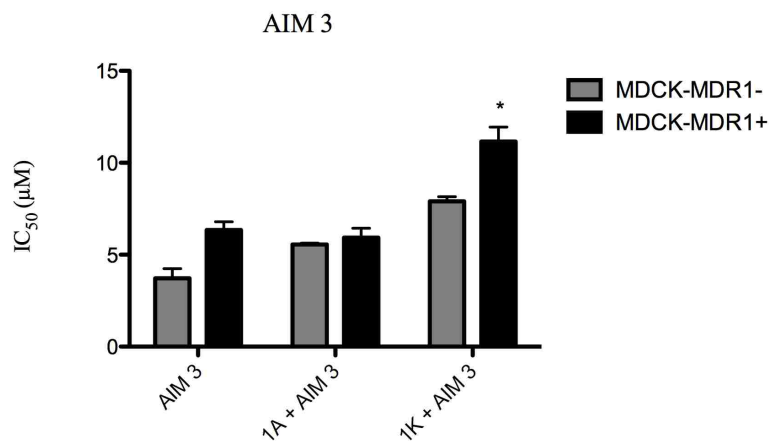


Figure 4.7. Pre-treatment with IDHPs and effects on AIM 3 cytotoxicity. Histograms reveal results from modified MTT viability assays following co-dosing with IDHP. IDHP effect on cytotoxicity of AIM 3 is indicated. IC₅₀ values in MDCK-MDR1⁻ cells (grey) compared to P-gp expressing MDCK-MDR1⁺ cells (black) are shown. * p_≤0.05, ** p_≤0.001, *** p_≤0.0001.

*indicates a p_≤0.05 from AIM 3 before IDHP pre-treatment.

Figure 4.8

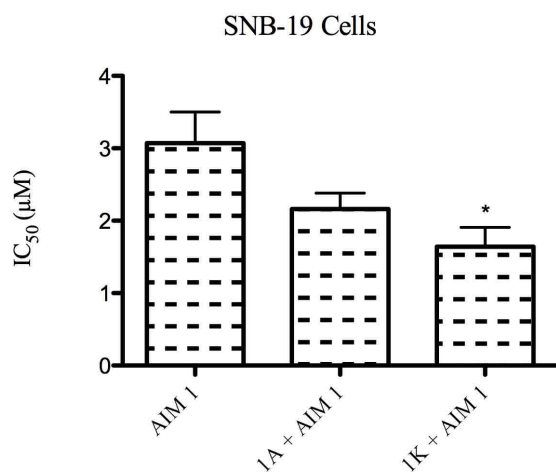


Figure 4.8. Effects of IDHPs on AIM 1 in SNB-19 cells. Pre-treatment of SNB-19 cells with IDHPs increases the cytotoxicity of AIM 1. Histogram details IC₅₀ of AIM 1 with IDHP. * p < 0.05.

AIM 3 is less cytotoxic to SNB-19 cells following IDHP exposure. As observed in MDCK-MDR1⁻ and MDCK-MDR1⁺ cells, pre-treatment of IDHPs resulted in a reduction of AIM 3 cytotoxicity in SNB-19 cells (Figure 4.9). With the addition of both IDHPs 1A and 1K, AIM 3 became significantly less toxic to SNB-19 cells, which was unexpected.

Figure 4.9

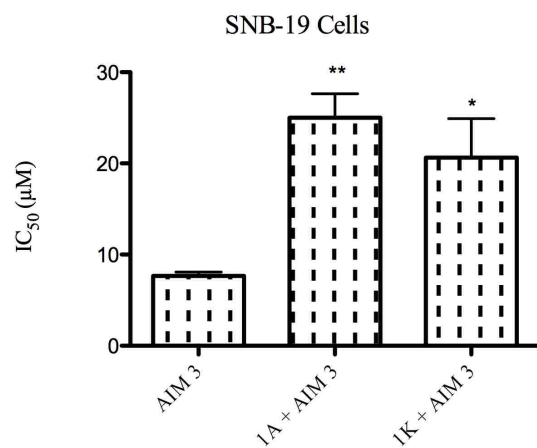


Figure 4.9. Effects of IDHPs on AIM 3 in SNB-19 cells. Pre-treatment of SNB-19 cells with IDHPs decreases the cytotoxicity of AIM 3. Histogram details IC₅₀ of AIM 1 with IDHP. * $p \leq 0.05$, ** $p \leq 0.01$.

DISCUSSION

Results of this study demonstrate the potential to use IDHPs as P-gp inhibitors. The two IDHPs examined in this study, 1A and 1K, possess significant P-gp inhibition properties and increase the cytotoxicity of P-gp substrates, doxorubicin and AIM 1. NCI-60 cell line screening results strongly suggest AIM 1 is indeed a P-gp substrate and our results both in MDCK-MDR1⁺ cells and SNB-19 cells corroborate these findings. AIM 3, a single tail AIM, does not appear to act in the same manner as doxorubicin and AIM 1. When the results of the MTT assays with doxorubicin, AIM 1, and AIM 3 are examined closely, we can conclude that while AIM 3 is significantly more cytotoxic in MDCK- MDR1⁻ cells, the extent to which this is true is much less than that of doxorubicin and AIM 1. MTT results considered together with the results of the NCI-60 cell line screening that show AIM 3 is less sensitive to the P-gp effects of ADR-RES cells, suggest that if AIM 3 is a P-gp substrate, it is functioning as a very weak P-gp substrate.

Results with IDHP 1K, which PDSP data showed produced the most P-gp inhibition, are not straightforward. In cases with doxorubicin and AIM 1, 1K pre-treatment results in a significant increase in substrate cytotoxicity. However, when 1K is dosed with AIM 3, the cytotoxicity is decreased significantly in MDCK-MDR1⁺ cells and SNB-19 cells; we would expect the cytotoxicity to be unchanged before and after 1K exposure. In these cases, there may

be an interaction between 1K and AIM 3, which results in one drug outcompeting the other for an enzyme or binding site (non P-gp related). AIM 3 might also be inducing P-gp, leading to an overall decrease in the cytotoxicity of the compound (Matheny *et al.*, 2001). This could result in AIM 3 not being able to achieve the cytotoxic effects that are seen before 1K exposure.

IDHP exposure effects in SNB-19 cells are preliminary—P-gp expression was not calculated in these cells— but do support the data that suggest efflux transporters exist not only within endothelial cells of the BBB, but other CNS cells as well (Abe *et al.*, 1995; Dallas *et al.*, 2006). While the modified MTT assay demonstrated a decrease in mean IC₅₀ values when AIM 1 was co-dosed with IDHP 1A, results were only significant following exposure to 1K. Baseline P-gp expression was not evaluated in SNB-19 cells; however, the significant effects observed only with exposure to 1K with AIM 1 in SNB-19 cells could be due to an inherent high expression of P-gp in SNB-19 cells. That is, a more potent IDHP (such as 1K, which produces more P-gp inhibition than 1A) would be necessary to achieve significant increases in cytotoxicity compared to the cytotoxicity before IDHP exposure. 1K is also inherently more cytotoxic than 1A (as demonstrated by MTT viability assays) and this cytotoxicity could be contributing to the effects observed following treatment with 1K and AIM 1.

Results from this study demonstrate IDHPs are capable of increasing the cytotoxicity of

doxorubicin in P-gp expressing cell lines to a greater extent than other P-gp inhibitors reported in the literature (Dantzig *et al.*, 2001). Pre-treatment with IDHPs also increases the cytotoxicity of AIM 1 significantly more efficiently than other anticancer agents being evaluated in conjunction with P-gp inhibitors (Zhou *et al.*, 2005b). While the development of P-gp inhibitors is an active field, there have been several limiting factors to their use. First generation P-gp inhibitors such as cyclosporin A, quinidine, and reserpine inhibited P-gp but were somewhat non-specific for the transporter and less potent than later generation P-gp inhibitors (Bansal *et al.*, 2009). In addition, doses required to achieve inhibition were often accompanied by significant toxicity. Second generation modulators such as biricodar and analogues of cyclosporin A had similar problems with not producing significant P-gp inhibition at tolerable doses. Issues with second generation inhibitors were compounded when it was discovered that many of these agents were also substrates for CYP3A4—competition between anticancer agents and these P-gp inhibitors for CYP 3A4 activity resulted in unpredictable pharmacokinetic interactions leading to toxic levels of anticancer drugs (Liscovitch and Lavie, 2002). Third generation P-gp inhibitors, such as tariquidar, have been improved to reduce the affinity to be metabolized by CYP3A4, as well as increase the overall potency and activity for P-gp (Palmeira *et al.*, 2012; Bansal *et al.*, 2009). One of the biggest improvements that has been made with new P-gp inhibitors is their ability to

be dosed within the nanomolar range (Krishna and Mayer, 2000). While great strides have been made in the development of third generation P-gp inhibitors, results from our studies with IDHPs are still superior in the extent to which pre-treatment increases the cytotoxicity of known substrates; one of the highest reported values is a 13 fold increase in cytotoxicity of doxorubicin following P-gp inhibitor exposure (Dantzig *et al.*, 2001). Our IDHPs exceed this value.

In vitro assays detailed in this study dosing at 10-50 μM IDHPs is an acceptable range for preliminary investigation. It is possible that effects would be replicated at doses even lower, but as results were significant with AIM 1 co-dosed with IDHPs, a dose response was not evaluated in this study. It is the ultimate goal of this research to continue the synthesis of IDHPs and develop increasingly potent P-gp inhibitors that are highly selective only for the P-gp efflux transporter. In the meantime, it is important to continue to evaluate the IDHPs to determine exactly how they interact with P-gp (to include a more detailed structure-activity analysis and identify IDHP activity as competitive or non-competitive inhibitors of P-gp) and how these effects can be accentuated to produce the most P-gp inhibition in the absence of undesirable or unpredictable toxicity.

AWKNOWLEDGEMENTS

The authors wish to thank Dr. Nicholas Natale and Scott Steiger for their generous contributions in the synthesis of the IDHPs. We are grateful for their insight and expertise.

REFERENCES

- Abe, T., Koike, K., Ohga, T., Kubo, T., Wada, M., Kohno, K., Mori, T., Hidaka, K., and Kuwano, M. (1995). Chemosensitisation of spontaneous multidrug resistance by a 1,4-dihydropyridine analogue and verapamil in human glioma cell lines overexpressing MRP or MDR1. *Br J Cancer* **72**, 418-423.
- Agarwal, S., Hartz, A. M. S., Elmquist, W. F., and Bauer, B. (2011). Breast cancer resistance protein and P-glycoprotein in brain cancer: two gatekeepers team up. *Curr Pharm Des* **26**, 2793-2802.
- Avendano, C., and Menendez, J. C. (2002). Inhibitors of multidrug resistance to antitumor agents (MDR). *Curr Med Chem* **2**, 159-193.
- Bansal, T., Jaggi, M., Khar, R. K., and Talegaonkar, S. (2009). Emerging significance of flavonoids as P-glycoprotein inhibitors in cancer chemotherapy. *J Pharm Sci* **1**, 46-78.
- Boer, R., Haas, S., and Schodl, A. (1994). Influence of dexniguldipine-HCl on rhodamine-123 accumulation in a multidrug-resistant leukemia cell line: comparison with other chemosensitisers. *Eur J Cancer* **30A**, 1117-1123.
- Dallas, S., Miller, D. S., and Bendayan, R. (2006). Multidrug resistance-associated proteins: expression and function in the central nervous system. *Pharmacol Rev* **2**, 140-161.
- Dantzig, A. H., Law, K. L., Cao, J., and Starling, J. J. (2001). Reversal of multidrug resistance by the P-glycoprotein modulator, LY335979, from the bench to the clinic. *Curr Med Chem* **1**, 39-50.
- Hawkins, B. T., and Davis, T. P. (2005). The blood-brain barrier/neurovascular unit in health and disease. *Pharmacol Rev* **2**, 173-185.
- Hulubei, V., Meikrantz, S. B., Quincy, D. A., Houle, T., McKenna, J. I., Rogers, M. E., Steiger, S., and Natale, N. R. (2012). 4-isoxazolyl-1,4-dihydropyridines exhibit binding at the multidrug-resistance transporter. *Bioorg Med Chem* **22**, 6613-6620.
- Krishna, R., and Mayer, L. D. (2000). Multidrug resistance (MDR) in cancer mechanisms, reversal using modulators of MDR and the role of MDR modulators in influencing the pharmacokinetics of anticancer drugs. *Eur J Pharm Sci* **11**, 265-283.
- Liscovitch, M., and Lavie, Y. (2002). Cancer multidrug resistance: A review of recent drug discovery research. *IDrugs* **5**, 1-7.
- Matheny, C. J., Lamb, M. W., Brouwer, K. R., and Pollack, G. M. (2001). Pharmacokinetic and pharmacodynamics implications of P-glycoprotein modulation. *Pharmacotherapy* **7**, 778-796.

- Palmeira, A., Sousa, E., Vasconcelos, M. H., and Pinto, M. M. (2012). Three decades of P-gp inhibitors: skimming through several generations and scaffolds. *Curr Med Chem* **13**, 1946-2025.
- Pardridge, W. M. (1999). Blood-brain barrier biology and methodology. *J Neurovirol* **6**, 556-569.
- Pleban, K., and Ecker, G. F. (2005). Inhibitors of p-glycoprotein-lead identification and optimization. *Mini Rev Med Chem* **2**, 153-163.
- Teodori, E., Dei, S., Scapecchi, S., and Gualtieri, F. (2002). The medicinal chemistry of multidrug resistance (MDR) reversing drugs. *Farmaco* **57**, 385-415.
- Tsuji, A. (1998). P-glycoprotein-mediated efflux transport of anticancer drugs at the blood-brain barrier. *Ther Drug Monit* **5**, 588-590.
- Tsuruo, T., Iida, H., Tsukagoshi, S., and Sakurai, Y. (1981). Overcoming of vincristine resistance in P388 leukemia in vivo and in vitro through enhanced cytotoxicity of vincristine and vinblastine by verapamil. *Cancer Res* **5**, 1967-1972.
- Vilpo, J., Koski, T., and Vilpo, L. (2000). Calcium antagonists potentiate P-glycoprotein-independent anticancer drugs in chronic lymphocytic leukemia cells *in vitro*. *Haematologica* **85**, 806-813.
- Yusa, K., and Tsuruo, T. (1989). Reversal mechanism of multidrug resistance by Verapamil: direct binding of verapamil to P-glycoprotein on specific sites and transport of verapamil outward across the plasma membrane of K562/ADM cells. *Cancer Res* **49**, 5002-5006.
- Zhou, X-F., Coburn, R. A., and Morris, M. E. (2005). Effects of new 4-aryl-1,4-dihydropyridines and 4-arylpyridines on drug efflux mediated by multidrug resistance-associated protein 1. *J Pharm Sci* **10**, 2256-2265.
- Zhou, X-F., Zhang, L., Tseng, E., Scott-Ramsay, E., Schentag, J. J., Coburn, R. A., Morris, M. E. (2005). New 4-aryl-1,4-dihydropyridines and 4-arylpyridines as P-glycoprotein inhibitors. *Drug Metab Dispos* **3**, 321-328.

CHAPTER 5

Synthesis of new quinolinequinone derivatives and preliminary exploration of their cytotoxic properties

Adapted from the *Journal of Medicinal Chemistry*

Authors

Alison K. Kearns, Charles M. Keyari, Philippe Diaz and Howard D. Beall

Corresponding Author

Dr. Howard D. Beall

Address: University of Montana

Department of Biomedical and Pharmaceutical Sciences

32 Campus Drive, Skaggs

Missoula, MT 59812

Telephone: 406-243-5112

Fax: 406-243-2807

Email: Howard.Beall@umontana.edu

ABSTRACT

A series of 7-amino- and 7-acetamidoquinoline-5,8-diones with aryl substituents at the 2-position were synthesized, characterized, and evaluated as potential NAD(P)H:quinone oxidoreductase (NQO1)-directed antitumor agents. NQO1 is an important drug target in cancer research; it is upregulated in many solid tumors and is capable of bioactivating compounds to increase toxicity and selectivity to cancerous cells. Aside from reducing quinone substrates to potentially more active hydroquinone alkylating agents that target cancer cells, NQO1 also functions as a cytoprotective enzyme. Through the detoxification of quinones, NQO1 aids in reducing harmful exposure and regulates the health of the cellular environment. In the present study we utilized several techniques to assay potential NQO1 substrates. Results of metabolism studies demonstrated that 7-amino analogues were generally better substrates for NQO1 than 7-amido analogues, as were compounds with smaller heteroaromatic substituents at the C-2 position. Two compounds, 7-acetamido-2-(8'-quinolinyl)quinoline-5,8-dione (11) and 7-amino-2-(2-pyridinyl)quinoline-5,8-dione (23), showed selective cytotoxicity toward the NQO1-expressing MDA468-NQ16 breast cancer cells versus the NQO1-null MDA468-WT cells. For all other compounds tested, NQO1 protected against quinoline-5,8-dione cytotoxicity. Compound 22 showed potent activity against human breast cancer cells expressing and not expressing

NQO1, with respective IC_{50} values of 190 nM and 140 nM and a low NQO1-mediated reduction rate, suggestive of a mode of action for 22 that differs from that of lavendamycin and involves an unidentified target(s).

INTRODUCTION

Lavendamycin is a quinolinequinone antibiotic with antitumor activity that was isolated from *Streptomyces lavendulae* (Balitz *et al.*, 1982; Doyle *et al.*, 1981). Lavendamycin is structurally related to streptonigrin, which was first isolated from *Streptomyces flocculus* (Rao and Cullen, 1959; Rao *et al.*, 1963). Streptonigrin is known for its potent cytotoxic properties, antitumor activity, *in vitro* and *in vivo* antiviral properties, and potent, broad-spectrum antimicrobial properties. Although lavendamycin is not suitable for clinical use due to its toxicity, its analogues are less toxic and have potential as antitumor agents (Podeszwa *et al.*, 2007). Recent findings suggest that some indolequinones and quinolinequinones are excellent substrates for the quinone reductase enzyme NAD(P)H:quinone oxidoreductase 1 (NQO1) and are selectively cytotoxic to cancer cell lines that overexpress NQO1 (Hassani *et al.*, 2005; Fryatt *et al.*, 2004; Beall *et al.*, 1998; Swann *et al.*, 2001; Hassani *et al.*, 2008; Cai *et al.*, 2010).

NQO1 is a ubiquitous flavoenzyme that catalyzes the two-electron reduction of quinones to hydroquinones, and it is highly expressed in many solid tumors (Colucci *et al.*, 2008). The upregulation of NQO1 in cancer is a feature that can be exploited to target drugs that are reduced by NQO1 and that become active through metabolism by the enzyme. This forms the basis for the synthesis of novel quinolinequinones structurally related to lavendamycin as potential

NQO1-directed antitumor agents. The primary role of NQO1, however, is not necessarily the bioactivation of substrates, but rather the detoxification of potentially harmful quinones. Two-electron reduction of quinones to hydroquinones results in bypass of formation of the highly reactive semiquinones from one-electron reduction. Formation of semiquinones, with one unpaired electron on the oxygen atom, can undergo redox cycling in the presence of molecular oxygen to generate additional reactive oxygen species (ROS) including superoxide, singlet oxygen, and hydroxyl radicals (Thor *et al.*, 1982). Semiquinones can also reduce other compounds. For example, when iron is reduced by a semiquinone, hydroxyl radicals can be formed by way of the Fenton reaction. The resulting ROS generated from the reactive semiquinone are toxic to the cells—consequences of ROS accumulation include lipid peroxidation, enzyme inactivation, and modification of DNA (Lind *et al.*, 1982). Conversely, the two electron reduction by NQO1 favors the formation of the stable hydroquinone that can be readily conjugated and excreted (Losito *et al.*, 1967).

In this study we utilize an efficient and direct approach from commercially available hydroxyquinolines that results in the synthesis of our series of 7-aminoquinoline quinones. Included in this study are metabolism and cytotoxicity studies on the quinoline-5,8-diones. Additionally, we report NMR spectra indicating the extent to which this series of quinones binds

Zn^{2+} , as metal complexation is believed to be an important factor in NQO1-mediated reduction and the resulting toxicity of quinones. Results from this study provide important information as to the mechanisms by which this series of lavendamycin analogues function.

MATERIALS AND METHODS

Chemicals. Synthetic chemistry of quinolinequinone derivatives was performed by Charles M. Keyari in the laboratory of Dr. Philippe Diaz at the University of Montana (Missoula, MT).

Cell Culture. MDA-MB-468 (MDA468) human breast cancer cells and stably NQO1-transfected MDA468-NQ1632 were a gift from Dr. David Ross (University of Colorado, Denver, Denver, CO). MDA468 cells had no measurable NQO1 activity whereas activity in MDA468-NQ16 cells was $1070 \text{ nmol}\cdot\text{min}^{-1}(\text{mg of total cell protein})^{-1}$, with dichlorophenolindophenol (DCPIP) as the standard electron acceptor. Cells were grown in RPMI 1640 medium with L-glutamine and penicillin/streptomycin, supplemented with 10% fetal bovine serum (FBS). Cell culture medium and supplements were obtained from Invitrogen (Carlsbad, CA). The cells were incubated at 37°C under a humidified atmosphere containing 5% CO_2 .

Spectrophotometric Cytochrome c Assay. Quinolinequinone reduction was monitored by a spectrophotometric assay in which the rate of reduction of cytochrome c was quantified at 550 nm. Briefly, the assay mixture contained cytochrome c ($70 \mu\text{M}$), reduced nicotinamide adenine dinucleotide (NADH; 1 mM), recombinant human NQO1 ($0.1\text{--}10 \mu\text{g}$) (gift from Dr. David Ross,

University of Colorado, Denver, Denver, CO), and quinolinequinones (25 μM) in a final volume of 1 mL of Tris-HCl (25 mM, pH 7.4) containing 0.7 mg/mL bovine serumalbumin (BSA) and 0.1% Tween-20. Reactions were carried out at room temperature and started by the addition of NADH. Rates of reduction were calculated from the initial linear part of the reaction curve (0–30 s), and results were expressed in terms of micromoles of cytochrome c reduced per minute per milligram of NQO1 by use of a molar extinction coefficient of $21.1 \text{ mM}^{-1} \cdot \text{cm}^{-1}$ for cytochrome c. All reactions were carried out at least in triplicate.

Oxygen Consumption. Oxygen concentration was monitored with a MI-730 micro-oxygen electrode (Microelectrodes, Bedford, NH) with concentrations adjusted for temperature (25 °C). Assay mixtures contained 25 μM quinolinequinones, 200 μM NADH, and 1 $\mu\text{g/mL}$ NQO1 in a 2 mL Tris-HCl/BSA/Tween (0.1%) buffer system. Reactions were started with NADH and measured over 3-min intervals at room temperature. All reactions were carried out in triplicate.

Cell Viability Assay. Growth inhibition was determined by the MTT colorimetric assay. Cells were plated in 96-well plates at a density of 10,000 cells/mL and allowed to attach overnight (16 h). Quinolinequinone solutions were applied in medium for 2 h, removed, and replaced with

fresh medium, and the plates were incubated at 37 °C under a humidified atmosphere containing 5% CO₂ for 3–5 days. MTT (50 µg) was added and the cells were incubated for another 4 h. Medium/MTT solutions were removed carefully by aspiration, the MTT formazan crystals were dissolved in 100 µL of DMSO, and absorbance was determined on a plate reader at 560 nm. IC₅₀ values (concentration at which cell survival equals 50% of control) were determined from semilog plots of percent of control versus concentration. Selectivity ratios were defined as IC₅₀ value for the MDA468 cell line divided by IC₅₀ value for the MDA468-NQ16 cell line.

RESULTS

Parameters relating to NQO1 substrate specificity. For this study, a series of derivatives of lavendamycin were synthesized (Figure 5.1). Several parameters were assessed to determine the ability of each compound to be efficiently reduced by NQO1 (Table 5.1). First, quinolinequinone metabolism by recombinant human NQO1 was determined using a spectrophotometric assay with cytochrome c as the terminal electron acceptor. For this study, the larger the value the more efficiently the compound is reduced by NQO1, indicating good substrate specificity for the enzyme. Results of metabolism studies demonstrated that 7-amino analogues were generally better substrates for NQO1 than 7-amido analogues, as were compounds with smaller

heteroaromatic substituents at the C-2 position. Although unusual, higher rates for acetylated analogues have been observed in other series (Hassani *et al.*, 2005; Cai *et al.*, 2010). No clear trend in reduction rates was observed in regard to the aromatic substitutions at the C-2 position, other than that bulkier groups generally decreased reduction rates. Oxygen consumption, the measure of the ability of a hydroquinone to redox-cycle following reduction by NQO1, was also assessed for select compounds. The trend of oxygen consumption was similar to reduction rates for these compounds. In addition, reduction potential versus ferrocene was also measured. Reduction potential versus ferrocene is a measure of the electronic effects and a consequence of chemical reduction. Reduction rates by NQO1 are more suitable in determining the effect to which quinones can be reduced enzymatically by NQO1.

Selective cytotoxicity of quinoline-5,8-diones. MTT cell viability assays were performed to determine selective toxicity of each compound to a NQO1 expressing (MDA468-NQ16) and non-NQO1 expressing (MDA468-WT) human breast cancer cell line (Table 5.2). Preferential cytotoxicity toward MDA468-NQ16 cells is reflected by a selectivity ratio of >1 . Surprisingly, almost all compounds tested had a selectivity ratio of <1 , indicating greater selectivity toward MDA-468-WT cells.

Figure 5.1



Figure 5.1. Structures of lavendamycin and streptonigrin. Streptonigrin is structurally related to lavendamycin, however, toxicity of these compounds limits their use. The series of quinolinequinones detailed in this study are structurally similar to lavendamycin.

Table 5.1

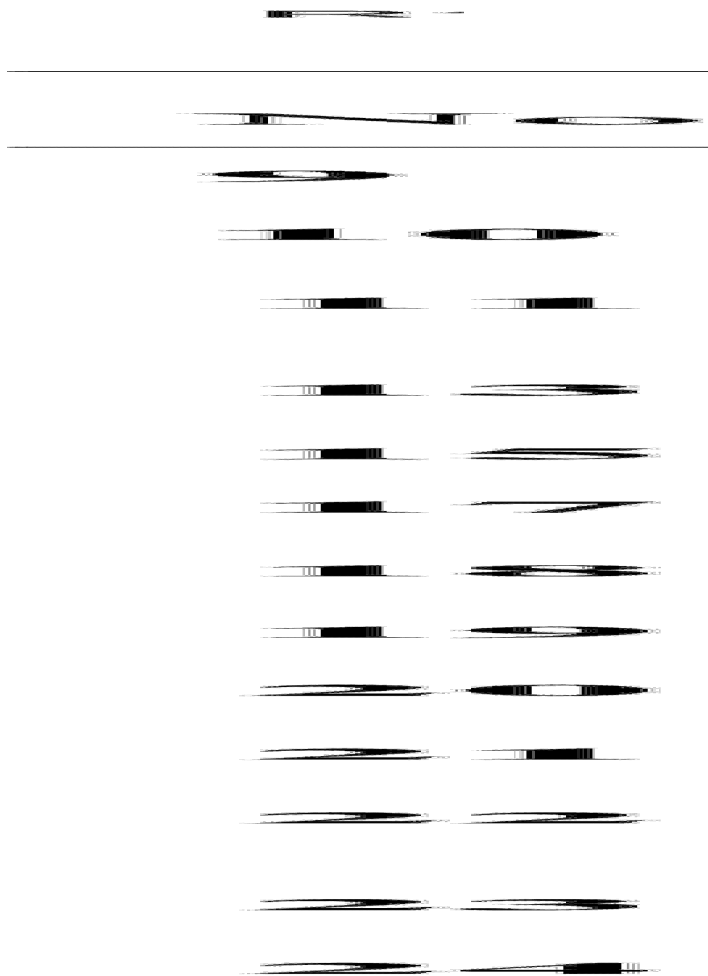


Table 5.1. Reduction rates and oxygen consumption as a result of quinoline-5,8-dione metabolism by recombinant human NQO1. ^aSpectrophotometric assay with cytochrome c as terminal electron acceptor (550 nm). ^bOxygen concentration monitored via an oxygen electrode. ^c $E_{1/2}$ values calculated as $(E_{pc}+E_{pa})/2$ are average values from voltammograms recorded at potential sweep rate of 50 mV/s. E_{pc} = cathodic peak potential; E_{pa} = anodic peak potential. ^dnr = nonreversible, anodic peak only.

Table 5.2

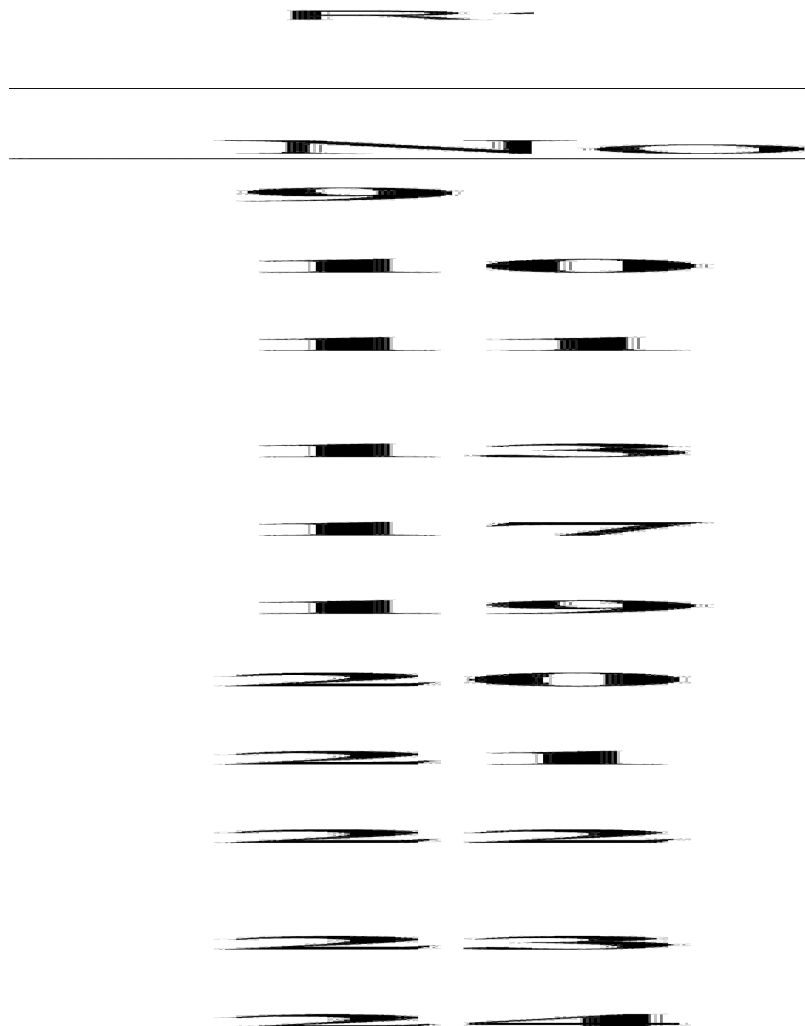


Table 5.2. Cytotoxicity of quinoline-5,8-diones toward MDA468-WT (NQO1-deficient) and MDA468-NQ16 (NQO1-rich) human breast cancer cell lines. IC₅₀ values are mean representation +/- standard deviation (SD) from triplicate experiments.

Metal complexation. For the purposes of this paper, two compounds were selected to highlight the differences in compound interactions with cationic metal. Compounds 19 and 22 were subjected to varying equivalents of Zn^{2+} and analyzed by NMR (Figure 5.2). Results of this experiment demonstrate that 19 does not efficiently bind Zn^{2+} . In contrast, NMR spectra with 22 indicates substantial proton shift with all equivalents of Zn^{2+} (Figure 5.3). Only one equivalent of Zn^{2+} was sufficient to produce a shift in protons, indicating that 22 complexes metal very efficiently compared to 19.

Figure 5.2

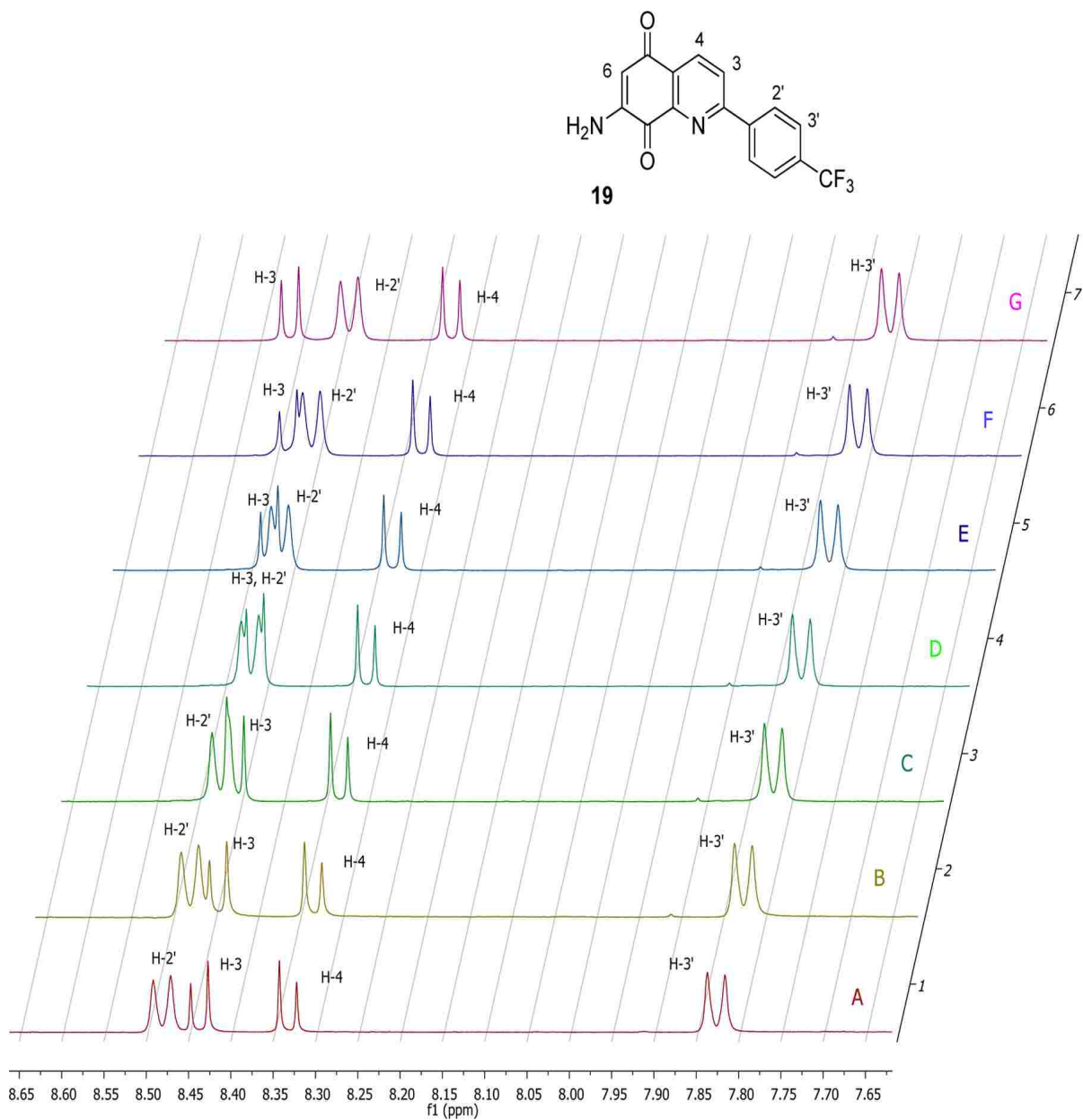


Figure 5.2. NMR spectra of 19 with Zn²⁺. Aromatic proton region of NMR spectrum of 19 upon addition of increasing equivalents of Zn(SO₃CF₃)₂ in THF-d₈. Note the change in δ of H-2' and H-3 upon addition of Zn²⁺. Equivalents of Zn²⁺: A = 0, B = 1, C = 2, D = 3, E = 4, F = 5, and G = 10.

Figure 5.3

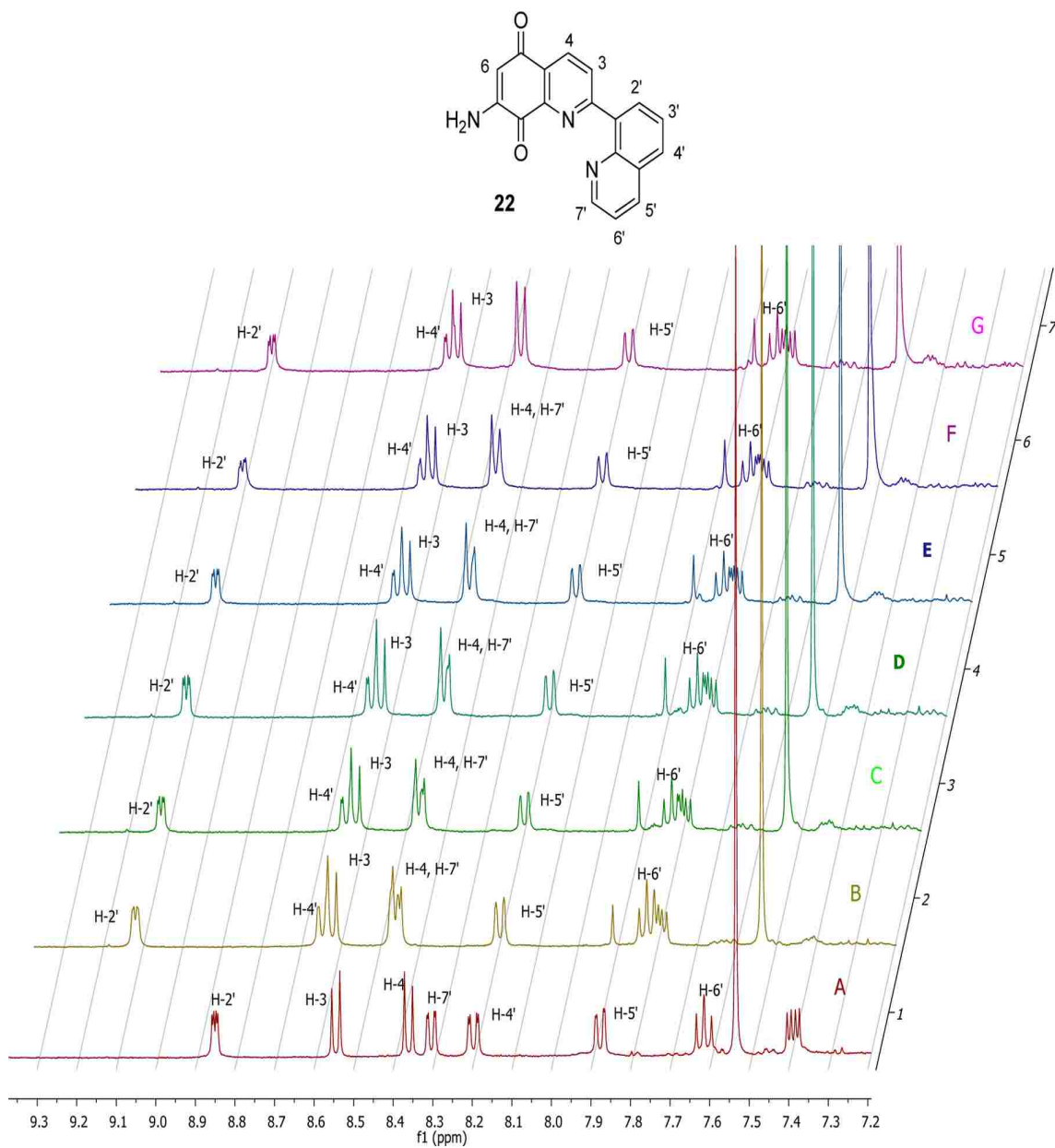


Figure 5.2. NMR spectra of **22** with Zn^{2+} . Aromatic protons region NMR spectra of **22** upon addition of increasing equivalents of $\text{Zn}(\text{SO}_3\text{CF}_3)_2$ in THF- d_8 . Equivalents of Zn^{2+} : A = 0, B = 1, C = 2, D = 3, E = 4, F = 5, and G = 10.

DISCUSSION

The purpose of this study was to design new lavendamycin derivatives that are NQO1 substrates and possess selective toxicity toward NQO1 expressing cancer cells. Of all the quinolinequinones evaluated in this series, only two compounds 11 and 23, were selective for NQO1 expressing cells. Results from cytochrome c reduction rates by NQO1, however, showed that both compounds were not the best substrates in the series for the enzyme. To this end, almost all of the quinolinequinones were cytotoxic to the MDA468 cell lines in the single digit micromolar range, with selectivity ratios <1 . These results are indicative of the compounds being selectively more cytotoxic to the non-NQO1 expressing cell line and suggest that NQO1 is cytoprotective in this case, rather than functioning to activate these quinones (Ross *et al.*, 2000). Results from this study indicate that the best NQO1 substrates (13, 20, 24) were among the least active compounds in NQO1 expressing cells. In contrast, compounds that were poor NQO1 substrates (22, 11) exhibit the best activity in both cell lines tested. The explanation for the overall absence of selective cytotoxicity to MDA468-NQ16 cells in this series of compounds is unclear, but it is consistent with the primary role of NQO1 as a detoxification enzyme.

To explain the results of this study, it is important to note that the mechanism of action of both lavendamycin and streptonigrin is not clearly understood. One feature that is necessary to the function of both streptonigrin and lavendamycin as NQO1 substrates is the ability to chelate

divalent cationic metal ions (Harding and Long, 1997). The precise mechanism for which metal complexation confers downstream cytotoxic effects is poorly understood. With iron for example, complexation might lead to iron shuttling into cells, catalyzing the production of reactive oxygen species through a Fenton reaction. This chelation may also result in the depletion of intracellular cationic metals, leading to cell death (Budimir, 2011). The NMR data reported in this study indicate that compound 22 (as well as compounds 13 and 23; NMR spectra for these compounds not shown) binds Zn^{2+} more efficiently than compound 19. Compounds 13 and 22 were also the most cytotoxic to NQO1 non-expressing cells with IC_{50} values of approximately 530 nM and 140 nM, respectively. As supported by NMR data, one possible explanation for this effect is that these two compounds bind metals more efficiently and are therefore better able to either generate ROS or shuttle iron into the cell, leading to cytotoxicity and eventual cell death. In addition, compound 23, which exhibits lower activity than compound 13, an acetylated amino analogue, may be less active due to a tautomeric shift to an inactive quinoid. Acetylated analogues cannot undergo tautomeric shift. It has been proposed that metals assist tautomeric shift from an active quinone compound to an inactive quinoid that is isoelectronic with biologically inactive azastreptonigrin (Gibson *et al.*, 1992). This tautomeric shift provides an explanation for the decrease in activity of compound 23.

The most active compounds in this study 11, 13, and 22 are potential tridentate ligands for metals. Our results seem to indicate that these compounds exert toxic effects at least partially due to metal chelation. In our series of aryl-substituted quinolinequinones, the active molecules appear to be the quinone derivatives and not derivatives of hydroquinones or semiquinones. These data suggest a mode of action that differs from that of previously studied lavendamycin analogues that are activated by NQO1 reduction and may involve an unidentified target (Hassani *et al.*, 2005; Hassani *et al.*, 2008; Cai *et al.*, 2010). Collectively, our data with this series of aryl-substituted quinolinequinones derivatives represent a promising class of cytotoxic agents with potential novel therapeutic value.

REFERENCES

- Balitz, D. M., Bush, J. A., Bradner, W. T., Doyle, T. W., O'Herron, F. A., and Nettleton, D. E. (1982). Isolation of lavendamycin, a new antibiotic from *Streptomyces lavendulae*. *J Antibiot* **35**, 259– 265.
- Beall, H. D., Winski, S., Swann, E., Hudnott, A. R., Cotterill, A. S., O'Sullivan, N., Green, S. J., Bien, R., Siegel, D., Ross, D., and Moody, C. J. (1998). Indolequinone antitumor agents: Correlation between quinone structure, rate of metabolism by recombinant human NAD(P)H:quinone oxidoreductase, and in vitro cytotoxicity. *J Med Chem* **41**, 4755– 4766.
- Budimir, A. (2011). Metal ions, Alzheimer's disease and chelation therapy. *Acta Pharm* **61**, 1-14.
- Cai, W., Hassani, M., Karki, R., Walter, E. D., Koelsch, K. H., Seradj, H., Lineswala, J. P., Mirzaei, H., York, J. S., Olang, F., Sedighi, M., Lucas, J. S., Eads, T. J., Rose, A. S., Charkharrin, S., Hermann, N. G., Beall, H. D., and Behforouz, M. (2010). Synthesis, metabolism and in vitro cytotoxicity studies on novel lavendamycin antitumor agents. *Bioorg Med Chem* **18**, 1899– 1909.
- Colucci, M. A., Couch, G. D., and Moody, C. J. (2008). Natural and synthetic quinones and their reduction by the quinone reductase enzyme NQO1: From synthetic organic chemistry to compounds with anticancer potential. *Org Biomol Chem* **6**, 637– 656.
- Doyle, T. W., Balitz, D. M., Grulich, R. E., Nettleton, D. E., Gould, S. J., Tann, C.-H., and Moews, A. E. (1981). Structure determination of lavendamycin, a new antitumor antibiotic from *Streptomyces lavendulae*. *Tetrahedron Lett* **22**, 4595– 4598.
- Fryatt, T., Pettersson, H. I., Gardipee, W. T., Bray, K. C., Green, S. J., Slawin, A. M. Z., Beall, H. D., and Moody, C. J. (2004). Novel quinolinequinone antitumor agents: structure-metabolism studies with NAD(P)H:quinone oxidoreductase (NQO1). *Bioorg Med Chem* **12**, 1667– 1687.
- Gibson, N. W., Hartley, J. A., Butler, J., Siegel, D., and Ross, D. (1992). Relationship between DT-diaphorase-mediated metabolism of a series of aziridinylbenzoquinones and DNA damage and cytotoxicity. *Mol Pharmacol* **42**, 531-536.
- Harding, M. M., and Long, G. V. (1997). Interaction of the antitumor antibiotic streptonigrin with metal ions and DNA. *Curr Med Chem* **4**, 405-420.
- Hassani, M., Cai, W., Holley, D. C., Lineswala, J. P., Maharjan, B. R., Ebrahimian, G. R., Seradj, H., Stocksdales, M. G., Mohammadi, F., Marvin, C. C., Gerdes, J. M., Beall, H. D., and Behforouz, M. (2005). Novel lavendamycin analogues as antitumor agents:

- Synthesis, in vitro cytotoxicity, structure–metabolism, and computational molecular modeling studies with NAD(P)H:quinone oxidoreductase 1. *J Med Chem* **48**, 7733–7749.
- Hassani, M., Cai, W., Koelsch, K. H., Holley, D. C., Rose, A. S., Olang, F., Lineswala, J. P., Holloway, W. G., Gerdes, J. M., Behforouz, M., and Beall, H. D. (2008). Lavendamycin antitumor agents: Structure-based design, synthesis, and NAD(P)H:quinone oxidoreductase 1 (NQO1) model validation with molecular docking and biological studies. *J Med Chem* **51**, 3104–3115.
- Lind, C., Hochstein, P., and Ernester, L. (1982). DT-diaphorase as a quinone reductase: a cellular control device against semiquinone and superoxide radical formation. *Arch Biochem Biophys* **216**, 178-185.
- Losito, R., Owen, C. A., and Flock, E. V. (1967). Metabolism of [¹⁴C]menadione. *Biochem* **6**, 62-68.
- Podeszwa, B., Niedbala, H., Polanski, J., Musiol, R., Tabak, D., Finster, J., Serafin, K., Milczarek, M., Wietrzyk, J., Boryczka, S., Mol, W., Jampilek, J., Dohnal, J., Kalinowski, D. S., and Richardson, D. R. (2007). Investigating the antiproliferative activity of quinoline-5,8-diones and styrylquinolinecarboxylic acids on tumor cell lines. *Bioorg Med Chem Lett* **17**, 6138–6141.
- Rao, K. V., and Cullen, W. P. (1959). Streptonigrin, an antitumor substance. I. Isolation and characterization. *Antibiot Annu* **7**, 950–953.
- Rao, K. V., Biemann, K., and Woodward, R. B. (1963). The structure of streptonigrin. *J Am Chem Soc* **85**, 2532–2533.
- Ross, D., Kepa, J. K., Winski, S. L., Beall, H. D., Anwar, A., and Siegal, D. (2000). NAD(P)H:quinone oxidoreductase 1 (NQO1): chemoprotection, bioactivation, gene regulation and genetic polymorphisms. *Chem Biol Interact* **129**, 77-97.
- Swann, E., Barraja, P., Oberlander, A. M., Gardipee, W. T., Hudnott, A. R., Beall, H. D., and Moody, C. J. (2001). Indolequinone antitumor agents: Correlation between quinone structure and rate of metabolism by recombinant human NAD(P)H:quinone oxidoreductase. Part 2. *J Med Chem* **44**, 3311–3319.
- Thor, H., Smith, M. T., Hartzell, P., Bellomo, G., Jewell, S. A., and Orrenius, S. (1982). The metabolism of menadione (2-methyl-1,4-naphthoquinone) by isolated hepatocytes. A study of the implication of oxidative stress in intact cells. *J Biol Chem* **257**, 12419-12425.

CHAPTER 6: CONCLUSIONS

Cancer is a common, complex, and difficult to treat disease. Understanding the underlying biology of cancer is vital to the development of new anticancer agents. Cancer is challenging to cure due in part to the characteristics of tumor cells: sustained proliferative signaling, evasion of growth suppressors, resistance to apoptosis, replicative immortality, induced angiogenesis, and invasion and metastasis capacity (Hanahan and Weinberg, 2000). Drug resistance and undesirable systemic toxicity add additional complexity to effective cancer treatment. Despite these barriers, cancer drug discovery research is an active and dynamic field with new approaches being identified frequently. To this end, the research detailed in our studies is an important contribution to the field of anticancer drug discovery. The following sections highlight the conclusions of these studies and future directions to expand on our results.

G-quadruplex ligand AIM 1 exerts effects on the mitochondria

Identification of G-quadruplex ligands capable of inhibiting telomerase was first reported in the literature in 1991 by Zahler and colleagues (Zahler *et al.*, 1991). Since this discovery, G-quadruplex DNA has been extensively studied as a drug target for telomerase inhibition in the context of cancer (Hemann *et al.*, 1999; Han *et al.*, 1999; Federoff *et al.*, 1998; Ou *et al.*, 2008).

To this end, we developed a series of anthracenyl isoxazole amides (AIMs) designed to bind to G-quadruplex DNA and inhibit telomerase. The first goal of this project was to identify which AIMs from the series were the most cytotoxic to SNB-19 human glioblastoma cells. In addition to determining relevant toxicities, fluorescent properties of the AIMs were examined by a series of LSC and confocal microscopy experiments. The inherent fluorescence of the AIMs was truly an advantage to all fluorescent microscopy experimentation that proceeded from this point and led to the identification of a possible alternate mechanism of action of AIM 1 in the mitochondria. Fluorescence was also a unique property to the AIMs that makes them distinctly different from other commercially available G-quadruplex ligands (Brooks and Hurley, 2010).

Following selection of AIM 1 as the lead compound, we demonstrated that AIM 1 binds telomeric G-quadruplex DNA and is localized to the mitochondria, and not the nucleus as originally expected. The discovery that AIM 1 was present in the mitochondria led to further investigation into the mitochondrial-specific effects that AIM 1 exerts, including activation of caspase-9 and apoptosis, decrease in mitochondrial membrane potential ($\Delta\Psi$ M), generation of mitochondrial superoxide, and facilitation of the export of hTERT from the nucleus. The presence of AIM 1 in the mitochondria as well as the induction of mitochondrial-apoptosis represents a novel mechanism for G-quadruplex ligands. We concluded using NMR

spectroscopy that AIM 1 is a G-quadruplex ligand; if AIM 1 is binding G-quadruplex DNA and is localized to the mitochondria (which we have shown by multiple fluorescent microscopy experiments), we hypothesize that AIM 1 is binding within mitochondrial DNA. Research suggests that G-quadruplex can form within mitochondrial DNA (Wanrooij *et al.*, 2012; Capra *et al.*, 2010; Ngo *et al.*, 2013). The first step to testing this hypothesis is to isolate mitochondria and determine via NMR spectroscopy that AIM 1 binds to G-quadruplex structures within the mitochondrial DNA. Electron microscopy would also be necessary to visualize the location of AIM 1 bound to mitochondrial DNA. Conversely, it is possible that the mitochondrial effects detailed in this study are unrelated to G-quadruplex binding. In this case, AIM 1 could be functioning as a mitochondrial complex inhibitor, a potent generator of reactive oxygen species (ROS), or altering mitochondrial metabolism in some other way (Fulda *et al.*, 2010).

A new series of P-gp inhibitors effectively increase cytotoxicity of P-gp substrates

The second goal of this project was to assay a series of 4-isoxazolyl-1,4-dihydropyridines (IDHPs) that function as P-gp inhibitors to determine their contribution to enhanced cytotoxicity of the AIMs when co-dosed together *in vitro*. Because so many anticancer agents are substrates for P-gp and are therefore limited in their ability to reach intended targets, the development of P-

gp inhibitors is an important area of research (Tsuji, 1998). Once it was determined that two of the IDHPs, 1A and 1K, produced substantial P-gp inhibition, the effect of co-dosing the IDHPs with the AIMs was examined. For these experiments, we developed a modified MTT assay that allowed for the determination of the effects of co-treatment of IDHPs with the AIMs. Results from these experiments indicated that IDHPs were superior to other dihydropyridine (DHP) P-gp inhibitors being reviewed by others; IDHPs increased the cytotoxicity of known P-gp substrate doxorubicin greater than these P-gp inhibitors being investigated (Dantzig *et al.*, 2001). Findings also demonstrate that AIM 1 is likely a P-gp substrate—a result that is not all together surprising, as many anticancer agents are P-gp substrates ((Loscher and Potschka, 2005). However, because AIM 1 was effectively administered with IDHPs and the resulting effect was increased cytotoxicity in the presence of high expression of P-gp, we have two conclusions. First, IDHPs represent a viable class of P-gp inhibitors and second, the P-gp substrate properties of AIM 1 can be overcome and does not limit its use *in vitro*. Understanding the mechanisms of drug resistance and continuing to develop strategies to overcome these effects is an important area of research to be expanded. In this way, continued synthesis of additional IDHPs is a viable component to drug discovery research.

Quinolinequinone lavendamycin derivatives as NQO1-directed antitumor agents

NQO1 is a bioreductive enzyme that is overexpressed in solid tumors and is well characterized in the literature (Lin *et al.*, 1972; Ross *et al.*, 1994; Workman, 1994; Colucci *et al.*, 2008). Based on previous research investigating the use of lavendamycin as a potent NQO1 substrate, we developed a series of quinoline-5,8-diones structurally similar to lavendamycin (Podeszwa *et al.*, 2007). The goal of this study was to determine the NQO1 substrate potential of this series of quinolinequinones and assess their corresponding antitumor potential. The first data that we collected on the quinolinequinones was reduction rates by NQO1. Surprisingly, we discovered that reduction rates varied substantially—compound 13 displayed the highest reduction rate by NQO1, although it was the only acetylated analogue in the series with such a high rate of reduction. In all other cases, it was the 7-amino compounds that possessed the highest rates of reduction compared to 7-acetamido counterparts. Bulkier groups at the C2 position also appeared to reduce reduction rates. Also unexpected, we discovered that only two compounds (23 and 11) were preferentially more cytotoxic to NQO1 expressing cells as compared to non-NQO1 expressing counterparts. These two compounds were not among the compounds possessing the highest reduction rates by NQO1 and a correlation was not found between the two assays in regards to these compounds.

In an effort to explain the mechanisms of this series of quinolinequinones that lack specificity for NQO1 as bioreductive agents, we added NMR experiments investigating quinone-metal complexation. The Zn^{2+} complexation studies were an important element to this investigation; research suggests that one feature that is necessary to the activity of both streptonigrin and lavendamycin is the ability to chelate divalent cationic metal ions (Harding and Long, 1997). We discovered that the ability to complex metal did appear to be an important component with our most active compounds and conclude that the activity can be explained at least in part by the capability to chelate metal. Collectively, in our series of aryl-substituted quinolinequinones, the active molecules appear to be the quinone derivatives and not derivatives of hydroquinones or semiquinones. These data suggest a mode of action that differs from that of previously studied lavendamycin analogues that are activated by NQO1 reduction (Hassani *et al.*, 2005; Hassani *et al.*, 2008; Cai *et al.*, 2010) and may involve an unidentified target. The data in this study represent a promising class of cytotoxic agents with potential novel therapeutic value.

This project involved three separate but related studies that fall under the category of anticancer drug discovery as a whole. Our investigation into the yet untapped extra-nuclear mechanisms and site of action of G-quadruplex ligands is an important contribution not only to G-quadruplex research but mitochondrial medicine for cancer as well. Our use of novel P-gp

inhibitors that are capable of increasing the cytotoxicity of P-gp substrates contributes not only to P-gp related research but adds to the understanding of how our AIMs function as antitumor agents as well. In regards to NQO1-directed antitumor pharmacology, we demonstrated that our lavendamycin analogues function in a manner that is different from lavendamycin itself and may involve another target. While this project focused on the general targeting of solid tumors, the type of tumor explicitly studied varied from brain cancer to breast cancer and encompassed multiple drug targets. Collectively the results of this study are expansive and offer much to the field of anticancer drug discovery.

REFERENCES

- Brooks, T. A., and Hurley, L. H. (2010). Targeting MYC expression through G-quadruplexes. *Genes Cancer* **6**, 641-649.
- Cai, W., Hassani, M., Karki, R., Walter, E. D., Koelsch, K. H., Seradj, H., Lineswala, J. P., Mirzaei, H., York, J. S., Olang, F., Sedighi, M., Lucas, J. S., Eads, T. J., Rose, A. S., Charkharrin, S., Hermann, N. G., Beall, H. D., and Behforouz, M. (2010). Synthesis, metabolism and in vitro cytotoxicity studies on novel lavendamycin antitumor agents. *Bioorg Med Chem* **18**, 1899– 1909.
- Capra, J. A., Paeschke, K., Singh, M., and Zakian, V. A. (2010). G-quadruplex DNA sequences are evolutionarily conserved and associated with distinct genomic features in *Saccharomyces cerevisiae*. *PLOS Comput Biol* **6**, 1-13.
- Colucci, M. A., Couch, G. D., and Moody, C. J. (2008). Natural and synthetic quinones and their reduction by the quinone reductase enzyme NQO1: From synthetic organic chemistry to compounds with anticancer potential. *Org Biomol Chem* **6**, 637– 656.
- Fedoroff, O., Salazar, M., Han, H., Chemeris, V. V., Kerwin, S. M., and Hurley, L. H. (1998) NMR-based model of a telomerase-inhibiting compound bound to G-quadruplex DNA. *Biochemistry* **37**, 12367–12374.
- Fulda, S., Galluzzi, L., and Kroemer, G. (2010). Targeting mitochondria for cancer therapy. *Nat Rev Drug Disc* **9**, 447-464.
- Han, F.X., Wheelhouse, R. T., and Hurley, L. H. (1999) Interaction of TMPyP4 and TMPyP2 with quadruplex DNA. Structural basis for the differential effects on telomerase inhibition. *J Am Chem Soc* **121**, 3561–3570.
- Hanahan, D., and Weinberg, R.A. (2000). The hallmarks of cancer. *Cell* **100**, 57–70.
- Harding, M. M., and Long, G. V. (1997). Interaction of the antitumor antibiotic streptonigrin with metal ions and DNA. *Curr Med Chem* **4**, 405-420.
- Hassani, M., Cai, W., Holley, D. C., Lineswala, J. P., Maharjan, B. R., Ebrahimian, G. R., Seradj, H., Stocksdales, M. G., Mohammadi, F., Marvin, C. C., Gerdes, J. M., Beall, H. D., and Behforouz, M. (2005). Novel lavendamycin analogues as antitumor agents: Synthesis, in vitro cytotoxicity, structure–metabolism, and computational molecular modeling studies with NAD(P)H:quinone oxidoreductase 1. *J Med Chem* **48**, 7733–7749.
- Hassani, M., Cai, W., Koelsch, K. H., Holley, D. C., Rose, A. S., Olang, F., Lineswala, J. P., Holloway, W. G., Gerdes, J. M., Behforouz, M., and Beall, H. D. (2008). Lavendamycin antitumor agents: Structure-based design, synthesis, and

- NAD(P)H:quinone oxidoreductase 1 (NQO1) model validation with molecular docking and biological studies. *J Med Chem* **51**, 3104–3115.
- Hemann, M.T. and Greider, C.W. (1999) G-strand overhangs on telomeres in telomerase-deficient mouse cells. *Nucleic Acids Res* **27**, 3964–3969.
- Lin, A. J., Cosby, L. A., Shansky, C. W., and Sartorelli, A. C. (1972). Potential bioreductive alkylating agents. 1. Benzoquinone derivatives. *J Med Chem* **15**,1247-1252.
- Loscher, W., and Potschka, H. (2005). Blood-brain barrier active efflux transporters: ATP-binding cassette gene family. *NeuroRx* **1**, 86-98.
- Ngo, J. K., Pomatto, L. C. D., and Davies, K. J. A. (2013). Upregulation of the mitochondrial Lon protease allows adaptation to acute oxidative stress but dysregulation is associated with stress, disease, and aging. *Redox Biol* **1**, 258-264.
- Ou, T-M., Lu, Y-J., Tan, J-H., Huang, Z-S., Wong, K-Y., and Gu, L-Q. (2008). G-quadruplexes: targets in anticancer drug design. *Chem Med Chem* **3**, 690-713.
- Podeszwa, B., Niedbala, H., Polanski, J., Musiol, R., Tabak, D., Finster, J., Serafin, K., Milczarek, M., Wietrzyk, J., Boryczka, S., Mol, W., Jampilek, J., Dohnal, J., Kalinowski, D. S., and Richardson, D. R. (2007). Investigating the antiproliferative activity of quinoline-5,-diones and styrylquinolinecarboxylic acids on tumor cell lines. *Bioorg Med Chem Lett* **17**, 6138-6141.
- Ross, D., Beall, H., Traver, R. D., Seigel, D., Phillips, R. M., and Gibson, N. W. (1994). Bioactivation of quinones by DT-diaphorase. Molecular, biochemical and chemical studies. *Oncol Res* **6**, 493-500.
- Tsuji, A. (1998). P-glycoprotein-mediated efflux transport of anticancer drugs at the blood-brain barrier. *Ther Drug Monit* **5**, 588-590.
- Wanrooij, P. H., Uhler, J. P., Westerlund, F., Falkenberg, M., and Gustaffson, C. M.(2012). A hybrid G-quadruplex structure formed between RNA and DNA explains the extraordinary stability of the mitochondrial R-loop. *Nucleic Acids Res* **20**, 10334-10344.
- Workman, P. (1994). Enzyme directed bioreductive drug development revisited: A commentary on recent progress and future prospects with emphasis on quinone anticancer agents and quinone metabolizing enzymes, particularly DT-diaphorase. *Oncol Res* **6**, 461-475.
- Zahler, A. M., Williamson, J. R., Cech, T. R., and Prescott, D. M. (1991). Inhibition of telomerase by G-quartet DNA structures. *Nature* **350**, 718-720.

APPENDIX I

Synthesis of New Quinolinequinone Derivatives and Preliminary Exploration of their Cytotoxic Properties

Charles M. Keyari, Alison K. Kearns, Nathan S. Duncan, Emily A. Eickholt, Geoffrey Abbott,

Howard D. Beall and Philippe Diaz

Published in the *Journal of Medicinal Chemistry*

2013 May 23;56(10):3806-19

Synthesis of New Quinolinequinone Derivatives and Preliminary Exploration of their Cytotoxic Properties

Charles M. Keyari, Alison K. Kearns, Nathan S. Duncan, Emily A. Eickholt, Geoffrey Abbott,
Howard D. Beall* and Philippe Diaz*

*Core Laboratory for Neuromolecular Production, Department of Biomedical and
Pharmaceutical Sciences, The University of Montana, Missoula, MT 59812, USA*

ABSTRACT

A series of 7-amino- and 7-acetamidoquinoline-5,8-diones with aryl substituents at the 2-position were synthesized, characterized and evaluated as potential NAD(P)H:quinone oxidoreductase (NQO1)-directed antitumor agents. The synthesis of lavendamycin analogs is illustrated. Metabolism studies demonstrated that 7-amino- analogues were generally better substrates for NQO1 than 7-amido- analogues as were compounds with smaller heteroaromatic substituents at the C-2 position. Surprisingly, only two compounds, 7-acetamido-2-(8'-quinolinyl)quinoline-5,8-dione (**11**) and 7-amino-2-(2-pyridinyl)quinoline-5,8-dione (**23**) showed selective cytotoxicity toward the NQO1-expressing MDA468-NQ16 breast cancer cells

versus the NQO1-null MDA468-WT cells. For all other compounds, NQO1 protected against quinoline-5,8-dione cytotoxicity. Compound **22** showed a potent activity against human breast cancer cells expressing or not expressing NQO1 with IC50 values of respectively 190 nM and 140 nM and a low NQO1 mediated reduction rate, which suggests that the mode of action of **22** differs from lavendamycin and involves an unidentified target(s).

KEYWORDS: Lavendamycin, Suzuki coupling, microwave irradiation, palladium (0) catalysis, quinolinequinones, NQO1, antitumor, cytotoxicity

INTRODUCTION

Lavendamycin (Figure 1) is a quinolinequinone antibiotic with antitumor activity first isolated from *Streptomyces lavendulae* by Balitz et al in 1982.¹⁻² It is structurally related to Streptonigrin which was first isolated from *Streptomyces flocculus*.³⁻⁴ Streptonigrin is known for its potent cytotoxic properties, antitumor activity, and *in vitro* and *in vivo* antiviral properties and potent, broad spectrum antimicrobial properties. Although lavendamycin is not suitable for clinical use due to its toxicity, its analogs are less

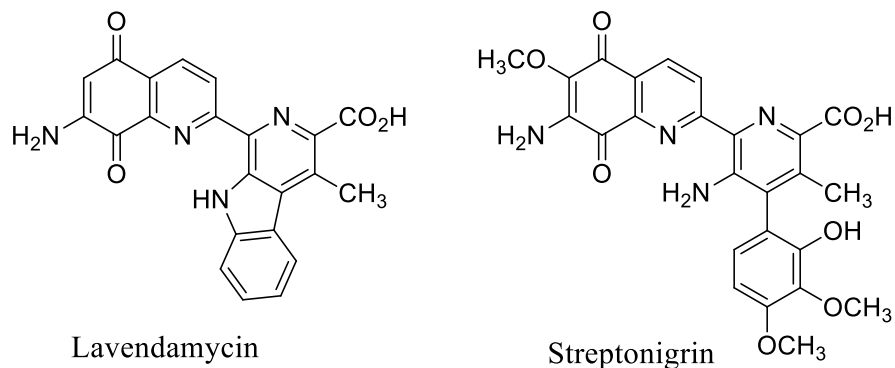


Figure 1. Natural quinolinequinone antibiotics

toxic and hence have potential as antitumor agents.⁵ Recent findings⁶⁻¹¹ suggest that some indolequinones and quinolinequinones are excellent substrates for the quinone reductase enzyme, NAD(P)H:quinone oxidoreductase 1 (NQO1), and are selectively cytotoxic to cancer cell lines that overexpress NQO1. NQO1 is a ubiquitous flavoenzyme that catalyzes the 2-electron reduction of quinones to hydroquinones, and it is highly expressed in many solid tumors.¹² This forms the basis for the synthesis of novel quinolinequinones structurally related to lavendamycin as potential NQO1-directed antitumor agents.

Behforouz *et al.* (1996)¹³ first demonstrated that 7-aminoquinoline-5,8-diones can be efficiently prepared from commercially available 8-hydroxy-2-methylquinoline. Fryatt and co-workers⁷ also showed that by starting with 6-methoxyquinoline, 6-methoxy-2-chloroquinoline-5,8-dione was prepared and subsequent palladium(0) catalyzed reaction with boronic acids gave novel quinoline quinones under reflux for 24 hours. Further, in 2004,¹⁴ arylboronic acids were

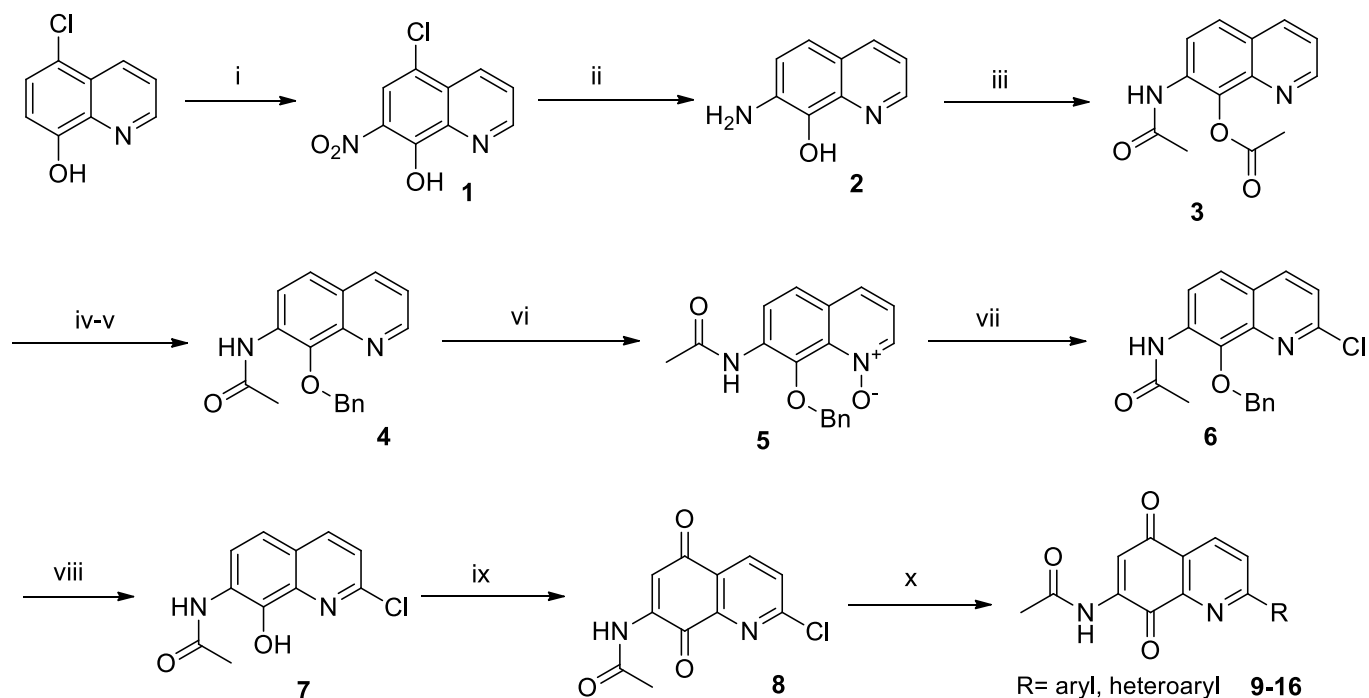
shown to be more reactive than their counterparts, the arylpinacolboronate esters when reacted with indole bromides in Suzuki couplings under reflux. The lower reactivity was attributed to steric factors in the arylpinacolboronate esters. Also, 3-aryl-indazoles have been synthesized by the reaction of haloindazoles (3-bromoindazole and 3-iodoindazole) with aryl boronic acids under Pd(0) catalysis in Suzuki type cross couplings.¹⁵ The reaction times ranged from 1 -18 hours under reflux conditions. In this present study we report a direct more efficient approach to 7-aminoquinoline quinones starting from commercially available 7-amino-8-hydroxyquinoline under microwave conditions where the reaction times are shorter. Computational, metabolism and cytotoxicity studies on the quinoline-5,8-diones are also described.

CHEMISTRY

The synthesis commenced with the nitration of 5-chloro-8-hydroxyquinoline under HNO₃/H₂SO₄ according to a procedure reported by Musser *et al.*¹⁶ to give the 5-chloro-7-nitro-8-hydroxyquinoline (**1**) in good yield (79%). Hydrogenation under Pd/C-catalysis at 40-50 psi not only reduced the nitro group to the free amine but also removed the chloride to provide the desired 7-amino-8-hydroxyquinoline (**2**) in excellent yield (99%). A direct approach to the amino alcohol **2** involves the heating of a mixture of 8-hydroxyquinoline and N-methyl-N-phenylhydrazine at 90°C, albeit very low yields were obtained.¹⁷ Our attempt to synthesize the

amino alcohol by heating in a microwave between 130-160°C did not improve the yield. Acetylation proceeded smoothly where both the amino and hydroxyl groups were protected. The resulting diacetylated product (**3**) was hydrolyzed in MeOH/H₂O under reflux to form 7-acetamido-8-hydroxyquinoline. Subsequent benzylation of the free hydroxyl was effected by reacting with BnBr/K₂CO₃ in DMF at 50°C for 24 hrs to give the 7-acetamido-8-benzyloxyquinoline (**4**) in 90% yield. Oxidation using *m*CPBA in 1,2-dichloroethane at rt for 48 hrs gave the N-oxide (**5**) in 82% yield.¹⁸ The key intermediate in the synthesis, the 2-chloro-7-acetamido-8-benzyloxyquinoline (**6**), was obtained in 62% yield by refluxing the N-oxide with POCl₃ in CHCl₃.¹⁹ The high regioselectivity of the reaction can be rationalized in terms of sterics as well as formation of an oxyphosphorane adduct anion in a rapid concerted mechanism.²⁰ We also attempted refluxing the N-oxide **5** with SO₂Cl₂ as reported in literature,⁹ but only resulted in massive decomposition of the starting material. Deprotection of the benzyl group was effected with BCl₃•SMe₂ in CH₂Cl₂ and subsequent oxidation using Fremy's salt (potassium nitrosodisulfonate-(KO₃S)₂NO) gave the 7-acetamido-2-chloro-quinoline-5,8-dione (**8**) in 71% yield.⁷ The results are summarized in Scheme 1 below.

Scheme 1^a

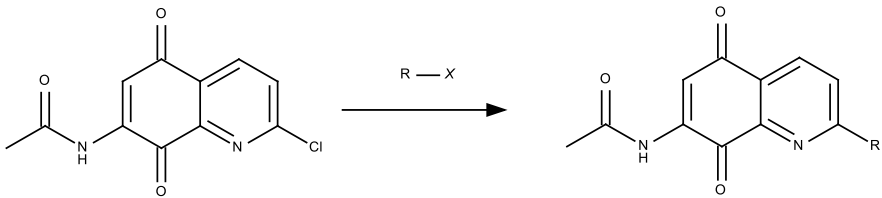


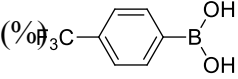
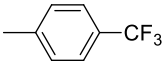
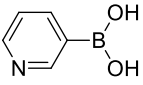
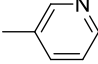
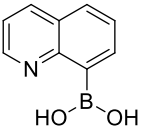
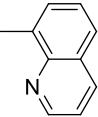
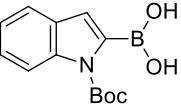
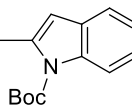
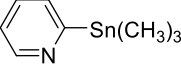
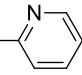
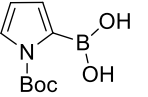
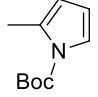
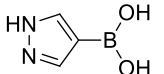
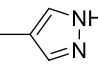
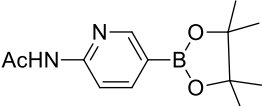
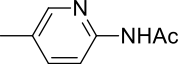
^aReagents and conditions: (i) $\text{HNO}_3/\text{H}_2\text{SO}_4$; (ii) $\text{H}_2/\text{Pd-C}$, MeOH, 40-50psi, overnight; (iii) CH_3COCl , DIEA, THF, 2hrs.; (iv) $\text{H}_2\text{O-MeOH}$, reflux, 1hr; (v) BnBr , K_2CO_3 , DMF, 50°C , 24 hrs; (vi) *m*CPBA, $\text{ClCH}_2\text{CH}_2\text{Cl}$, 48hrs; (vii) POCl_3 , CHCl_3 , reflux, 2 hrs; (viii) $\text{BCl}_3 \cdot \text{SMe}_2$, CH_2Cl_2 , overnight; (ix) Fremy's salt, rt, 1 hr; (x) RB(OH)_2 , $\text{Pd(PPh}_3)_4$, 110-140 $^\circ\text{C}$, MW 20-25 min.

After the successful formation of the quinolinequinone **8**, the stage was now set for Suzuki coupling chemistry. This was accomplished by reaction with different boronic acids under Pd(0) catalysis in a microwave as illustrated in Table 1 below. Generally, the reactions were complete within 20-30 minutes in good yields except for the arylboronate ester where only 27% of the

product (**16**) was obtained. The mechanistic details of the reaction have been well studied in which case oxidative addition, transmetallation and reductive elimination being the most critical

Table 1. Suzuki coupling products



R-X	Reaction conditions	R	Yield
	Pd(PPh ₃) ₄ , DME/Na ₂ CO ₃ 140°C, 20 min	 (9)	70
	Pd(PPh ₃) ₄ , DME/Na ₂ CO ₃ 120°C, 20 min	 (10)	41
	Pd(PPh ₃) ₄ , DME/Na ₂ CO ₃ 120°C, 20 min	 (11)	51
	Pd(PPh ₃) ₄ , DME/Na ₂ CO ₃ 110°C, 25 min	 (12)	67
	*Pd(PPh ₃) ₄ , p-dioxane 120°C, 20 min	 (13)	71
	Pd(PPh ₃) ₄ , DME/Na ₂ CO ₃ 110°C, 25 min	 (14)	53
	Pd(PPh ₃) ₄ , DME/Na ₂ CO ₃ 120°C, 20 min	 (15)	42
	PdCl ₂ (dppf), p-dioxane, K ₃ PO ₄ 120°C, 30 min	 (16)	27

*Stille coupling reaction

steps.²¹ Interestingly, the 7-amino-2-(2-pyridyl)quinoline-5,8-dione was prepared in 9 steps starting from 3-hydroxybenzoic acid where the key step was a * Friedlander condensation of 2-acetylpyridine and 2-amino-3-benzyloxy-4-bromobenzaldehyde to give the 8-benzyloxy-7-bromo-2-(2'-pyridyl)quinoline.²² Although this seems an attractive strategy, the method lacks the flexibility needed to create a library of lavendamycin analogs.

The final step in the synthesis involved the removal of the acetate protecting group which was effected by reaction with H₂SO₄-MeOH at rt. The Boc-protected derivatives were also subjected to TFA/CH₂Cl₂ at rt for 2 hrs to provide the 7-acetamido derivatives.

ELECTROCHEMISTRY

Electrochemistry was performed to compare the electrochemical behavior of the quinolinequinones with their reduction rates by NQO1, and the data are shown in Table 2. Tetrahydrofuran was used as the solvent for all compounds except **15**, which was run in DMSO. The compounds were run against a Ag/AgCl electrode cathodic and anodic peak potentials, E_{pc} and E_{pa}, respectively, were measured at a potential sweep rate of 50 mV/sec, and the midpoint of the peak potentials was used to determine E_{1/2} values, (E_{pc} + E_{pa})/2. Unfortunately, many of the

analogues did not show reversible electrochemistry, and in some cases, there were multiple reduction peaks. This makes interpretation of the numbers somewhat difficult, but some conclusions can be drawn. For instance, most of the acetylated quinolinequinones had a reduction peak between -1.08V and -1.18V, an indication that they are easier to reduce than the non-acetylated compounds due to the presence of this electron-withdrawing group. This is consistent with what we reported previously for lavendamycins. However, there was no correlation between reduction potentials and reduction rates by NQO1, in line with previous publications on this topic.^{6-8, 23, 24} This suggests that steric interactions are more likely to be predictive of substrate efficiency than reduction potentials.

NMR SPECTROSCOPY AND SPECTROPHOTOMETRY

Complexation of zinc(II) triflate by compounds **19**, **22** and **23** was studied using ¹H NMR spectroscopy. No new peaks were observed in NMR spectra, indicating that free and complexed forms of zinc(II) triflate were in a rapid exchange relative to NMR timescale. The aromatic region of the NMR spectrum of compound **19** in THF-D₈ at room temperature is shown below in Figure 2.

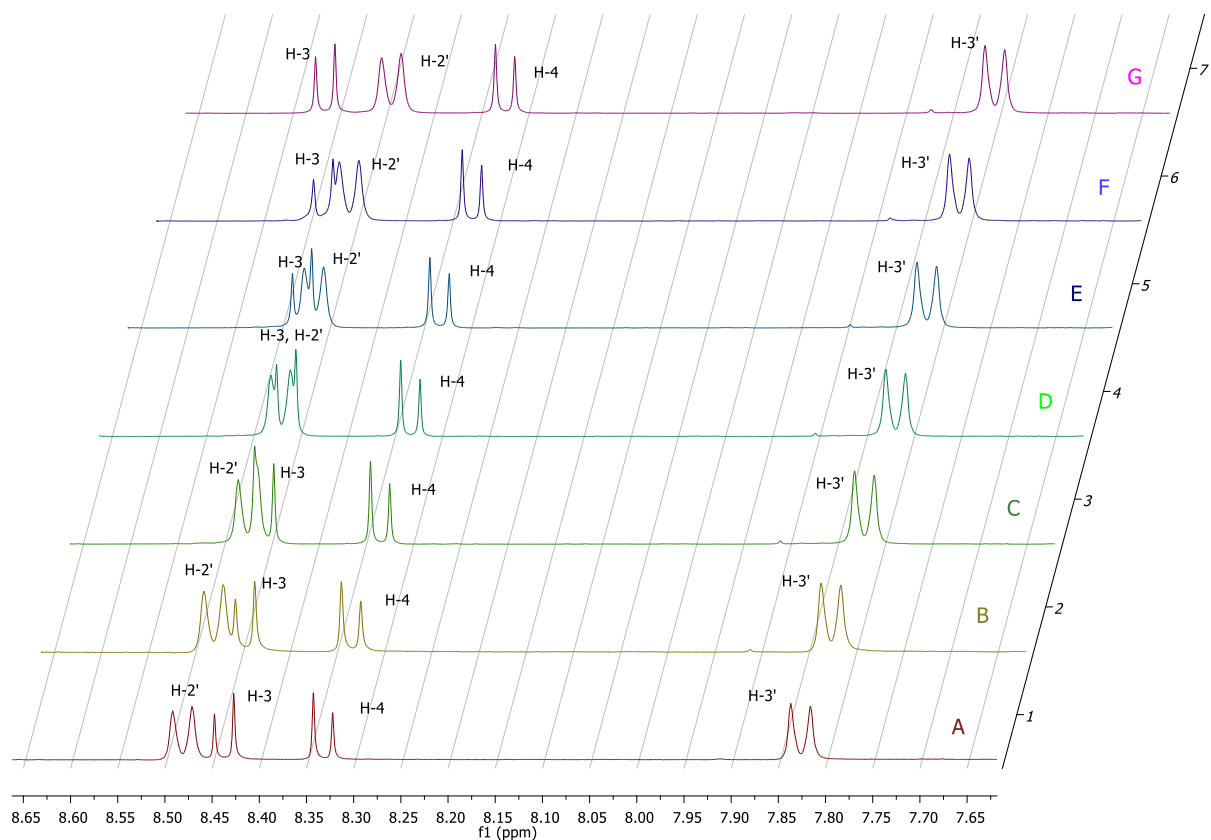
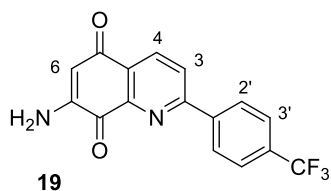


Figure 2. Aromatic proton region NMR spectra of **19** upon addition of increasing equivalent of $\text{Zn}(\text{SO}_3\text{CF}_3)_2$ in $[\text{}^2\text{H}_8]\text{THF}$. Note the change in δ of H-2' and H-3 on addition of Zn^{2+} . Equivalents of Zn^{2+} : A=0, B=1, C=2, D=3, E=4, F=5 and G=10.

There was a small difference in chemical shifts of H-2' (moving upfield) and H-3 (moving downfield) after addition of one equivalent zinc(II) triflate to the NMR solution (Table S1 and Figure 2) whereas the changes in δ of the other protons were barely noticeable. The biggest

change in δ of H-2' (-0.04 ppm) and H-3' (+0.07 ppm) occurs after addition of ten equivalents of $\text{Zn}(\text{SO}_3\text{CF}_3)_2$. This suggests that weak binding occurs at low Zn^{2+} concentration.

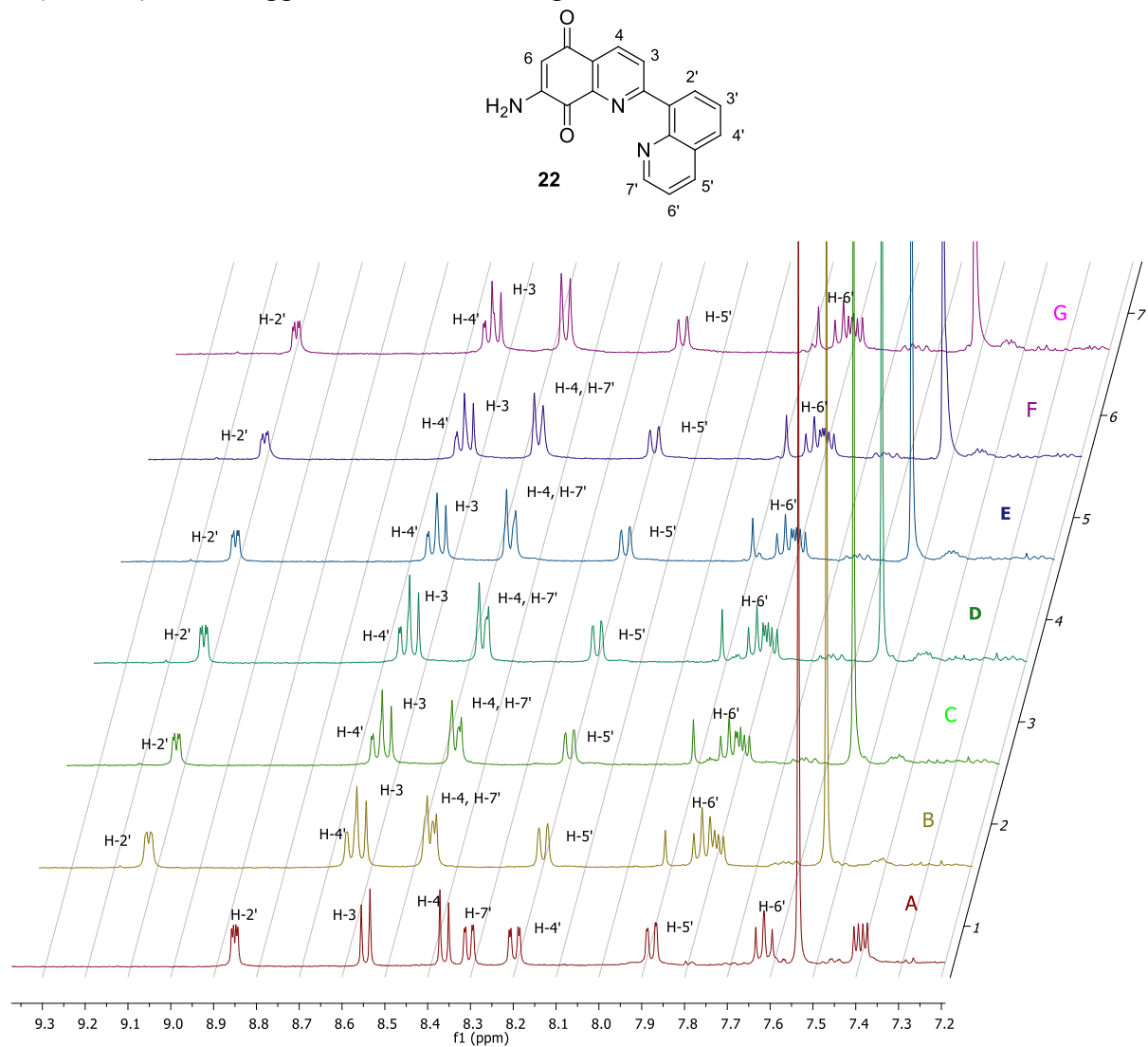


Figure 3. Aromatic protons region NMR spectra of **22** upon addition of increasing equivalent of $\text{Zn}(\text{SO}_3\text{CF}_3)_2$ in $[\text{}^2\text{H}_8]\text{THF}$. Equivalents of Zn^{2+} : A=0, B=1, C=2, D=3, E=4, F=5 and G=10.

In contrast, addition of only one equivalent of $\text{Zn}(\text{SO}_3\text{CF}_3)_2$ to compound **22** caused larger chemical shift variations of all the protons (Table S2 and Figure 3) Increasing the amount of Zn^{2+}

(2-10 equiv.) added to compound **22** made little or no difference in δ afterwards (>0.01 ppm).

This means that the quinoline derivative binds the Zn^{2+} more efficiently than compound **19** and only one equivalent of Zn^{2+} is enough to cause chemical shift variations.

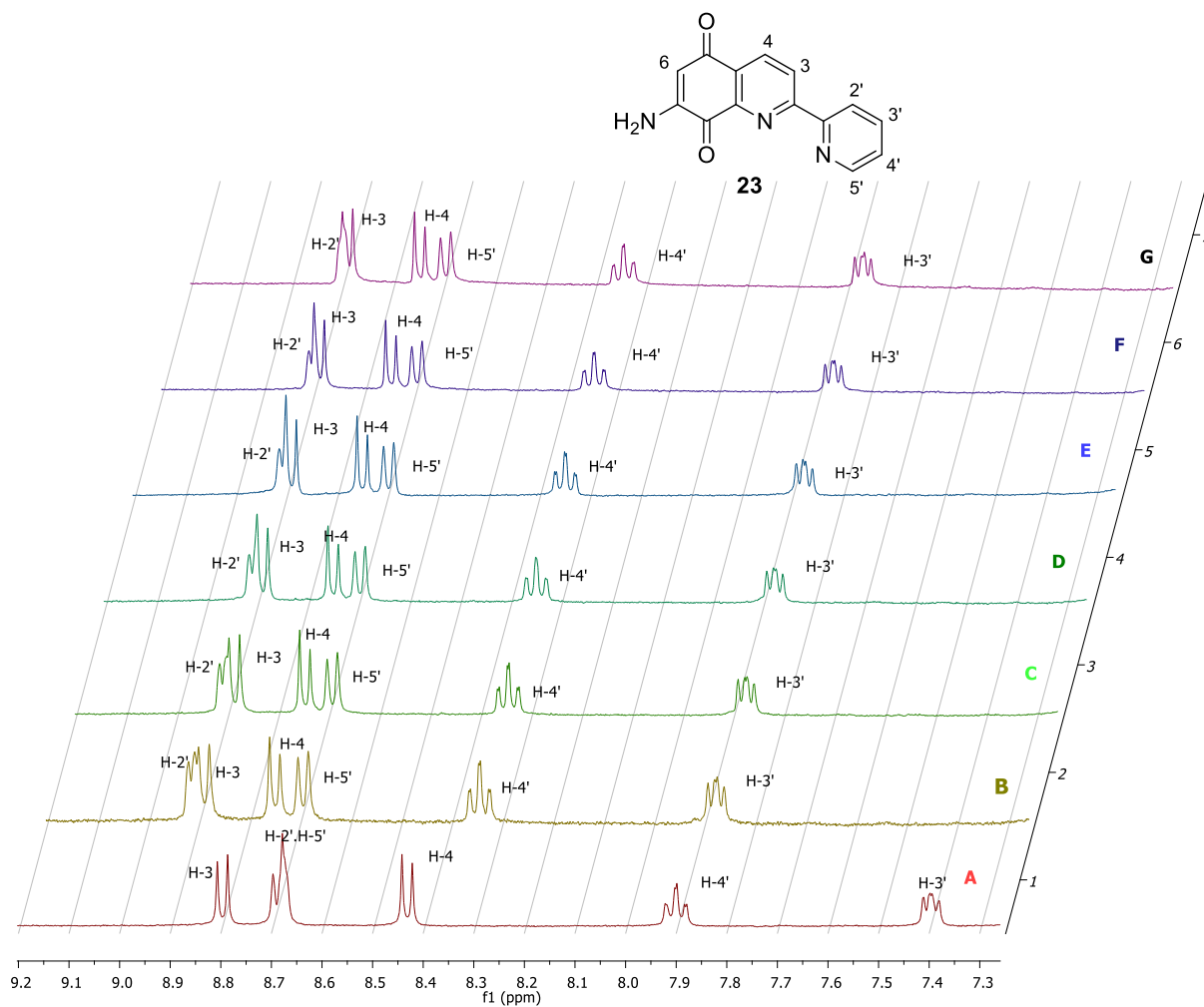


Figure 4. Aromatic proton region NMR spectra of **23** upon addition of increasing equivalent of $Zn(SO_3CF_3)_2$ in $[^2H_8]THF$. Equivalents of Zn^{2+} : A=0, B=1, C=2, D=3, E=4, F=5 and G=10.

Similar observations were made with compounds **23** (Table S3 and Figure 4) and **13** (Table S4). This is consistent with the results reported by Long and Harding²⁵ where they demonstrated that the 1:1 bipyridyl complex of streptonigrin was the major complex formed at room temperature by performing an NMR study in [²H₈]THF with addition of Zn²⁺. Titration of compound **23** with Zn²⁺ in a mixture of dimethylsulfoxide-methanol (1:3) was monitored by a spectrophotometer as reported in literature.²⁶ A plot of $D\lambda_{355}$ against Zn²⁺ concentration gave a moderate affinity constant of $1.41 \times 10^4 \text{ M}^{-1}$ for compound **23** binding with Zn²⁺.

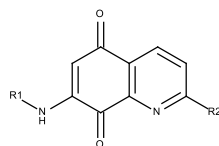
RESULTS AND DISCUSSION

Quinolinequinone metabolism by recombinant human NQO1 was examined using a spectrophotometric assay that employs cytochrome c as the terminal electron acceptor. Initial rates of reduction ($\mu\text{mol cytochrome c reduced/min/mg NQO1}$) were calculated from the linear portion (0-30 s) of the reaction graphs. The 7-acetamido-2-(2-pyridinyl) compound **13** displayed the highest reduction rate by NQO1 (Table 2), although it was the only acetylated analogue with a high reduction rate. In all other cases, 7-amino compounds had much higher reduction rates than corresponding 7-acetamido compounds with identical substituents at the quinoline-2-position. Although unusual, higher rates for acetylated analogues have been observed in other series.^{6, 11} With regard to the aromatic substituents at the quinoline-2-position, no clear trend in

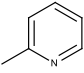
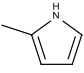
reduction rates was observed except that bulkier groups generally decreased reduction rates.

Oxygen consumption is a measure of the ability of the reduced quinone (hydroquinone) to redox cycle following reduction by NQO1. This could lead to production of toxic reactive oxygen species and ultimately to cell death. Oxygen consumption was measured for select quinolinequinones, and the trend, if not the magnitude, mirrored the reduction rates. (Table 2).

Table 2. Reduction rates^a and oxygen consumption^b as a result of quinoline-5,8-dione metabolism by recombinant human NQO1 and electrochemical reduction potentials vs ferrocene^c. Reduction rates were determined by spectrophotometric cytochrome *c* assay and oxygen uptake by oxygen electrode.



No.	R1	R2	Reduction rate by hNQO1 (μmol cyt <i>c</i> reduced /min/mg NQO1)	Oxygen Consumption ($\mu\text{mol}/\text{min}/\text{mg}$ NQO1)	Reduction Potential ($E_{1/2}(\text{V})$ vs Fc)
9	CH ₃ CO		4.5 +/- 0.5	5.2 +/- 1.0	-1.93 nr ^d
10	CH ₃ CO		25 +/- 4	-	-1.17, -1.92 nr
11	CH ₃ CO		7.0 +/- 0.3	-	-1.18, -1.68, -1.77
13	CH ₃ CO		480 +/- 200	34 +/- 3	-1.90 nr
15	CH ₃ CO		16 +/- 1	-	-1.08, -1.36, -1.58
17	CH ₃ CO		2.8 +/- 0.2	-	-1.10, -1.60, -1.94
18	CH ₃ CO		31 +/- 9	-	-
19	H		78 +/- 7	-	-
20	H		170 +/- 30	-	-1.99 nr
21	H		80 +/- 8	-	-1.84 nr
22	H		18 +/- 6	-	-1.53, -1.65

23	H		71 +/- 13	-	-1.85 nr
24	H		120 +/- 10	8.5 +/- 1.6	-

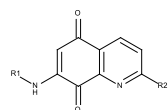
^aSpectrophotometric assay using cytochrome c as terminal electron acceptor (550 nm).

^bOxygen concentration monitored using an oxygen electrode. ^c $E_{1/2}$ values calculated as $(E_{pc}+E_{pa})/2$ are average values from voltammograms recorded potential sweep rate of 50 mV/sec.

E_{pc} = cathodic peak potential; E_{pa} = anodic peak potential. ^dnr = non-reversible, anodic peak only.

Cell survival was measured using the MTT colorimetric assay. In previous work, we demonstrated that IC_{50} values generated from standard clonogenic assays and MTT assays were positively correlated suggesting that the MTT assay is a reliable indicator of cytotoxicity. ⁶ We utilized MDA-MB-468 human breast cancer cells stably transfected with human NQO1 cDNA (MDA468-NQ16) along with the non-transfected wild type cells (MDA468) to compare the cytotoxicity of the quinolinequinones (Table 3).²⁷

Table 3. Cytotoxicity of quinoline-5,8-diones toward MDA468-WT (NQO1-deficient) and MDA468-NQ16 (NQO1-rich) human breast cancer cell lines.



No.	R1	R2	IC ₅₀ (μM)		Selectivity Ratio
			MDA468-WT	MDA468-NQ16	IC ₅₀ (WT)/ IC ₅₀ NQ16
9	CH ₃ CO		1.7 +/- 0.8	2.4 +/- 1.9	0.73
10	CH ₃ CO		3.3 +/- 0.1	6.3 +/- 0.2	0.52
11	CH ₃ CO		0.80 +/- 0.33	0.64 +/- 0.41	1.2
13	CH ₃ CO		0.53 +/- 0.27	2.2 +/- 0.5	0.24
17	CH ₃ CO		7.4 +/- 5.0	19.1 +/- 5.9	0.39
19	H		5.3 +/- 0.8	17 +/- 5	0.31
20	H		5.6 +/- 1.3	15 +/- 2	0.37
21	H		4.8 +/- 0.9	10 +/- 1	0.47
22	H		0.14 +/- 0.02	0.19 +/- 0.04	0.75
23	H		19 +/- 12	5.3 +/- 2.1	3.5
24	H		4.5 +/- 1.9	17 +/- 2	0.26

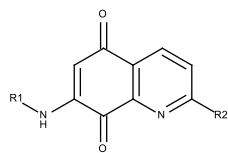
Quinolinequinone cytotoxicity (IC_{50}) to MDA468 cells was generally in the single digit micromolar range following 2-h exposures with some in the high nanomolar range (**11**, **13**, **22**). Surprisingly, selectivity ratios [IC_{50} (MDA468) / IC_{50} (MDA468-NQ16)] were generally <1 meaning that the quinolinequinones were less cytotoxic to the NQO1-rich MDA468-NQ16 cells rather than more cytotoxic. This suggests that NQO1 was protective to the cells rather than functioning as an activating enzyme.²⁷ Only two compounds (**11**, **23**) were selectively cytotoxic to the MDA468-NQ16 cells. The reason for the general absence of selective cytotoxicity with this particular series of compounds is unclear, but it is consistent with NQO1's primary role as a detoxification enzyme.²⁷

Molecular docking of the quinolinequinones in the NQO1 active site was performed using Sybyl 8.1.1 and GOLD 5.1 for scoring. Three good NQO1 substrates (**13**, **20**, **24**) and three poor NQO1 substrates (**9**, **11**, **17**) were docked and scored using ChemPLP and ChemScore (Table 4). The highest scores representing a good fit for the model were found for **20** and **24** consistent with the metabolism data. The exception again was **13**, which scored the lowest, but was the best substrate. Interatomic distances between quinolinequinone carbonyl groups and FAD N5 and His161 were shortest for **20**, but all were within a reasonable distance for hydride transfer from

FAD when the dynamic effects of the quinone-enzyme interaction are considered. Figure 5 shows possible docking conformations for **20** and **11** with NQO1. All quinolinequinones orient with the quinone ring above the FAD isoalloxazine ring as needed for hydride transfer.

The mechanism of action of lavendamycin and streptonigrin is not clearly understood. However previous studies demonstrated that quinone moieties are reduced by NQO1 to the corresponding hydroquinones which undergo auto-oxidation producing activated oxygen species including not only the semiquinone derivatives but also superoxide and hydroxyl radicals.²⁸ In addition, both streptonigrin and lavendamycin chelate divalent cationic metal ions. This property might confer to streptonigrin and lavendamycin the ability to shuttle iron cations into the cells which in turn can catalyze production of reactive oxygen species through a Fenton reaction. On the other hand, this chelation can result in depletion of intracellular cationic metals which might result in cell death.²⁹ Generation of the semiquinone radical, after reduction of the quinone to the hydroquinone followed by auto-oxidation, results in a decrease of activity in 9 compounds. The best NQO1 substrates are less active compounds (**13**, **20**, **24**) in NQO1 expressing cells. In contrast, poor NQO1 substrates such as compound **22** or **11**, exhibit the best activity in both cancer cells expressing NQO1 and not expressing NQO1. According to the NMR experiments, the quinoline derivative **22** and compound **13** binds the Zn^{2+} more efficiently than compound **19**;

and only one equivalent of Zn^{2+} is enough to cause important chemical shift variations. Similar observations were made with compound **23**, which was less cytotoxic than compound **22**. Even though metal chelation by these compounds is still a plausible mechanism to explain their activity against breast cancer cells, another mode of action cannot be discarded. Most active compounds (**11**, **13** and **22**) are potential tridentate ligands for metals. Compound **23** exhibits lower activity than the corresponding acetylated amino analogue **13**. It was proposed that metals can assist tautomeric shift from the active quinone analogues to the quinoid analogue which has an isoelectronic structure with the biologically inactive azastreptonigrin.²⁴ This tautomeric shift can explain the decrease of activity of the amino derivative compared to the amido derivative. In our series of aryl substituted quinonequinolines the active molecule is the quinone derivatives and not the semiquinone derivatives. A similar mode of action than the bidentate metal ligands derivatives 8-hydroxyquinone is currently under investigation.^{30, 31}

Table 4. Computational parameters for selected quinoline-5,8-diones.

No.	R ¹	R ²	ChemPLP	ChemScore	C=O8... NH5 ((Å))	C=O5... His161NE2 (Å)
9	CH ₃ CO		63.2	22.6	3.9	3.6
11	CH ₃ CO		63.8	22.6	4.7	3.3
13	CH ₃ CO		57.6	21.4	4.3	3.5
17	CH ₃ CO		63.8	22.1	4.2	3.3
20	H		72.8	26.0	3.6	3.2
24	H		67.3	22.7	4.1	3.3

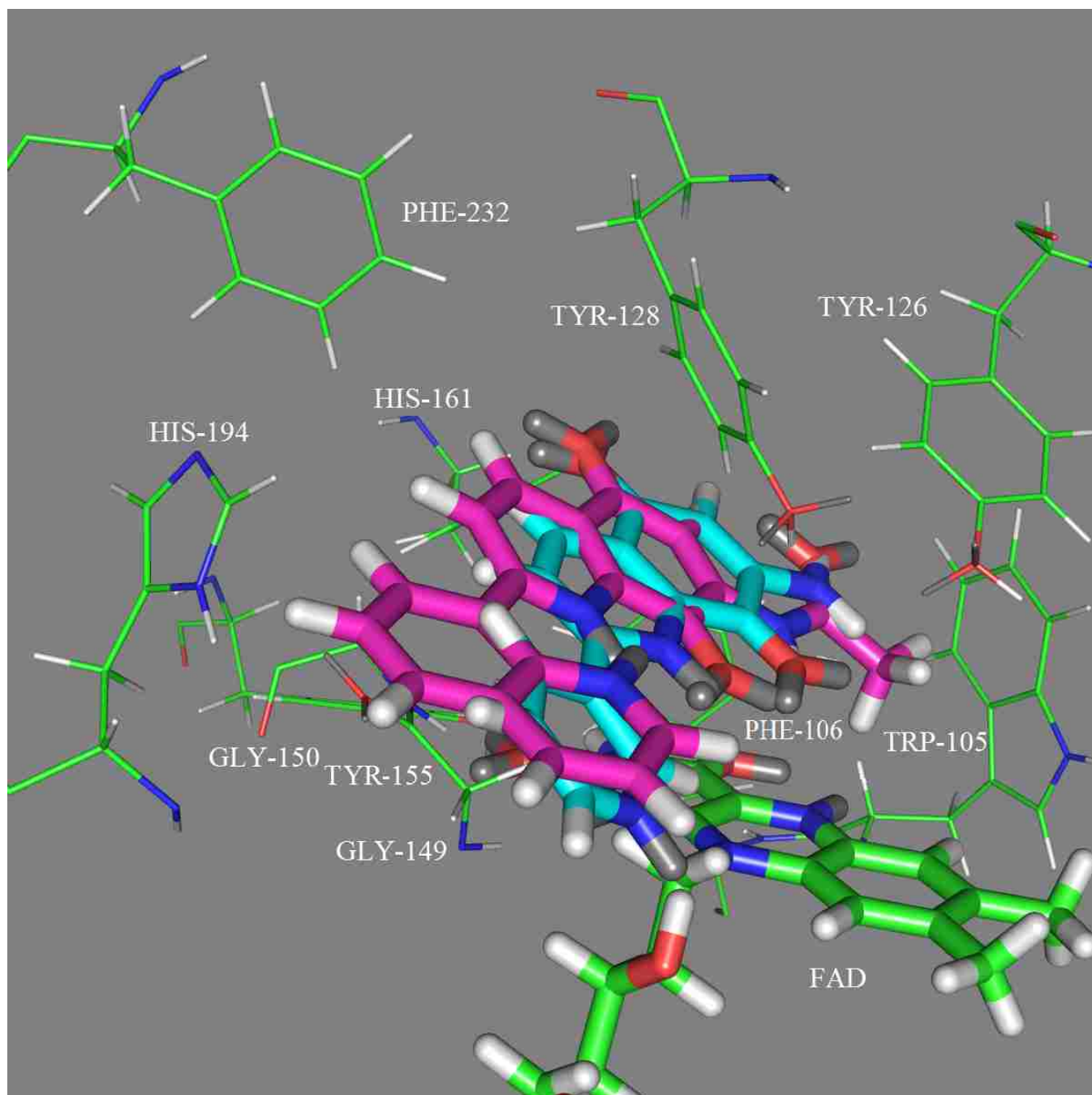


Figure 5. Quinolinequinones docked in NQO1 active site: **20**, cyan; **11**, magenta; FAD, green.

CONCLUSIONS

A six step synthetic scheme led to good yields for quinolinequinone analogs of lavendamycin projected as NQO1-directed antitumor agents. Unexpectedly, ten of eleven analogs demonstrated excellent cytotoxicity (IC₅₀ values of single digit micromolar or better) towards MDA468 breast cancer cells, but only two were selectively cytotoxic to NQO1-expressing MDA468-NQ16 cells. Compounds **22** and **11** are poor NQO1 substrates and exhibit the best activity against breast cancer cells. In our novel series of aryl substituted quinonequinolines the active molecule appears to be the quinone derivatives and not the semiquinone derivatives resulting from NQO1 reduction, suggesting that the mode of action of this novel series differs from lavendamycin and involves an unidentified target. Quinolinequinone derivatives **11**, **13** and **22** cytotoxicities (IC₅₀) to MDA468 cells were in the high nanomolar range. Our results seem to indicate that compounds **11**, **13** and **22** effects could be also, at least partially, mediated by metal chelation. These aryl quinonequinoline derivatives represent a novel promising class of cytotoxic agents with a potential novel therapeutic value.

EXPERIMENTAL SECTION

Cell Culture. MDA-MB-468 (MDA468) human breast cancer cells and stably NQO1-transfected MDA468-NQ16³² were a gift from Dr. David Ross (University of Colorado-Denver, Denver, CO). MDA468 cells had no measurable NQO1 activity whereas activity in MDA468-NQ16 cells was 1070 nmol/min/mg total cell protein using dichlorophenolindophenol (DCPIP) as the standard electron acceptor. Cells were grown in RPMI 1640 medium with L-glutamine and penicillin/streptomycin, and supplemented with 10% fetal bovine serum (FBS). Cell culture medium and supplements were obtained from Invitrogen (Carlsbad, CA). The cells were incubated at 37 °C under a humidified atmosphere containing 5% CO₂.

Spectrophotometric cytochrome c assay. Quinolinequinone reduction was monitored using a spectrophotometric assay in which the rate of reduction of cytochrome c was quantified at 550 nm. Briefly, the assay mixture contained cytochrome c (70 μM), NADH (1 mM), recombinant human NQO1 (0.1-10 μg) (gift from Dr. David Ross, University of Colorado-Denver, Denver, CO) and quinolinequinones (25 μM) in a final volume of 1 mL Tris-HCl (25 mM, pH 7.4) containing 0.7 mg/mL BSA and 0.1% Tween-20. Reactions were carried out at room temperature and started by the addition of NADH. Rates of reduction were calculated from the initial linear part of the reaction curve (0-30 s) and results were expressed in terms of μmol of

cytochrome c reduced/min/mg of NQO1 using a molar extinction coefficient of $21.1 \text{ mM}^{-1} \text{ cm}^{-1}$ for cytochrome c. All reactions were carried out at least in triplicate.

Oxygen Consumption. Oxygen concentration was monitored using a MI-730 Micro-Oxygen Electrode (Microelectrodes, Bedford, NH) with concentrations adjusted for temperature ($25 \text{ }^{\circ}\text{C}$). Assay mixtures contained $25 \text{ }\mu\text{M}$ quinone/quinones, $200 \text{ }\mu\text{M}$ NADH and $1 \text{ }\mu\text{g/mL}$ NQO1 in a 2 mL Tris-HCl-BSA/Tween (0.1%) buffer system. Reactions were started with NADH and measured over 3 minute intervals at room temperature. All reactions were carried out in triplicate.

Electrochemistry. Cyclic Voltammograms were collected for 10 analogues using a BAS CV-50W electrochemical analyzer using a standard 3 electrode cell. Experiments were performed using an Ag/AgCl reference electrode, a glossy carbon working electrode and a platinum wire auxiliary electrode. The reported potentials are referenced by the Ferrocene (0/+) couple in the solvent used, primarily THF, which occurs at $+0.60\text{V}$ vs. Ag/AgCl. The compounds were run at concentrations of 1mM in THF, except compound 15 which was run in DMSO, with a 0.1M concentration of tetrabutylammonium hexafluorophosphate as a supporting electrolyte. All samples were purged and run under an Ar atmosphere during the course of the experiment, and the electrodes were washed and wiped down between each sample. Each CV was collected at a

sweep rate of 50mV/s in the potential range of 0V to -2V at room temperature of 21°C.

NMR spectroscopy. One-dimensional ^1H NMR spectra were recorded at room temperature on Bruker Avance IIIITM spectrometer (The Woodlands, Texas) at 400 MHz using a 5-mm probe and a simple pulse-acquire sequence. Acquisition parameters consisted of spectral width of 4000 Hz with an acquisition time 3.98 s, number of scans of 128, and relaxation delay of 1 s.

Complexes were prepared in a mixture of CDCl_3 and THF-D_8 .

Cell Viability Assay. Growth inhibition was determined using the MTT colorimetric assay. Cells were plated in 96-well plates at a density of 10,000 cells/mL and allowed to attach overnight (16 h). Quinolinequinone solutions were applied in medium for 2 hours, removed and replaced with fresh medium, and the plates were incubated at 37 °C under a humidified atmosphere containing 5% CO_2 for 3-5 days. MTT (50 μg) was added and the cells were incubated for another 4 hours. Medium/MTT solutions were removed carefully by aspiration, the MTT formazan crystals were dissolved in 100 μL DMSO, and absorbance was determined on a plate reader at 560 nm. IC_{50} values (concentration at which cell survival equals 50% of control) were determined from semi-log plots of percent of control vs. concentration. Selectivity ratios were defined as the IC_{50} value for the MDA468 cell line divided by the IC_{50} value for the MDA468-NQ16 cell line.

Molecular Modeling. For docking purposes, the crystallographic coordinates of the human NQO1 complex with 3-(hydroxymethyl)-5-(2-methylaziridin-1-yl)-1-methyl-2-phenylindole-4,7-dione (**25**) were obtained from the Brookhaven Database (PDB code 1H69³³ and resolution 1.86Å) and was edited accordingly to provide a monomer of the protein. The protein complex was then minimized within Sybyl 7.3 (Tripos Ltd., St Louis) while holding all heavy atoms stationary. The ligand was then removed to leave the receptor complex which was used for the subsequent docking studies. For preparation of ligand structures, fragments from Sybyl 8.1.1 were used to construct the compounds and all symmetric compounds were prepared as monoanionic ligands. Ligands were subject to 1000 iterations of energy minimization using the Powell method with MMFF94s force field standard method. For computational docking, the GOLD 5.1 software was used in combination with the ChemPLP³⁴ scoring function (rescoring with ChemScore.³⁵ The active site was defined as being any volume within 8Å of the quinone scaffold of **25** in its crystal pose in 1H69. Each GA run comprised using the default parameters of: 100000 genetic operations on an initial population of 100 members divided into five subpopulations with weights for crossover, mutation, and migration being set to 95, 95, and 10, respectively. GOLD allows a user-definable number of GA runs per ligand, each of which starts from a different orientation. For these experiments, the number of GA runs was set to 10, and

scoring of the docked poses was performed with the ChemPLP scoring function using ChemScore rescore. Each GOLD run was saved and the strongest scoring binding pose of each ligand (subject to a rmsd default distance threshold of 1.5Å) was compared to that of the reference ligand position observed in the crystal structure. The best output pose (orientations) of the ligands generated were analyzed based on its ChemPLP/ChemScore score, feasibility of hydride transfer process and H-bonding to the enzyme. The best pose(s) were visualized using PyMOL Molecular Graphics System version 1.3.

Chemistry. All moisture sensitive reactions were performed in an inert, dry atmosphere of argon in flame dried glassware. Air sensitive liquids were transferred via syringe or cannula through rubber septa. Reagent grade solvents were used for extraction and flash chromatography. THF was distilled from Na/benzophenone under argon; dichloromethane (CH₂Cl₂) and chloroform (CHCl₃) were distilled from CaH₂ under argon. All other reagents and solvents which were purchased from commercial sources, were used directly without further purification. The progress of reactions was checked by analytical thin-layer chromatography (Sorbent Technologies, Silica G TLC plates w/UV 254). The plates were visualized first with UV illumination followed by charring with ninhydrin (0.3% ninhydrin (w/v), 97:3 EtOH-AcOH). Flash column chromatography was performed using prepacked Biotage SNAP cartridges on a

Biotage Isolera One instrument. Microwave reactions were performed using a Biotage Initiator instrument. The solvent compositions reported for all chromatographic separations are on a volume/volume (v/v) basis. ^1H NMR spectra were recorded at 400 or 500 MHz and are reported in parts per million (ppm) on the δ scale relative to tetramethylsilane as an internal standard. ^{13}C NMR spectra were recorded at 100 or 125 MHz and are reported in parts per million (ppm) on the δ scale relative to CDCl_3 (δ 77.00). Melting points were determined on a Stuart melting point apparatus from Bibby Scientific Limited and are uncorrected. High Resolution mass spectrometry (HRMS) was performed on a Waters/Micromass LCT-TOF instrument. All compounds were more than 95% pure.

5-chloro-8-hydroxy-7-nitroquinoline (1). This compound was prepared according to the literature ¹² procedure to yield a yellow solid, 4.40 g (79%). M.p. 198-200°C, [lit. ¹², m.p. 192-194°C]; ^1H NMR (500 MHz, DMSO) δ 9.09 (dd, $J = 4.2, 0.5$ Hz, 1H), 8.58 (dd, $J = 8.5, 0.8$ Hz, 1H), 8.18 (s, 1H), 7.94 (dd, $J = 8.5, 4.3$ Hz, 1H). ^{13}C NMR (126 MHz, DMSO) δ 150.5, 150.1, 139.9, 133.6, 132.3, 128.5, 125.9, 122.0, 117.9. HRMS (TOF MS ES+) for $\text{C}_9\text{H}_6\text{ClN}_2\text{O}_3^+$ (MH+) calcd. 225.0067, found 225.0055.

7-Amino-8-hydroxyquinoline (2). Compound **1** (2.4 g, 10.69 mmol) was placed in a hydrogenation apparatus equipped with a magnetic stir bar and methanol added. Pd/C (150 mg)

in a small amount of MeOH (60 mL) was added and stirring commenced. H₂ gas was introduced at a pressure of 40-50 psi and reacted at rt overnight. TLC showed full conversion. The black solution was filtered using a celite pad and concentrated under reduced pressure to yield **2** as a black oil, 99% yield. ¹H NMR (500 MHz, CDCl₃) δ 8.66 (dd, *J* = 4.4, 1.6 Hz, 1H), 8.03 (dd, *J* = 8.2, 1.6 Hz, 1H), 7.24 (d, *J* = 8.7 Hz, 1H), 7.17 (dd, *J* = 8.2, 4.4 Hz, 1H), 7.10 (d, *J* = 8.7 Hz, 1H). ¹³C NMR (126 MHz, CDCl₃) δ 148.0, 137.9, 136.6, 136.1, 132.1, 122.4, 119.3, 118.5, 117.7. HRMS (TOF MS ES+) for C₉H₉N₂O⁺ (MH⁺) calcd. 161.0715, found 161.0707.

7-acetamido-8-acetyloxyquinoline (3). Compound **2** (330 mg, 2.06 mmol) was dissolved in dried THF (10 mL) and DIEA added with stirring. AcCl (176 μL) in 1mL THF was added drop wise while stirring and reacted at rt for 2 hrs. Then concentrated under reduced pressure followed by redissolving in CH₂Cl₂ (20 mL) and water (10 mL). The two layers were allowed to partition and extracted 2x 20 mL CH₂Cl₂. The combined organic layers were dried over MgSO₄, filtered and concentrated under reduced pressure. Then purified on a Biotage SNAP cartridge (25 g) at a flow rate of 25 mL/min to yield an orange solid, 382 mg (76%); m.p. 151-153°C; ¹H NMR (500 MHz, CDCl₃) δ 8.85 (dd, *J* = 4.1, 1.3 Hz, 1H), 8.49 (d, *J* = 9.1 Hz, 1H), 8.13 (dd, *J* = 8.3, 1.5 Hz, 1H), 7.70 (d, *J* = 9.1 Hz, 1H), 7.67 (s, 1H), 7.36 (dd, *J* = 8.2, 4.2 Hz, 1H), 2.56 (s, 1H), 2.04 (s, 1H); ¹³C NMR (126 MHz, CDCl₃) δ 169.7, 168.5, 150.6, 140.7, 135.8, 134.9, 130.8, 125.8, 125.6,

121.3, 120.6, 24.5, 21.0; HRMS (TOF MS ES+) for $C_{13}H_{13}N_2O_3^+$ (MH+) calcd. 245.0926, found 245.0923.

7-acetamido-8-benzyloxyquinoline (4). To a solution of **3** (1.2 g, 4.91 mmol) in MeOH (100 mL) was added water (10 mL) and the reaction stirred under reflux for 1 hr. The black solution was concentrated and in vacuo and flash chromatographed on a KP-Sil 100 g Biotage SNAP cartridge using MeOH: DCM as the solvent (0-5% MeOH). A white solid (0.9 g) obtained and used for the next step directly. $R_f = 0.11$ (5% MeOH:CH₂Cl₂).

To a solution of 7-acetamido-8-hydroxyquinoline (2.27 g, 11.23 mmol) in 40 mL DMF was added K₂CO₃ (2.33 g, 16.80 mmol) and BnBr (2 mL, 16.80 mmol) respectively. The reaction was stirred at 50°C for 24 hrs after which TLC showed almost all the starting material was consumed. The reaction mixture was diluted with 30 mL CH₂Cl₂, filtered with a pad of celite and concentrated under reduced pressure. The residue was loaded onto a 100 g Biotage SNAP cartridge by dissolving in a small amount of CH₂Cl₂ and eluted with EtOAc:heptane gradient (0-50%). Yield 2.95 g (90%) of a yellow oil was obtained. $R_f = 0.50$ (60% EtOAc:heptane). ¹H NMR (500 MHz, CDCl₃) δ 8.95 (dd, $J = 4.2, 1.7$ Hz, 1H), 8.58 (d, $J = 9.0$ Hz, 1H), 8.14 (dd, $J = 8.3, 1.7$ Hz, 1H), 7.77 (s, 1H), 7.57 (d, $J = 9.0$ Hz, 1H), 7.40 – 7.35 (m, 6H), 5.49 (s, 2H), 1.93 (s, 4H). ¹³C NMR (126 MHz, CDCl₃) δ 168.3, 150.0, 142.0, 141.0, 137.4, 136.2, 132.0, 128.9,

128.8, 128.8, 126.0, 124.0, 120.0, 120.0, 77.3, 24.6. HRMS (TOF MS ES+) for $C_{18}H_{17}N_2O_2^+$ (MH+) calcd. 293.1290, found 293.1264.

7-acetamido-8-(benzyloxy)quinoline-1-oxide (5). The starting material (**4**) (428 mg, 1.46 mmol) was dissolved in 4.3 mL 1,2-dichloroethane with stirring. The *m*CPBA (340 mg, 1.76 mmol) was added (0.5 M) and the reaction stirred at rt for 48 hrs. TLC showed almost all the starting material was consumed. The precipitated *m*CPBA was filtered and washed with 5 mL 1, 2-dichloroethane. The filtrate was concentrated under reduced pressure and flash chromatographed on a KP-sil 100 g Biotage SNAP cartridge using a 5% MeOH: DCM gradient at a flow rate of 25 mL/min to yield a yellow solid, 373 mg (82%). M.p. 145-147°C; R_f 0.24 (5%MeOH:DCM). 1H NMR (500 MHz, DMSO) δ 9.45 (s, 1H), 8.46 (d, $J = 6.1$ Hz, 1H), 8.20 (d, $J = 8.9$ Hz, 1H), 7.81 (d, $J = 8.3$ Hz, 1H), 7.77 (d, $J = 9.0$ Hz, 1H), 7.58 – 7.50 (2H), 7.40 – 7.30 (aromatic, 4H). ^{13}C NMR (126 MHz, DMSO) δ 168.9, 139.8, 138.1, 137.1, 136.4, 133.3, 129.8, 129.1, 128.1, 128.0, 124.7, 124.4, 120.8, 77.7, 23.8. HRMS (TOF MS ES+) for $C_{18}H_{17}N_2O_3^+$ (MH+) calcd. 309.1239, found 309.1227.

7-acetamido-8-benzyloxy-2-chloroquinoline (6). Phosphoryl chloride (280 μ L, 3.0 mmol) in $CHCl_3$ (1.0 mL) was added to a stirred solution of the oxide **5** (770 mg, 2.50 mmol) in 21 mL $CHCl_3$ and stirred for 15 min. The mixture was then refluxed for 2 hrs, cooled and poured into

ice (50 g) and the pH adjusted to 12 with NaOH (aq.). The aq. layer was extracted with 2 x 50 mL CH₂Cl₂, washed with 2 x 20 mL H₂O, dried over MgSO₄, filtered and concentrated under reduced pressure to yield a brown oil. Then purified on a HP-Sil 25 g Biotage SNAP cartridge using EtOAc:heptane gradient (0-50%) as the solvent. Yield 504 mg (62%) of an off-white solid was obtained. R_f = 0.58 (60% EtOAc:heptane); M.P. 92-94°C; ¹H NMR (500 MHz, CDCl₃) δ 8.60 (d, *J* = 9.0 Hz, 1H), 8.06 (d, *J* = 8.5 Hz, 1H), 7.81 (s, 1H), 7.54 (d, *J* = 9.0 Hz, 1H), 7.45 – 7.35 (m, 1H), 7.32 (d, *J* = 8.5 Hz, 1H), 5.48 (s, 1H), 1.96 (s, 1H). ¹³C NMR (126 MHz, CDCl₃) δ 168.4, 150.5, 141.4, 140.3, 139.0, 137.2, 133.0, 128.9, 128.8, 128.8, 124.3, 123.3, 121.1, 120.1, 77.4, 24.7. HRMS (TOF MS ES+) for C₁₈H₁₆ClN₂O₂⁺ (MH⁺) calcd. 327.0900, found 327.0936.

7-acetamido-2-chloro-8-hydroxyquinoline (7). To a solution of **6** (330 mg, 1.01 mmol) in CH₂Cl₂ (10.1 mL) under an Ar atmosphere was added BCl₃•SMe₂ (10.1 mL) via a syringe and stirred at rt overnight. TLC showed the reaction was complete. The reaction was then quenched with saturated NaHCO₃(aq.) and extracted with 2x20 mL CH₂Cl₂. The organic layers were combined, dried over MgSO₄, filtered and concentrated under reduced pressure. The residue was purified on 50 g KP-Sil Biotage SNAP cartridge using a MeOH: CH₂Cl₂ gradient (0-5% MeOH) at a flow rate of 25 mL/minute to give a yellow solid, 198 mg (82%). M.P. 176-178°C; R_f = 0.50 (5% MeOH:CH₂Cl₂). ¹H NMR (400 MHz, CDCl₃) δ 8.60 (d, *J* = 9.0 Hz, 1H), 8.05 (d, *J* = 8.5

Hz, 1H), 7.82 (brs, 1H), 7.72 (s, 1H), 7.35 (d, $J = 9.0$ Hz, 1H), 7.30 (d, $J = 8.5$ Hz, 1H), 2.29 (s, 3H). ^{13}C NMR (101 MHz, CDCl_3) δ 168.6, 149.7, 138.9, 138.2, 137.1, 124.4, 123.3, 121.5, 121.3, 118.0, 24.9. HRMS (TOF MS ES+) for $\text{C}_{11}\text{H}_{10}\text{ClN}_2\text{O}_2^+$ (MH+) calcd. 237.0431, found 237.0424.

7-Acetamido-2-chloroquinoline-5,8-dione (8). To a solution of **7** (300 mg, 1.27 mmol) in acetone (30 mL) was added a solution of Fremy's salt in NaH_2PO_4 buffer (0.3 M, 30 mL) and the mixture stirred at rt for 1 hr. A further solution of Fremy's salt in the buffer (0.3M, 30 mL) was added and stirring continued for 2 hrs. The acetone was removed under reduced pressure and the residue extracted with 2 x 50 mL CH_2Cl_2 . The CH_2Cl_2 phases were combined, dried over MgSO_4 and concentrated under reduced pressure. The residue was purified on a 25 g HP-Sil Biotage SNAP cartridge using EtOAc:heptanes gradient (0-60%) to obtain a yellow solid, 225 mg (71% over 2 steps); m.p. 224-226°C (decomposes into a black mass), $R_f = 0.49$ (60% EtOAc:heptane). ^1H NMR (500 MHz, CDCl_3) δ 8.41 (s, 1H), 8.39 (d, $J = 8.2$ Hz, 1H), 7.97 (s, 1H), 7.74 (d, $J = 8.2$ Hz, 1H), 2.34 (s, 3H). ^{13}C NMR (126 MHz, CDCl_3) δ 183.4, 178.1, 169.5, 156.7, 145.9, 140.4, 137.2, 129.9, 128.0, 116.3, 25.1. HRMS (TOF MS ES+) for $\text{C}_{11}\text{H}_8\text{ClN}_2\text{O}_3^+$ (MH+) calcd. 251.0223, found 250.0203.

General procedure for Suzuki coupling under microwave conditions. The 7-acetamido-2-chloroquinoline-5,8-dione **8** (21 mg, 0.08 mmol) was dissolved in 4 mL dimethoxyethane (DME) and degassed under reduced pressure. The palladium (0) catalyst, Pd(PPh₃)₄ (10 mg, 0.084 mmol) was added and the solution degassed further. The mixture was stirred under Ar atmosphere for 10 minutes. Na₂CO₃ solution (0.2 mL, 2.0 M) was added followed by the boronic acid (0.126 mmol). The mixture was then heated using a Biotage microwave initiator at 110-140°C for 20 minutes. After cooling, TLC showed all the starting material was consumed. The reaction mixture was poured into DCM and washed with 2 x 10 mL water. Then dried over MgSO₄, filtered and concentrated under reduced pressure. The residue was purified on HP-Sil 25 g Biotage SNAP cartridge using EtOAc:heptane gradient (0-50%) at a flow rate of 20 mL/min. For very polar products, MeOH:CH₂Cl₂ (0-10%MeOH) was used as solvent for purification.

7-acetamido-2-(4-(trifluoromethyl)phenyl)quinoline-5,8-dione (9). Yield 21 mg (70%) of a yellow solid was obtained. R_f = 0.47 (50% EtOAc:heptane); m.p. 250°C(decomposes); ¹H NMR (500 MHz, CDCl₃) δ 8.53 (d, *J* = 8.2 Hz, 1H), 8.45 (s, 1H), 8.27 (d, *J* = 8.1 Hz, 2H), 8.17 (d, *J* = 8.2 Hz, 1H), 7.99 (s, 1H), 7.80 (d, *J* = 8.2 Hz, 2H), 2.35 (s, 4H). ¹³C NMR (126 MHz, CDCl₃) δ 184.1, 179.1, 169.5, 160.1, 146.1, 140.6, 135.7, 128.3, 128.0, 126.0, 126.0, 126.0, 125.3, 116.5, 25.2; HRMS (TOF MS ES⁺) for C₁₈H₁₂F₃N₂O₃⁺(MH⁺) calcd. 361.0800, found 361.0834.

7-acetamido-2-(3-pyridinyl)quinoline-5,8-dione (10). Yield 21 mg (41%) of a yellow solid obtained, $R_f = 0.19$ (5% MeOH:DCM); m.p. $>300^\circ\text{C}$ (decomposes); ^1H NMR (500 MHz, CDCl_3) δ 9.29 (s, 1H), 8.72 (d, $J = 3.9$ Hz, 1H), 8.56 (d, $J = 8.2$ Hz, 1H), 8.55 (m, 1H), 8.21 (d, $J = 8.2$ Hz, 1H), 8.00 (s, 1H), 7.56 (dd, $J = 8.0, 4.9$ Hz, 1H), 2.35 (s, 3H). ^{13}C NMR (126 MHz, CDCl_3) δ 184.2, 179.0, 170.4, 158.9, 150.7, 148.1, 146.1, 140.9, 135.7, 135.7, 128.1, 125.3, 116.6, 24.6; HRMS (TOF MS ES+) for $\text{C}_{16}\text{H}_{12}\text{N}_3\text{O}_3^+\text{MH}^+$ calcd. 294.0879, found 294.0914. *7-amino-2-(3-pyridinyl)quinoline-5,8-dione*: 6 mg (12%) of a red solid was obtained. $R_f = 0.13$ (5% MeOH:DCM); m.p. $195\text{-}197^\circ\text{C}$ (decomposes, turns black); ^1H NMR (500 MHz, CDCl_3) δ 9.29 (d, $J = 1.7$ Hz, 1H), 8.67 (dd, $J = 4.9, 1.4$ Hz, 1H), 8.58 (ddd, $J = 8.0, 2.2, 1.7$ Hz, 1H), 8.52 (d, $J = 8.2$ Hz, 1H), 8.22 (d, $J = 8.2$ Hz, 1H), 7.59 (ddd, $J = 8.0, 4.9, 0.7$ Hz, 1H), 6.07 (s, 1H). ^{13}C NMR (126 MHz, CDCl_3) δ 181.9, 179.8, 157.0, 150.4, 149.6, 147.6, 146.3, 135.4, 135.0, 133.5, 129.4, 124.7, 123.8, 102.1. HRMS (TOF MS ES+) for $\text{C}_{14}\text{H}_{10}\text{N}_3\text{O}_2^+\text{MH}^+$ calcd. 252.0773, found 252.0795.

7-acetamido-2-(8'-quinolinyl)quinoline-5,8-dione (11). Yield 31 mg (51%) of a yellow solid was obtained. $R_f = 0.25$ (70% EtOAc:heptane), crystallized from MeOH/ CH_2Cl_2 ; m.p. 295°C (decomposes); ^1H NMR (500 MHz, CDCl_3) δ 8.93 (dd, $J = 4.2, 1.8$ Hz, 1H), 8.53 (d, $J = 8.1$ Hz, 1H), 8.48 (d, $J = 8.1$ Hz, 1H), 8.34 (dd, $J = 8.3, 1.8$ Hz, 1H), 8.22 (dd, $J = 7.2, 1.4$ Hz, 1H), 8.04

(dd, $J = 8.2, 1.4$ Hz, 1H), 8.00 (s, 1H), 7.76 (dd, $J = 8.1, 7.3$ Hz, 1H), 7.54 (dd, $J = 8.3, 4.2$ Hz, 1H), 2.34 (s, 3H). ^{13}C NMR (126 MHz, CDCl_3) δ 184.8, 179.1, 170.9, 161.9, 150.5, 145.7, 145.1, 140.9, 136.7, 136.5, 133.3, 131.9, 131.7, 130.2, 128.4, 127.6, 126.3, 121.4, 116.5, 24.2. HRMS (TOF MS ES+) $\text{C}_{20}\text{H}_{14}\text{N}_3\text{O}_3^+$ (MH+) calcd. 344.1035, found 344.1022.

7-acetamido-2-(2-(1-tert-butoxycarbonylindolyl))quinoline-5,8-dione (12). Yield 63mg (67%) of an orange was obtained. $R_f = 0.40$ (50% EtOAc:heptane); m.p. 191-193°C (decomposes); ^1H NMR (500 MHz, CDCl_3) δ 8.47 (s, 1H), 8.45 (d, $J = 8.1$ Hz, 1H), 8.15 (d, $J = 8.4$ Hz, 1H), 7.97 (s, 1H), 7.89 (d, $J = 8.1$ Hz, 1H), 7.60 (d, $J = 7.8$ Hz, 1H), 7.40 (t, $J = 7.8$ Hz, 1H), 7.27 (dd, $J = 9.1, 5.9$ Hz, 1H), 6.98 (s, 1H), 2.33 (s, 3H), 1.41 (s, 9H). ^{13}C NMR (126 MHz, CDCl_3) δ 184.2, 179.0, 169.6, 157.4, 149.7, 145.3, 140.4, 138.1, 137.5, 134.2, 128.6, 127.9, 127.6, 126.0, 123.3, 121.5, 116.5, 115.2, 114.0, 84.2, 27.8, 25.1. HRMS (TOF MS ES+) $\text{C}_{24}\text{H}_{22}\text{N}_3\text{O}_5^+$ (MH+) calcd. 432.1559, found 432.1568.

7-acetamido-2-(2-pyridinyl)quinoline-5,8-dione (13). Yield 37 mg (71%) of a yellow solid was obtained. $R_f = 0.19$ (5% MeOH: CH_2Cl_2), crystallized from MeOH/ CH_2Cl_2 ; m.p. 255-258°C (decomposes); ^1H NMR (500 MHz, DMSO) δ 10.08 (s, 1H), 8.78 (ddd, $J = 4.8, 1.6, 0.8$ Hz, 1H), 8.53 (d, $J = 7.9$ Hz, 1H), 8.46 (d, $J = 8.2$ Hz, 1H), 8.08 (td, $J = 7.7, 1.8$ Hz, 1H), 7.77 (s, 1H), 7.58 (ddd, $J = 7.5, 4.7, 1.1$ Hz, 1H), 2.28 (s, 3H). ^{13}C NMR (126 MHz, DMSO) δ 184.6, 178.4,

171.5, 158.6, 153.6, 149.8, 146.4, 142.5, 137.8, 135.0, 128.5, 125.5, 124.6, 121.7, 115.3, 24.7.

HRMS (TOF MS ES+) $C_{16}H_{12}N_3O_3^+$ (MH+) calcd. 294.0879, found 294.0914.

7-acetamido-2-(2-(1-tert-butoxycarbonylpyrrolyl))quinoline-5,8-dione (14). Yield 36 mg (53%)

of a yellow solid was obtained. R_f = 0.30 (50% EtOAc:heptane); m.p. 191-193°C (decomposes),

recrystallized from methanol; 1H NMR (500 MHz, $CDCl_3$) δ 8.42 (s, 1H), 8.39 (d, J = 8.2 Hz,

1H), 7.95 (s, 1H), 7.79 (d, J = 8.2 Hz, 1H), 7.42 (dd, J = 3.2, 1.7 Hz, 1H), 6.64 (dd, J = 3.4, 1.7

Hz, 1H), 6.29 (t, J = 3.3 Hz, 1H), 2.32 (s, 3H), 1.43 (s, 9H). ^{13}C NMR (126 MHz, $CDCl_3$) δ

184.3, 179.2, 169.5, 156.9, 148.8, 145.3, 140.3, 134.0, 132.5, 128.0, 127.3, 125.5, 118.6, 116.4,

111.2, 84.4, 27.7, 25.1. HRMS (TOF MS ES+) $C_{20}H_{20}N_3O_5^+$ (MH+) calcd. 382.1403, found

382.1381.

7-acetamido-2-(4-pyrazolyl)quinoline-5,8-dione (15). Yield 31 mg (42%) of a brown solid was

obtained. R_f = 0.33 (5% MeOH: CH_2Cl_2); m.p. 270°C (decomposes), recrystallized from

methanol; 1H NMR (500 MHz, DMSO) δ 13.34 (s, 1H), 9.97 (s, 1H), 8.55 (s, 1H), 8.25 (d, J =

8.2 Hz, 1H), 8.21 (s, 1H), 8.11 (d, J = 8.2 Hz, 1H), 7.69 (s, 1H), 2.26 (s, 3H). ^{13}C NMR (126

MHz, DMSO) δ 184.6, 178.6, 171.4, 156.1, 146.6, 142.1, 134.2, 126.1, 123.8, 121.2, 115.1, 24.6.

HRMS (TOF MS ES+) $C_{14}H_{11}N_4O_3^+$ (MH+) calcd. 283.0831, found 283.0846.

7-acetamido-2-(3-(2-acetamido-pyridinyl))quinoline-5,8-dione (16). The quinone **8** (71 mg, 0.28 mmol) was dissolved in 2 mL 1,4-dioxane and degassed under reduced pressure. PdCl₂(dppf) (20 mg), K₃PO₄ (238 mg) and the boronate were added and the solution degassed further. The mixture was stirred under Ar atmosphere for 10 minutes. The mixture was then heated using a Biotage microwave initiator at 120°C for 30 minutes. After cooling, the reaction mixture was poured into CH₂Cl₂ and washed with 2 x 10 mL water and extracted 2x 30 mL DCM. The combined organic phases were dried over MgSO₄, filtered and concentrated under reduced pressure. The residue was purified on a HP-Sil 25 g Biotage SNAP cartridge using MeOH:CH₂Cl₂ gradient (0-5%) at a flow rate of 20 mL/min. Yield 23mg (23%) of a brown solid was obtained. R_f = 0.32 (5% MeOH:CH₂Cl₂); m.p. 249°C (decomposes); ¹H NMR (500 MHz, DMSO) δ 10.82 (s, 1H), 10.04 (s, 1H), 9.17 (d, *J* = 2.5 Hz, 1H), 8.60 (dd, *J* = 8.8, 2.5 Hz, 1H), 8.45 (d, *J* = 8.3 Hz, 1H), 8.38 (d, *J* = 8.2 Hz, 1H), 8.27 (d, *J* = 8.8 Hz, 1H), 7.75 (s, 1H), 2.28 (s, 3H), 2.14 (s, 3H). ¹³C NMR (126 MHz, DMSO) δ 184.6, 178.5, 171.5, 169.7, 157.4, 153.6, 147.3, 146.6, 142.4, 137.0, 134.8, 128.0, 127.2, 124.1, 115.3, 113.0, 24.7, 24.0. HRMS (TOF MS ES+) C₁₈H₁₅N₄O₄⁺ (MH⁺) calcd. 351.1093, found 351.1064.

7-acetamido-2-(2-indolyl)quinoline-5,8-dione (17). The starting material **12** (39 mg, 0.09 mmol) was dissolved in 2.5 mL CH₂Cl₂ and cooled to 0°C using an ice bath. Trifluoroacetic acid (140

mL) was added dropwise and reacted at rt for 2 hrs. TLC showed full conversion. Then quenched with sat. NaHCO₃ (10 mL) and extracted 2x20 mL CH₂Cl₂. The organic layers were combined, dried over MgSO₄, filtered and concentrated under reduced pressure. The residue was purified on a HP-Sil 25 g Biotage SNAP cartridge using EtOAc:heptane gradient (0-70%) at a flow rate of 20 mL/min. Yield 17 mg (59%) of a red solid was obtained after recrystallization from MeOH. M.p. 185°C, decomposes; R_f = 0.38 (70% EtOAc:heptane). ¹H NMR (500 MHz, CDCl₃) δ 8.35 (d, *J* = 8.3 Hz, 1H), 8.14 (d, *J* = 8.3 Hz, 1H), 7.92 (s, 1H), 7.67 (d, *J* = 8.0 Hz, 1H), 7.49 (d, *J* = 8.3 Hz, 1H), 7.29 (t, *J* = 7.6 Hz, 1H), 7.23 (s, 1H), 7.13 (t, *J* = 7.4 Hz, 1H), 2.34 (s, 3H). ¹³C NMR (126 MHz, CDCl₃) δ 184.2, 180.4, 170.5, 154.7, 145.4, 140.3, 137.8, 134.7, 134.4, 128.3, 126.6, 124.4, 124.4, 121.5, 120.2, 117.0, 111.7, 104.4, 24.4. HRMS (TOF MS ES+) C₁₉H₁₄N₃O₃⁺ (MH⁺) calcd. 332.1035, found 332.1030.

7-acetamido-2-(2-(pyrrolyl))quinoline-5,8-dione (18). The starting material **14** (30 mg, 0.08 mmol) was dissolved in 3 mL CH₂Cl₂ and cooled to 0°C using an ice bath. Trifluoroacetic acid (150 μL) was added dropwise and reacted at rt for 2 hrs. TLC showed full conversion. Then quenched with sat. NaHCO₃ (10 mL) and extracted 2x20 mL CH₂Cl₂. The organic layers were combined, dried over MgSO₄, filtered and concentrated under reduced pressure. The residue was purified on a HP-Sil 25 g Biotage SNAP cartridge using EtOAc:heptane gradient (0-50%) at a

flow rate of 20 mL/min. Yield 21 mg (93%) of a red solid was obtained after recrystallization from MeOH. M.P. 255°C, decomposes. $R_f = 0.11$ (50% EtOAc:heptane). ^1H NMR (500 MHz, DMSO) δ 11.65 (s, 1H), 9.95 (s, 1H), 8.20 (d, $J = 8.4$ Hz, 1H), 8.05 (d, $J = 8.4$ Hz, 1H), 7.69 (s, 1H), 7.07 – 7.04 (m, 2H), 6.28 – 6.22 (m, 1H), 2.27 (s, 3H). ^{13}C NMR (126 MHz, DMSO) δ 184.6, 178.7, 171.4, 154.0, 146.6, 141.9, 133.9, 130.1, 125.3, 123.8, 121.8, 115.2, 111.9, 110.4, 24.7. HRMS (TOF MS ES+) $\text{C}_{15}\text{H}_{12}\text{N}_3\text{O}_3^+$ (MH+) calcd. 282.0879, found 282.0909.

General procedure for removal of the acetate group with MeOH-H₂SO₄. To the starting material (0.1 mmol) in a 20 mL vial was added 175 mL of H₂SO₄ in 3.0 mL MeOH and stirred at rt for 3 hrs. The red solution was then neutralized with 5 mL 5% NaHCO₃ (aq.) and extracted with 5 X 10 mL CH₂Cl₂. The combined organic extracts were dried over MgSO₄, filtered and concentrated under reduced pressure. Then purified on a HP-Sil 25 g Biotage SNAP cartridge using EtOAc:heptanes (0-70%) or MeOH:CH₂Cl₂ gradient (0-5%) at a flow rate of 20 mL/min.

7-Amino-2-(4-(trifluoromethyl)phenyl)quinoline-5,8-dione (19). The general procedure was used to obtain 6.0 mg (67%) of a red solid; $R_f = 0.38$ (60% EtOAc:heptane); m.p. 151-153°C (decomposes, turns black); ^1H NMR (500 MHz, CDCl₃) δ 8.28 (d, $J = 8.2$ Hz, 1H), 8.05 (d, $J = 8.2$ Hz, 2H), 7.95 (d, $J = 8.2$ Hz, 1H), 7.58 (d, $J = 8.3$ Hz, 2H), 5.84 (s, 1H). ^{13}C NMR (126 MHz, CDCl₃) δ 182.2, 180.1, 158.7, 150.3, 146.3, 140.6, 135.1, 129.4, 127.7, 125.5, 125.5,

125.1, 105.8, 102.4. HRMS (TOF MS ES+) $C_{16}H_{10}F_3N_2O_2^+$ (MH+) calcd. 319.0694, found 319.0666.

7-amino-2-(3-pyridinyl)quinoline-5,8-dione (20). The general procedure was used to obtain 10 mg (83%) of a red solid. $R_f = 0.16$ (5% MeOH:CH₂Cl₂); m.p. 195-197°C (decomposes, turns black). ¹H NMR (500 MHz, CDCl₃) δ 9.29 (d, $J = 1.7$ Hz, 1H), 8.67 (dd, $J = 4.9, 1.4$ Hz, 1H), 8.58 (ddd, $J = 8.0, 2.2, 1.7$ Hz, 1H), 8.52 (d, $J = 8.2$ Hz, 1H), 8.22 (d, $J = 8.2$ Hz, 1H), 7.59 (ddd, $J = 8.0, 4.9, 0.7$ Hz, 1H), 6.07 (s, 1H). ¹³C NMR (126 MHz, CDCl₃) δ 181.9, 179.8, 157.0, 150.4, 149.6, 147.6, 146.3, 135.4, 135.0, 133.5, 129.4, 124.7, 123.8, 102.1. HRMS (TOF MS ES+) for $C_{14}H_{10}N_3O_2^+$ (MH+) calcd. 252.0773, found 252.0795.

7-amino-2-(2-indolyl)quinoline-5,8-dione (21). The general procedure was used to obtain 19 mg (63%) of a dark-brown solid. $R_f = 0.22$ (70% EtOAc:heptane); m.p. 235°C decomposes. ¹H NMR (500 MHz, CDCl₃) δ 8.33 (d, $J = 8.3$ Hz, 1H), 8.10 (d, $J = 8.3$ Hz, 1H), 7.67 (d, $J = 8.0$ Hz, 1H), 7.49 (d, $J = 8.2$ Hz, 1H), 7.39 (s, 1H), 7.27 (ddd, $J = 8.1, 7.1, 1.1$ Hz, 1H), 7.19 (s, 1H), 7.12 (td, $J = 7.5, 0.8$ Hz, 1H), 6.01 (s, 1H). ¹³C NMR (126 MHz, CDCl₃) δ 182.6, 181.6, 153.6, 149.5, 145.9, 137.6, 135.0, 134.2, 128.3, 128.0, 124.1, 124.0, 121.3, 120.0, 111.7, 103.5, 102.9. HRMS (TOF MS ES+) for $C_{17}H_{12}N_3O_2^+$ (MH+) calcd. 290.0930, found 290.0900.

7-amino-2-(8-quinolinyl)quinoline-5,8-dione (22). The general procedure was used to obtain 55 mg (71%) of a brown solid. $R_f = 0.29$ (5% MeOH:CH₂Cl₂); m.p. 243-245°C, recrystallized from MeOH. ¹H NMR (500 MHz, CD₃OD) δ 8.92 (dd, $J = 4.2, 1.8$ Hz, 1H), 8.49 (d, $J = 8.1$ Hz, 1H), 8.40 (d, $J = 8.1$ Hz, 1H), 8.33 (dd, $J = 8.3, 1.8$ Hz, 1H), 8.21 (dd, $J = 7.2, 1.5$ Hz, 1H), 8.02 (dd, $J = 8.2, 1.4$ Hz, 1H), 7.75 (dd, $J = 8.1, 7.3$ Hz, 1H), 7.53 (dd, $J = 8.3, 4.2$ Hz, 1H), 6.06 (s, 1H). ¹³C NMR (126 MHz, CDCl₃) δ 182.8, 180.1, 160.5, 150.3, 150.2, 146.2, 145.2, 136.7, 136.7, 133.2, 131.6, 131.5, 129.8, 129.1, 128.4, 126.3, 121.2, 102.4. HRMS (TOF MS ES+) for C₁₈H₁₂N₃O₂⁺ (MH⁺) calcd. 302.0930, found 302.0939.

7-amino-2-(2-pyridinyl)quinoline-5,8-dione (23). The general procedure was used to obtain 16 mg (76%) of a red solid. $R_f = 0.25$ (20% MeOH:CH₂Cl₂), recrystallized from MeOH. ¹H NMR (500 MHz, DMSO) δ 8.75 (d, $J = 4.1$ Hz, 1H), 8.72 (d, $J = 8.2$ Hz, 1H), 8.50 (d, $J = 7.9$ Hz, 1H), 8.40 (d, $J = 8.1$ Hz, 1H), 8.05 (t, $J = 7.7$ Hz, 1H), 7.58 – 7.53 (m, 1H), 5.89 (s, 1H). HRMS (TOF MS ES+) for C₁₄H₁₀N₃O₂⁺ (MH⁺) calcd. 252.0773 found 252.0749.

7-Amino-2-(2-pyrrolyl)quinoline-5,8-dione (24). The general procedure was used to obtain 11 mg (78%) of a red solid. $R_f = 0.37$ (5% MeOH:CH₂Cl₂); m.p. 230°C (decomposes), recrystallized from MeOH. ¹H NMR (500 MHz, CDCl₃) δ 8.23 (d, $J = 8.4$ Hz, 1H), 7.84 (d, $J = 8.4$ Hz, 1H), 7.06 (dd, $J = 2.5, 1.3$ Hz, 1H), 6.91 (dd, $J = 3.7, 1.3$ Hz, 1H), 6.32 (dd, $J = 3.7, 2.6$

Hz, 1H), 5.97 (s, 1H). ^{13}C NMR (126 MHz, CDCl_3) δ 183.0, 181.7, 153.5, 149.4, 145.7, 133.9, 129.9, 126.6, 122.7, 122.3, 110.8, 110.3, 102.5. HRMS (TOF MS ES+) for $\text{C}_{13}\text{H}_{10}\text{N}_3\text{O}_2^+$ (MH+) calc. 240.0773, found 240.0779.

ASSOCIATED CONTENT

Supporting Information. Additional characterization data, ^1H and ^{13}C -NMR spectra. This material is available free of charge via the Internet at <http://pubs.acs.org>.

AUTHOR INFORMATION

***Corresponding Authors**

For chemistry: P.Diaz: phone: 406-243-4362; fax: 406-243-5228; email:

Philippe.diaz@umontana.edu.

For biology: H.D. Beall: phone, 406-243-5112; fax, 406-243-5228; email:

howard.beall@umontana.edu.

ACKNOWLEDGEMENT

This work was supported by NIH grants P30NS055022 (PD and CMK) and P20RR017670 (HDB). We thank Dr. Ayesha Sharmin for experimental assistance and the CBSD NIH CoBRE (P20GM103546), which supports the BioSpectroscopy Core and the Molecular Computational

Core Facility. Marvin was used for drawing, displaying and characterizing chemical structures, substructures and reactions included in the supporting information, Marvin 5.11.5, 2013, ChemAxon (<http://www.chemaxon.com>).

ABBREVIATIONS

NQO1, NAD(P)H: quinone oxidoreductase 1; MeOH, Methanol; BnBr, Benzyl bromide; DME, 1, 2-Dimethoxyethane; dppf, 1,1'-Bis(diphenylphosphino)ferrocene; E_{pc} = cathodic peak potential; E_{pa} = anodic peak potential

REFERENCES

- (1) Balitz, D. M. B., J. A.; Bradner, W. T.; Doyle, T. W.; O'Herron, F. A.; Nettleton, D. E. Isolation of lavendamycin. A new antibiotic from *Streptomyces lavendulae*. *J. Antibiot.* **1982**, *35*, 259-265.
- (2) Doyle, T. W.; Balitz, D. M.; Grulich, R. E.; Nettleton, D. E.; Gould, S. J.; Tann, C.-h.; Moews, A. E. Structure determination of lavendamycin- a new antitumor antibiotic from *streptomyces lavendulae*. *Tetrahedron Lett.* **1981**, *22*, 4595-4598.
- (3) P, R. K. V. C. W. Streptonigrin, an antitumor substance. I. Isolation and characterization. *Antibiot. Annu.* **1959**, *7*, 950-953.
- (4) Rao, K. V.; Biemann, K.; Woodward, R. B. The Structure of Streptonigrin. *J. Am. Chem. Soc.* **1963**, *85*, 2532-2533.
- (5) Podeszwa, B.; Niedbala, H.; Polanski, J.; Musiol, R.; Tabak, D.; Finster, J.; Serafin, K.; Milczarek, M.; Wietrzyk, J.; Boryczka, S.; Mol, W.; Jampilek, J.; Dohnal, J.; Kalinowski, D. S.; Richardson, D. R. Investigating the antiproliferative activity of quinoline-5,8-diones and styrylquinolinecarboxylic acids on tumor cell lines. *Bioorg. Med. Chem. Lett.* **2007**, *17*, 6138-6141.

- (6) Hassani, M.; Cai, W.; Holley, D. C.; Lineswala, J. P.; Maharjan, B. R.; Ebrahimian, G. R.; Seradj, H.; Stocksdales, M. G.; Mohammadi, F.; Marvin, C. C.; Gerdes, J. M.; Beall, H. D.; Behforouz, M. Novel Lavendamycin Analogues as Antitumor Agents: Synthesis, in Vitro Cytotoxicity, Structure–Metabolism, and Computational Molecular Modeling Studies with NAD(P)H:Quinone Oxidoreductase 1. *J. Med. Chem.* **2005**, *48*, 7733-7749.
- (7) Fryatt, T.; Pettersson, H. I.; Gardipee, W. T.; Bray, K. C.; Green, S. J.; Slawin, A. M. Z.; Beall, H. D.; Moody, C. J. Novel quinolinequinone antitumor agents: structure-metabolism studies with NAD(P)H:quinone oxidoreductase (NQO1). *Bioorg. Med. Chem.* **2004**, *12*, 1667-1687.
- (8) Beall, H. D.; Winski, S.; Swann, E.; Hudnott, A. R.; Cotterill, A. S.; O'Sullivan, N.; Green, S. J.; Bien, R.; Siegel, D.; Ross, D.; Moody, C. J. Indolequinone Antitumor Agents: Correlation between Quinone Structure, Rate of Metabolism by Recombinant Human NAD(P)H:Quinone Oxidoreductase, and in Vitro Cytotoxicity¹. *J. Med. Chem.* **1998**, *41*, 4755-4766.
- (9) Swann, E.; Barraja, P.; Oberlander, A. M.; Gardipee, W. T.; Hudnott, A. R.; Beall, H. D.; Moody, C. J. Indolequinone Antitumor Agents: Correlation between Quinone Structure and Rate of Metabolism by Recombinant Human NAD(P)H:Quinone Oxidoreductase. Part 21. *J. Med. Chem.* **2001**, *44*, 3311-3319.
- (10) Hassani, M.; Cai, W.; Koelsch, K. H.; Holley, D. C.; Rose, A. S.; Olang, F.; Lineswala, J. P.; Holloway, W. G.; Gerdes, J. M.; Behforouz, M.; Beall, H. D. Lavendamycin Antitumor Agents: Structure-Based Design, Synthesis, and NAD(P)H:Quinone Oxidoreductase 1 (NQO1) Model Validation with Molecular Docking and Biological Studies. *J. Med. Chem.* **2008**, *51*, 3104-3115.
- (11) Cai, W.; Hassani, M.; Karki, R.; Walter, E. D.; Koelsch, K. H.; Seradj, H.; Lineswala, J. P.; Mirzaei, H.; York, J. S.; Olang, F.; Sedighi, M.; Lucas, J. S.; Eads, T. J.; Rose, A. S.; Charkharrin, S.; Hermann, N. G.; Beall, H. D.; Behforouz, M. Synthesis, metabolism and in vitro cytotoxicity studies on novel lavendamycin antitumor agents. *Bioorg. Med. Chem.* **2010**, *18*, 1899-1909.
- (12) Colucci, M. A.; Couch, G. D.; Moody, C. J. Natural and synthetic quinones and their reduction by the quinone reductase enzyme NQO1: from synthetic organic chemistry to compounds with anticancer potential. *Org. Biomol. Chem.* **2008**, *6*, 637-656.

- (13) Behforouz, M.; Haddad, J.; Cai, W.; Arnold, M. B.; Mohammadi, F.; Sousa, A. C.; Horn, M. A. Highly Efficient and Practical Syntheses of Lavendamycin Methyl Ester and Related Novel Quinolindiones. *J. Org. Chem.* **1996**, *61*, 6552-6555.
- (14) Prieto, M.; Zurita, E.; Rosa, E.; Muñoz, L.; Lloyd-Williams, P.; Giralt, E. Arylboronic Acids and Arylpinacolboronate Esters in Suzuki Coupling Reactions Involving Indoles. Partner Role Swapping and Heterocycle Protection. *J. Org. Chem.* **2004**, *69*, 6812-6820.
- (15) Collot, V.; Dallemagne, P.; Bovy, P. R.; Rault, S. Suzuki-type cross-coupling reaction of 3-iodoindazoles with aryl boronic acids: A general and flexible route to 3-arylindazoles. *Tetrahedron* **1999**, *55*, 6917-6922.
- (16) Musser, J. H.; Jones, H.; Sciortino, S.; Bailey, K.; Coutts, S. M.; Khandwala, A.; Sonnino-Goldman, P.; Leibowitz, M.; Wolf, P.; Neiss, E. S. Synthesis and antiallergic activities of 1,3-oxazolo[4,5-h]quinolines. *J. Med. Chem.* **1985**, *28*, 1255-1259.
- (17) Tang, Q.; Zhang, C.; Luo, M. A New Method for N–N Bond Cleavage of N,N-Disubstituted Hydrazines to Secondary Amines and Direct Ortho Amination of Naphthol and Its Analogues. *J. Am. Chem. Soc.* **2008**, *130*, 5840-5841.
- (18) Campeau, L.-C.; Stuart, D. R.; Leclerc, J.-P.; Bertrand-Laperle, M. g.; Villemure, E.; Sun, H.-Y.; Lasserre, S.; Guimond, N.; Lecavallier, M.; Fagnou, K. Palladium-Catalyzed Direct Arylation of Azine and Azole N-Oxides: Reaction Development, Scope and Applications in Synthesis. *J. Am. Chem. Soc.* **2009**, *131*, 3291-3306.
- (19) LaMontagne, M. P.; Blumbergs, P.; Smith, D. C. Antimalarials. 16. Synthesis of 2-substituted analogs of 8-[(4-amino-1-methylbutyl)amino]-6-methoxy-4-methyl-5-[3-(trifluoromethyl)phenoxy]quinoline as candidate antimalarials. *J. Med. Chem.* **1989**, *32*, 1728-1732.
- (20) Rodríguez, J. G.; de los Rios, C.; Lafuente, A. Synthesis of n-chloroquinolines and n-ethynylquinolines (n=2, 4, 8): homo and heterocoupling reactions. *Tetrahedron* **2005**, *61*, 9042-9051.
- (21) Miyaura, N.; Suzuki, A. Palladium-Catalyzed Cross-Coupling Reactions of Organoboron Compounds. *Chem. Rev.* **1995**, *95*, 2457-2483.
- (22) Boger, D. L.; Duff, S. R.; Panek, J. S.; Yasuda, M. Inverse electron demand Diels-Alder reactions of heterocyclic azadienes. Studies on the total synthesis of lavendamycin: investigative studies on the preparation of the CDE .beta.-carboline ring system and AB quinoline-5,8-quinone ring system. *J. Org. Chem.* **1985**, *50*, 5782-5789.

- (23) Buffinton, G.; Ollinger, K.; Brunmark, A.; Cadenas, E. DT-diaphorase-catalysed reduction of 1,4-naphthoquinone derivatives and glutathionyl-quinone conjugates. Effect of substituents on autoxidation rates. *Biochem. J.* **1989**, *257*, 561-571.
- (24) Gibson, N. W.; Hartley, J. A.; Butler, J.; Siegel, D.; Ross, D. Relationship between DT-diaphorase-mediated metabolism of a series of aziridinylbenzoquinones and DNA damage and cytotoxicity. *Mol. Pharmacol.* **1992**, *42*, 531-536.
- (25) Long, G. V.; Harding, M. M. A proton nuclear magnetic resonance study of the interaction of zinc(II) with the antitumour drug streptonigrin. *J. Chem. Soc. Dalton Trans.* **1996**, 549-552.
- (26) Wei, X.; Ming, L.-J. Comprehensive 2D ¹H NMR Studies of Paramagnetic Lanthanide(III) Complexes of Anthracycline Antitumor Antibiotics. *Inorg. Chem.* **1998**, *37*, 2255-2262.
- (27) Ross, D.; Kepa, J. K.; Winski, S. L.; Beall, H. D.; Anwar, A.; Siegel, D. NAD(P)H:quinone oxidoreductase 1 (NQO1): chemoprotection, bioactivation, gene regulation and genetic polymorphisms. *Chem. Biol. Interact.* **2000**, *129*, 77-97.
- (28) Harding, M. M.; Long, G. V. Interaction of the antitumor antibiotic streptonigrin with metal ions and DNA. *Curr. Med. Chem.* **1997**, *4*, 405-420.
- (29) Budimir, A. Metal ions, Alzheimer's disease and chelation therapy. *Acta Pharm.* **2011**, *61*, 1-14.
- (30) Kraus, J.-L.; Conti, F.; Madonna, S.; Tchoghandjian, A.; Beclin, C. Alternative responses of primary tumor cells and glioblastoma cell lines to N,N-bis-(8-hydroxyquinoline-5-yl methyl)-benzyl substituted amines: cell death versus P53-independent senescence. *Int. J. Oncol.* **2010**, *37*, 1463-1470.
- (31) King, O. N. F.; Li, X. S.; Sakurai, M.; Kawamura, A.; Rose, N. R.; Ng, S. S.; Quinn, A. M.; Rai, G.; Mott, B. T.; Beswick, P.; Klose, R. J.; Oppermann, U.; Jadhav, A.; Heightman, T. D.; Maloney, D. J.; Schofield, C. J.; Simeonov, A. Quantitative high-throughput screening identifies 8-hydroxyquinolines as cell-active histone demethylase inhibitors. *PLoS One* **2010**, *5*, e15535.
- (32) Yan, C.; Kepa, J. K.; Siegel, D.; Stratford, I. J.; Ross, D. Dissecting the role of multiple reductases in bioactivation and cytotoxicity of the antitumor agent 2,5-diaziridinyl-3-(hydroxymethyl)-6-methyl-1,4-benzoquinone (RH1). *Mol. Pharmacol.* **2008**, *74*, 1657-1665.

- (33) Faig, M.; Bianchet, M. A.; Winski, S.; Hargreaves, R.; Moody, C. J.; Hudnott, A. R.; Ross, D.; Amzel, L. M. Structure-Based Development of Anticancer Drugs. Complexes of NAD(P)H:Quinone Oxidoreductase 1 with Chemotherapeutic Quinones. *Structure* **2001**, *9*, 659-667.
- (34) Verdonk, M. L.; Giangreco, I.; Hall, R. J.; Korb, O.; Mortenson, P. N.; Murray, C. W. Docking Performance of Fragments and Druglike Compounds. *J. Med. Chem.* **2011**, *54*, 5422-5431.
- (35) Verdonk, M. L.; Cole, J. C.; Hartshorn, M. J.; Murray, C. W.; Taylor, R. D. Improved protein-ligand docking using GOLD. *Proteins* **2003**, *52*, 609-623.

APPENDIX II

Improved synthesis of 3-aryl isoxazoles containing fused aromatic rings

Yousef R. Mirzaei, Matthew J. Weaver, Scott A. Steiger, Alison K. Kearns, Mariusz P. Gajewski, Kevin C. Rider, Howard D. Beall, and N.R. Natale

Published in *Tetrahedron*

2012 Dec 16;68(50):10360-10364

Improved synthesis of 3-aryl isoxazoles containing fused aromatic rings

Yousef R. Mirzaei, Matthew J. Weaver, Scott A. Steiger, Alison K. Kearns, Mariusz P. Gajewski, Kevin C. Rider, Howard D. Beall, and N.R. Natale*

Medicinal Chemistry Graduate Program

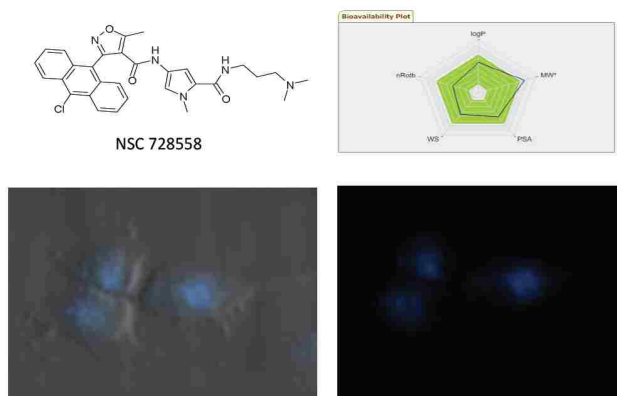
Department of Biomedical and Pharmaceutical Sciences

The University of Montana, Missoula MT 59812

Abstract— A critical comparison of methods to prepare sterically hindered 3-aryl isoxazoles containing fused aromatic rings using the nitrile oxide cycloaddition (NOC) reveal that modification of the method of Bode, Hachisu, Matsuura and Suzuki (BHMS), utilizing either triethyl amine as base or sodium enolates of the diketone, ketoester and ketoamide dipolarophiles, respectively was the method of choice for this transformation. © 2013 Elsevier Science. All rights reserved

Isoxazoles continue to be of interest for both their biological activities and synthetic utility.¹⁻⁴ The synthesis of aryl-isoxazoles is also the subject of on-going improvements.^{1,5-7} In connection with our studies on aryl isoxazole amides (AIMs)⁸⁻⁹ we have reported lead compounds which possess (1) useful antitumor activity and (2) photophysical properties which are of potential diagnostic use as "tumor paint".¹⁰

Figure 1. Structure, Symyx radar graph, and Laser Scanning Cytometry of NSC 728558.



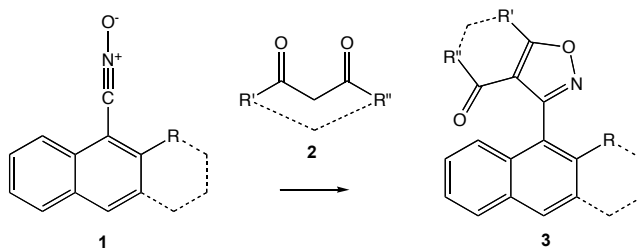
* Corresponding author. Tel.: 406-243-4132; fax: 406-243-5228; e-mail: nicholas.natale@umontana.edu

An illustration of the application of AIMs is shown in **Figure 1**. AIM NSC 728558 has exhibited a mid-graph mean point of -5.71-5.75 (log scale, which translate to single digit micromolar) for tumor cell line growth inhibition (GI_{50}) against the full panel in the NCI60 cell line antitumor screening protocol,⁸ and as a benchmark for comparison clinically used agents 5-fluorodeoxyuridine, bleomycin and rubidazole gave values of -4.7, -5.2 and -5.8 respectively in the same standard assay. The calculated physical property data for NSC 728558 fall within or close to values with useful bioavailability (radar graph, Symyx Draw v3.1; top right panel). Laser Scanning Cytometry shows that NSC 728558 does in fact permeate human glioma SNB-19 cells (the AIM is blue) and is localized within the nucleus. Surgical resection of many cancers, especially brain tumors or gliomas, have a poor success rate because of the difficulty of judging the border between cancerous and healthy tissue. Fluorescent agents with antitumor activity such as the AIMs hold promise for improvements in visualizing tumors during surgery.^{10b,c}

We required both improvements in the efficiency of the preparation of the isoxazole *and* concomitant economy of scale to prepare amounts of material sufficient to expand the scope of our investigations toward *in vivo* studies.

Isoxazoles prepared via nitrile oxide cycloaddition (NOC)¹¹ are most often prepared by dehydration of α -methylene nitro precursors,⁵ or chlorination/dehalogenation of oximes^{1,6,7} to form the nitrile oxide **1**.

Among the unsymmetrical dipolarophiles **2** which usually give rise to regioselective cycloaddition are enamines.



First pioneered by Stork and McMurry,¹² the use of enamines in the NOC works well for aliphatic and aromatic nitrile oxides on mole scales.¹ We have employed modifications of this synthesis in the preparation of isoxazole-oxazolines,¹³ antihypertensive 4-isoxazolyl-1,4-dihydropyridines,¹⁴ and we have championed the reaction as a learning tool for aspiring chemists.¹⁵ Our previous reports in the AIM series have used enamines as dipolarophiles,¹⁶ while for most cases modest yields in the range of 30-40% overall of **3** were obtained, sufficient

quantities of material were isolated for pharmacology studies. Upon scale-up however, we have observed a consistent diseconomy of scale using enamines and nitrile oxides derived from fused ring aromatics, to the extent that even a ten-fold increase in scale (from *ca.* 10 to 100 mM) produced only marginally more desired product, and purified yields plummeted to 10-20%. *We have found this is especially a limitation when using nitrile oxides derived from fused aromatic systems.* Careful examination of the reaction by-products after chromatographic isolation and characterization by LC-MS revealed that as the stability of aryl nitrile oxides **1** increases^{17,16b} their consequent reactivity to dipolarophiles slows, with concomitant increases in amine trapping of the nitrile oxide/oximidoyl chloride to give **7**, as well as self-condensation of the nitrile oxide to yield **8** as shown in **Scheme 1**.

Table 1. Nitrile oxide cycloaddition synthesis of hindered 3-acylaryl-isoquinolines

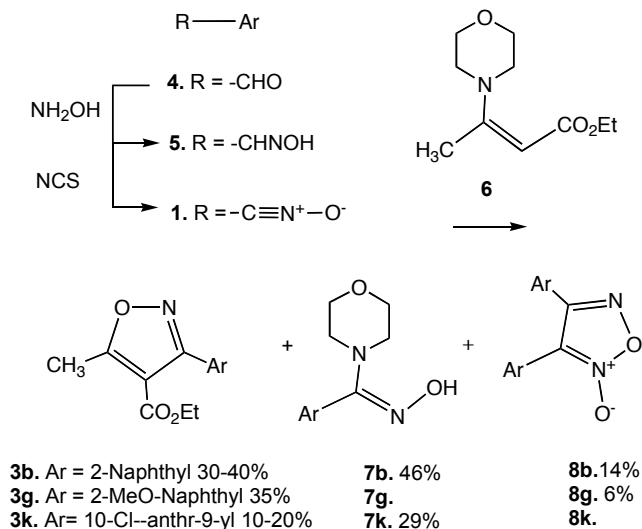
Entry	Nitrile oxide	Dipolarophile	Conditions	Product	Yield %
1	 1a, R ₁ = CH ₃	 2a, R ₁ = CH ₃	Et ₃ N EtOH	 3a, R ₁ = CH ₃ ; R ₂ = CH ₃	40
2	1a, R ₁ = CH ₃	2b, R ₁ = OCH ₂ CH ₃	Na/EtOH	3b, R ₁ = OCH ₂ CH ₃ ; R ₂ = CH ₃	70
3	1a, R ₁ = CH ₃	2c, R ₁ = C ₆ H ₅	Et ₃ N	3c, R ₁ = C ₆ H ₅ ; R ₂ = CH ₃	40
4	1a, R ₁ = CH ₃	 2d	Et ₃ N	 3d	71
5	 1b, R ₁ = OCH ₃	2a, R ₁ = CH ₃	Na/EtOH	 3e, R ₁ = CH ₃ ; R ₂ = OCH ₃	70
6	1b, R ₁ = OCH ₃	2a, R ₁ = OCH ₃	Na ₂ S ₂ O ₈ /CH ₂ Cl ₂	3e, R ₁ = OCH ₃ ; R ₂ = OCH ₃	60
7	1b, R ₁ = OCH ₃	2a, R ₁ = OCH ₃	Et ₃ N	3e, R ₁ = OCH ₃ ; R ₂ = OCH ₃	62
8	1b, R ₁ = OCH ₃	2b, R ₁ = OCH ₂ CH ₃	Na/EtOH	3g, R ₁ = OCH ₂ CH ₃ ; R ₂ = OCH ₃	30
9	1b, R ₁ = OCH ₃	2c, R ₁ = C ₆ H ₅	Na/EtOH	3h, R ₁ = C ₆ H ₅ ; R ₂ = OCH ₃	13
10	1b, R ₁ = OCH ₃	2c, R ₁ = C ₆ H ₅	Et ₃ N EtOH	3h, R ₁ = C ₆ H ₅ ; R ₂ = OCH ₃	22
11	1b, R ₁ = OCH ₃	2c, R ₁ = C ₆ H ₅	NaCl-Pt	3h, R ₁ = C ₆ H ₅ ; R ₂ = OCH ₃	43
12	1b, R ₁ = OCH ₃	 2d	Na EtOH	 3i	42
13	1b, R ₁ = OCH ₃	2d	Et ₃ N	3i	53
14	1b, R ₁ = OCH ₃	2d	NaCl-Pt	3i	57

*The reaction was conducted in similar conditions.

We therefore examined the methodology of Bode, Hachisu, Matsuura and Suzuki (BHMS), which use either the sodium enolates of ketoesters,⁶ or tertiary amines as base.⁷ The use of sodium enolates in the NOC was pioneered by Renzi and Dal Piaz,²⁰ and recently applied in 2,6-disubstituted aryl cases for the preparation of growth hormone secretagogue receptor antagonists.²¹ The BHMS procedure has been used to prepare particularly hindered

unsymmetrical 2,6-disubstituted aryl examples, including examples which appear to exist as atropisomers,⁷ which recommended its application to our examples.

Scheme 1. Synthesis of the isoxazoles used for the present study.



The comparison was especially dramatic for the anthryl isoxazole cases, shown in **Table 2**. Excellent yields were obtained for anthryl isoxazoles **3j**, 10-chloro analog **3k**, and 10-bromo analog **3m**. The yields with the enamine procedures were 35-45¹⁶ and 10-20%, for **3j** and **3k**, respectively. **Table 2**, Entry 3 illustrates the direct synthesis of a fused aromatic containing a C-4 tertiary amide, which is an uncommon example of a ketamide used as dipolarophile in the NOC.²² The ketamide was prepared from diketene and pyrrolidine,¹⁸ and cycloaddition provided the C-4 amide in synthetically reasonable yield. The sluggish reactivity we previously reported for nucleophilic addition to the C-4 ester of the 3-anthryl-isoxazole is exemplified by (1) slow hydrolysis rates (i.e., 60 h using refluxing aqueous LiOH)⁹ and (2) the observation that n-BuLi deprotonates the C-5 methyl at -78°C without noticeable addition to the C-4 ester.¹⁹ The C-4 functionalization prior to the NOC stage is a definite advantage for the preparation of AIMs, and will be the subject of further study.

Table 2. Nitrile oxide cyclization to form fused bicyclic 3-isoxazolo[4,5-b]pyridines

Entry	Nitrile oxide	Dipolarophile	Conditions ^a	Product	Yield (%)
1			Na/EtOH		88-94
2			Na/EtOH		90-92
3			Na/EtOH		30
4			Na/MeOH		82
5			Et ₃ N		72

^aThe reaction was conducted in anoxic conditions.

In summary, we have found that the *BHMS protocol* produced superior results, especially in sterically encumbered examples containing fused ring aromatic nitrile oxides and that these *conditions represent the methodology of choice* when standard enamine methodology fails. We will report on the chemical and pharmacological application of these novel isoxazoles in due course.

Experimental

General: All reactions were performed under inert atmosphere. Purification was carried out by column chromatography. Chemicals were purchased from TCI or Aldrich Chemical Company, all commercial reagents are routinely examined for purity by NMR and TLC, and recrystallized or distilled as appropriate. Solvents were reagent grade. Melting points were determined in open capillary tubes on a Melt-Temp apparatus and are uncorrected. NMR spectra were obtained using either a Varian 400 MHz Unity Plus or a Varian NMR systems 500 MHz spectrometer, in deuteriochloroform unless otherwise noted. Infrared spectra were obtained on a thermo-Nicolet 633 FT-IR spectrometer.

Chemical shifts (δ) are reported using CHCl_3 (7.26 ppm for ^1H), CDCl_3 (77 ppm for ^{13}C) as references. High resolution mass spectra (HRMS) were obtained using a Micromass electrospray ionization (ESI)/time-of-flight mass spectrometry (LCTOF). Mass spectrometer samples were introduced using a Waters model 2690 separations module HPLC fitted with a C-18 reversed

phase column (2.1 mm i.d., 5 cm). Elemental analyses for C, H, and N were performed by Midwest Microlab, Indianapolis, IN. All reactions were monitored by Thin Layer Chromatography (TLC). Purification was performed by flash column chromatography, and analytical samples were prepared by PTLC. Analytical LCMS (UV at 254 nm) and NMR were used to establish the purity of targeted compounds. All compounds that were evaluated in biochemical and biophysical assays had >95% purity as determined by ¹H NMR and LCMS NSC 728558 was prepared from **3k** as previously described.^{8,9}

1-(Pyrrolidin-1-yl)butane-1,3-dione.¹⁸ Pyrrolidine (0.539 g, 7.5 mmol) is dissolved in 10 mL of anhydrous DCM and diketene (0.925 g, 11.00 mmol) is added. The mixture is stirred at ambient temperature for 2.5 h, followed by removal of the solvent under vacuum to afford (1.163 g, 99%) as red brown liquid. ¹H NMR (500 MHz, CDCl₃): δ 3.46 (t, *J* = 6.62 Hz, 2H), 3.45 (s, 2H), 3.; ¹³C NMR (125 MHz, CDCl₃): δ 202.6, 165.0, 88.8, 51.3, 47.2, 45.9, 30.4, 26.0, 24.4; IR cm⁻¹; mass calculated for C₈H₁₃NO₂ 155.0946, found *m/z* 156.1902 (M +1, 100%).

NOC: sodium enolate method.

(3-(Anthracen-9-yl)-5-methylisoxazol-4-yl)(pyrrolidin-1-yl)methanone, 3l. To a solution of sodium ethoxide, prepared from 0.199 g of Na in 44.2 mL of absolute EtOH, was added 1-(Pyrrolidin-1-yl)butane-1,3-butane-1,3-dione (1.015 g, 6.54 mmol), and 9-anthrahydroximinoylchloride, (1.06, 4.105 mmol) successively and the resulting red solution was stirred under Ar atmosphere for 4h at ambient temperature. The red-brown solution was extracted with ethyl acetate (4 x 20 mL), washed with DI water (2 x 50 mL) and brine (50 mL), and dried over anhydrous Na₂SO₄. Filtration and concentration afforded the desired product **3l** as red-brown oil (1.40 g, 95%), which was further purified by silica column flash chromatography (Hexanes: EtOAc; 10:1), and PTLC to afford **3l** as off white solid (0.7375 g, 50 %).

NOC: triethyl amine method. Synthesis of 1-(5-methyl-3-(2-methylnaphthalene-1-yl)isoxazol-4-yl)ethanone, 3a. To 2,4-pentanedione (0.42 g, 4.11 mmol) in absolute ethanol (21ml) at ambient temperature was added triethylamine (0.47 g, 4.584 mmol) followed by addition of nitrile oxide (0.6 g, 3.28 mmol). The temperature was raised to 53°C and the mixture stirred under Ar atmosphere for 72 h. The pale yellow solution was extracted with chloroform (4 x 20 mL), washed with DI water (2 x 50 mL) and brine (50 mL), dried over anhydrous Na₂SO₄. Filtration, concentration and silica column flash chromatography (Hexanes: EtOAc: DCM; 5:1:1) afforded the desired product **3a** (0.289 g, 40 %):

Analytical data for 3-fused aryl isoxazole products.

1-(5-Methyl-3-(2-methylnaphthalene-1-yl)isoxazol-4-yl)ethanone, 3a. Oil, TLC SiO₂ hexane-DCM-EtOAc 4:1:1 R_f 0.77. ¹H NMR (500 MHz, CDCl₃) δ 7.80-7.75 (m, 2H), 7.38-7.32 (m, 4H), 2.76 (s, 3H), 2.26 (s, 3H), 1.56 (s, 3H); ¹³C NMR (125 MHz, CDCl₃) δ 192.3, 175.7, 159.6, 135.3, 132.3, 131.4, 129.5, 127.8, 126.8, 125.2, 124.0, 117.5, 28.6, 19.8, 13.6; HRMS Calc'd for C₁₇H₁₆NO₂ 266.1181; Found: 266.1193.

Ethyl 3-(2-methylnaphthalen-1-yl)-5-methylisoxazole-4-carboxylate, 3b. Oil, TLC SiO₂ hexane-DCM-EtOAc 4:1:1 R_f 0.6. ¹H-NMR (CDCl₃) δ 7.826 (d, 2H); 7.25-7.398 (m, 4H); 3.87 (q, 2H); 2.841 (s, 3H); 2.303 (s, 3H); 0.651 (t, 3H). ¹³C NMR (125 MHz, CDCl₃) δ 175.7, 161.4, 160.7, 135.0, 132.5, 131.4, 128.9, 127.9, 127.7, 126.2, 124.8, 124.6, 124.5, 110.1, 59.9, 20.1, 13.2, 13.0. HRMS calc'd for C₁₈H₁₈NO₃: 296.1287; Found: 296.1297.

Phenyl (5-methyl-3-(2-methylnaphthalen-1-yl)isoxazol-4-yl)methanone, 3c. Oil, TLC SiO₂ hexane-DCM-EtOAc 4:1:1 R_f 0.79 ¹H NMR (500 MHz, CDCl₃): δ 7.65 (d, *J* = 7.90, 1H), 7.60 (d, *J* = 8.50 Hz, 1H), 7.55 (d, *J* = 8.00 Hz, 1H), 7.37 (t, *J* = 6.60 Hz, 1H), 7.33 (m, 3H), 7.16 (m, 2H), 6.94 (t, *J* = 8.00 Hz, 2H), 3.38 (s, 3H), 2.64 (s, 3H); ¹³C NMR (125 MHz, CDCl₃): δ 189.8, 173.7, 171.0, 160.3, 137.1, 135.5, 132.4, 132.3, 131.4, 129.3, 129.2, 128.1, 128.0, 127.9, 127.8, 127.5, 125.0, 124.5, 124.4, 123.6, 117.8, 20.4, 14.0; HRMS Calc'd for C₂₂H₁₈NO₂: 328.1338; Found: 328.1370.

6,6-Dimethyl-3-(2-methylnaphthalen-1-yl)-6,7-dihydrobenzo[*d*]isoxazol-4(5*H*)-one 3d. Oil, TLC SiO₂ hexane-DCM-EtOAc 4:1:1 R_f 0.71. ¹H NMR (500 MHz, CDCl₃) δ 7.87 (d, *J* = 8.3, 1H), 7.84 (d, *J* = 8.3, 1H), 7.36-7.43 (m, 4H), 3.01 (s, 2H), 2.40 (d, *J* = 8.3, 2H), 2.31 (s, 3H), 1.22 (s, 3H), 1.19 (s, 3H); ¹³C NMR (125 MHz, CDCl₃) δ 190.8, 180.9, 171.1, 157.9, 135.6, 132.3, 131.7, 129.7, 129.6, 128.4, 128.2, 128.1, 128.0, 125.2, 125.0, 124.5, 124.3, 122.9, 52.4, 37.0, 35.5, 28.6, 28.5, 28.1, 28.0, 21.0, 14.2. HRMS Calc'd for C₂₀H₂₀NO₂: 306.1494; Found: 306.1516.

1-(3-(2-methoxynaphthalene-1-yl)-5-methylisoxazol-4-yl)ethanone, 3e. Oil, TLC SiO₂ hexane-DCM-EtOAc 4:1:1 R_f 0.53. ¹H NMR (500 MHz, CDCl₃) δ 8.01 (d, *J* = 9.30 Hz, 1H), 7.84 (d, *J* = 7.80 Hz, 1H), 7.48 (d, *J* = 8.30 Hz, 1H), 7.44 (t, *J* = 8.30 Hz, 1H), 7.39 (d, *J* = 7.90 Hz, 1H), 7.36 (d, *J* = 8.80 Hz, 1H), 3.90 (s, 3H), 2.81 (s, 3H), 1.76 (s, 3H); ¹³C NMR (125 MHz, CDCl₃) δ 193.2, 175.4, 157.7, 155.3, 133.3, 132.1, 128.7, 128.1, 127.8, 124.2, 123.9, 118.3, 112.6, 111.4, 56.4, 28.8, 14.0. HRMS Calc'd for M+H, C₁₇H₁₆NO₃ 282.1130; Found: 282.1150

(M +1, 100%). Anal Calc'd for C₁₇H₁₅NO₃: C, 72.58; H, 5.37; N, 4.98. Found: C, 71.81; H, 5.52; N, 4.56.

Methyl 3-(2-methoxynaphthalene-1-yl)-5-methylisoxazole-4-carboxylate, 3f. Oil, TLC SiO₂ hexane-DCM-EtOAc 4:1:1 R_f 0.56. ¹H NMR (500 MHz, CDCl₃): δ 7.96 (d, *J* = 9.05 Hz, 1H), 7.82 (d, *J* = 9.99 Hz, 1H), 7.55 (d, *J* = 9.99 Hz, 1H), 7.40 (t, *J* = 9.99 Hz, 1H), 7.35 (t, *J* = 9.99 Hz, 2H), 3.86 (s, 3H), 3.54 (s, 3H), 2.81 (s, 3H); ¹³C NMR (500 MHz, CDCl₃): δ 175.1, 162.1, 158.5, 155.3, 133.0, 131.3, 128.6, 127.9, 127.0, 124.0, 123.6, 112.6, 111.4, 110.4, 56.4, 51.3, 13.3; IR cm⁻¹; HRMS Calc'd for C₁₇H₁₆NO₄: 298.1079; Found 298.1111. Anal. Calc'd for C₁₇H₁₅NO₄: C, 68.68; H, 5.09; N, 4.71. Found: C, 66.81; H, 5.00; N, 4.53.

Ethyl 3-(2-methoxynaphthalen-1-yl)-5-methylisoxazole-4-carboxylate, 3g, as yellow solid (1.8 g, 60 %): mp 103-104°C; ¹H NMR (500 MHz, CDCl₃): δ 7.96 (d, *J* = 8.99 Hz, 1H), 7.81 (d, *J* = 8.07 Hz, 1H), 7.50 (d, *J* = 8.55 Hz, 1H), 7.39 (dd, *J* = 11.00, 6.84 Hz 1H), 7.34 (d, *J* = 9.05 Hz, 2H), 3.96 (q, *J* = 7.06 Hz, 2H), 3.88 (s, 3H), 2.82 (s, 3H), 0.79 (t, *J* = 7.06 Hz, 3H); ¹³C NMR (125 MHz, CDCl₃): δ 175.3, 161.9, 158.6, 155.3, 133.3, 131.3, 128.6, 127.9, 127.1, 124.1, 123.7, 112.7, 111.8, 110.6, 60.1, 56.5, 13.5, 13.3; ESI-MS Calculated for C₁₈H₁₇NO₄+H m/z 312.1428 (M +1, 100 %). Anal Calc'd for C₁₈H₁₇NO₄: C, 69.44; H, 5.50; N, 4.50. Found: C, 69.58; H, 5.47; N, 4.54.

Phenyl (3-(2-methoxynaphthalen-1-yl)-5-methylisoxazol-4-yl) methanone, 3h. mp 141-142 °C; ¹H NMR (500 MHz, CDCl₃): δ 8.06 (d, *J* = 8.50, 1H), 7.73 (d, *J* = 8.80 Hz, 2H), 7.51 (t, *J* = 8.40 Hz, 1H), 7.44 (d, *J* = 8.30 Hz, 2H), 7.36 (t, *J* = 7.55 Hz, 1H), 6.96 (t, *J* = 7.80 Hz, 2H), 6.90 (d, *J* = 9.30 Hz, 1H), 3.61 (s, 3H), 2.69 (s, 3H); ¹³C NMR (125 MHz, CDCl₃): δ 189.8, 173.2, 157.8, 154.5, 137.1, 132.7, 132.4, 131.7, 128.7, 128.5, 128.0, 127.7, 127.5, 124.2, 117.6, 111.6, 78.1 55.5, 29.7; ESI-MS for C₂₂H₁₇NO₃+Hm/z 344.1008 (M +1, 100%).

6,6-dimethyl-3-(2-methoxynaphthalen-1-yl)-6,7-dihydrobenzo[*d*]isoxazol-4(5H)-one, 3i. Oil, TLC SiO₂ hexane-DCM-EtOAc 4:1:1 R_f 0.46. ¹H NMR (500 MHz, CDCl₃) δ 7.96 (d, *J* = 9.1, 1H), δ 7.81 (d, *J* = 7.8 Hz, 1H), 7.69 (d, *J* = 8.6 Hz, 1H), 7.43 (dt, *J* = 9.8 Hz, 1.5 Hz, 1H), 7.36 (dd, *J* = 6.8 Hz, 1.3 Hz, 1H), 7.34 (d, *J* = 9.3 Hz, 2H), 3.85 (s, 3H), 2.90 (s, 2H), 2.36 (q, *J* = 14.7 Hz, 2H), 1.17 (s, 3H), 1.14 (s, 3H); ¹³C NMR (125 MHz, CDCl₃) δ 190.7, 180.2, 155.7, 155.4, 132.6, 131.7, 131.6, 128.6, 128.1, 128.0, 127.9, 127.8, 127.6, 127.2, 126.9, 123.9, 123.7, 123.4, 115.2, 112.9, 112.8, 112.6, 109.9, 56.4, 56.2, 52.3, 36.7, 35.1, 28.3, 28.0. HRMS Calculated for C₂₀H₂₀NO₃ 322.1443; Found: 322.1458.

Ethyl 3-(anthracen-9-yl)-5-methylisoxazole-4-carboxylate, 3j. mp 121-122°C; TLC SiO₂ hexane-EtOAc 10:1, R_f 0.30. ¹H NMR (500 MHz, CDCl₃): δ 8.58 (s, 1H), 8.05 (d, *J* = 8.31 Hz, 2H), 7.65 (d, *J* = 8.55 Hz, 2H), 7.40-7.49 (m, 4H), 3.71 (q, *J* = 7.21 Hz, 2H), 2.93 (s, 3H), 0.32 (t, *J* = 7.10 Hz, 3H); ¹³C NMR (500 MHz, CDCl₃): 176.2, 161.5, 160.5, 131.0, 130.8, 128.7, 128.5, 126.3, 125.4, 125.2, 122.7, 111.4, 60.1, 13.5, 12.8, spectral data are in accord with those reported previously.^{16a} ESI-MS for C₂₁H₁₇NO₃+H m/z 332.1441 (M +1, 100%).

Ethyl 3-(10-chloroanthracen-9-yl)-5-methylisoxazole-4-carboxylate, 3k. mp 123-124°C, lit. mp 119-120.^{16b} TLC SiO₂ hexane-EtOAc 10:1, R_f 0.28. ¹H NMR (500 MHz, CDCl₃): δ 8.59 (d, *J* = 8.80 Hz, 2H), 7.53 - 7.60 (m, 4H), 7.43 (d, *J* = 8.80 Hz, 2H), 3.72 (q, *J* = 7.1 Hz, 2H), 2.93 (s, 3H), 0.39 (t, *J* = 7.1 Hz, 3H); ¹³C NMR (500 MHz, CDCl₃): 177.3, 161.3, 161.2, 134.1, 131.1, 128.3, 126.7, 125.9, 125.1, 122.6, 111.5, 60.2, 13.2; ESI-MS for C₂₁H₁₆ClNO₃+H m/z 366.0886 (M +1, 95%).

[3-(Anthracen-9-yl)-5-methylisoxazol-4-yl](pyrrolidin-1-yl)methanone, 3l. mp 194-5°C. ¹H NMR (500 MHz, CDCl₃): δ 8.54 (s, 1H), 7.99 (d, *J* = 9.29 Hz, 2H), 7.95 (d, *J* = 10.0 Hz, 2H), 7.48-7.45 (m, 4H), 3.10 (t, *J* = 6.87 Hz, 2H), 2.73 (s, 3H), 2.60 (t, *J* = 6.61 Hz, 2H), 1.42 (pentet, *J* = 6.85 Hz, 2H), 1.29 (pentet, *J* = 6.60 Hz, 2H); ¹³C NMR (125 MHz, CDCl₃): δ 170.1, 161.3, 158.3, 131.0, 130.5, 129.4, 128.5, 126.9, 126.7, 125.8, 125.3, 125.0, 121.9, 116.5, 47.7, 45.3, 25.6, 23.7, 12.4; ESI-MS for C₂₃H₂₀N₂O₂+H, m/z 357.0757 [M +1, (100)]. Anal Calc'd for C₂₃H₂₀N₂O₂: C, 77.51; H, 5.66; N, 7.86. Found: C, 77.37; H, 5.45; N, 7.99.

Methyl 3-(10-bromoanthracen-9-yl)-5-methylisoxazole-4-carboxylate, 3m. R_f=0.45 Hex:EtOAc:DCM 4:1:1 ¹H NMR (500 MHz, CDCl₃): 8.63-8.60 (d,2H), 7.62-7.59 (m,4H), 7.47-7.43 (m,2H), 3.32 (s,3H), 2.93 (s,3H). ¹³C NMR (125 MHz, CDCl₃): 176.08, 163.32, 161.53, 131.12, 129.90, 127.96, 126.88, 126.39, 125.60, 123.12, 51.35, 13.42. HRMS Calc'd for M+H C₂₀H₁₄NO₃⁷⁹Br+H, m/z 396.0227; Found: 396.0235.

Laser Scanning Cytometry Methods: SNB-19 human glioblastoma cells (American Type Cell Culture Cat No. CRL-2266) were plated at a density of 2000 cells/mL on cover slips in RPMI medium (with L-glutamine and penicillin/streptomycin and supplemented with 10% fetal bovine serum). Cell culture medium and supplements were obtained from VWR (West Chester, PA). The cells were incubated at 37 °C under a humidified atmosphere containing 5% CO₂ and allowed to adhere. Medium was aspirated and replaced with 1 μM NSC 728558 for 24-h exposure. Drug was removed and cells were washed twice with phosphate buffered saline (PBS).

Cells were fixed in 4% paraformaldehyde (15 min, 21 °C) and washed once with PBS. Following two additional washes, slides were inverted to microscope slides and sealed using FluorSave Reagent (Calbiochem). Images were generated from scans from a CompuCyte iCys Laser Scanning Cytometer. (CompuCyte, Westwood, MA). Cells were scanned with a 405 nm 30 mW Diode laser. Fluorescent signals were measured in photo-multiplier detectors following a 440/30 Band-pass (BP) filter to detect NSC 728558 presence. Light absorption was also measured to produce a differential interference contrast (DIC)-like image for cell morphology. Each signal was given a pseudo-color and overlaid to produce images.

Acknowledgement

The authors thank the NIH for grants R21NS067466, P20RR017670 and P30NS055022 for financial support of this work.

References

1. (a) Zhu, S.; Shi, S.; Gerritz, S.W. *Tetrahedron Lett.* **2011**, *52*, 4001-4004. References 1-4 of this paper reviews recent bioactive isoxazoles in the patent literature. (b) Nakamura, M.; Kurihara, H.; Suzuki, G.; Mitsuya, M.; Ohkubo, M.; Ohta, H. *Bioorg. Med. Chem. Lett.*, **2010**, *20*, 726-729.
2. The Kurth group has provided a useful catalog of the bioactive isoxazole literature in their NOC synthesis papers over the years, the following are illustrative examples: (a) Yu, G.J.; Yang, B.; Verkman, A. S.; Kurth, M. J. *Synlett* **2010**, *7*, 1063-1066. (b) Meng, L.; Lorsbach, B.A.; Sparks, T.C.; Fettinger, J.C.; Kurth, M.J. *J. Comb. Chem.* **2010**, *12*, 129-136. (c) Butler, J.D.; Donald, M.B.; Ding, Z.; Fettinger, J.C.; Kurth, M.J. *Tetrahedron Lett.* **2009**, *50*, 5110-5112. (d) Choung, W.; Lorsbach, B.A.; Sparks, T.C.; Ruiz, J. M.; Kurth, M.J. *Synlett* **2008**, *19*, 3036-3040. (e) Quan, C.; Kurth, M. *J. Org. Chem.* **2004**, *69*, 1470-1474 (f) Hwang, S.H.; Kurth, M.J. *J. Org. Chem.* **2002**, *67*, 6564-6567.
3. In the course of their studies on glutamate receptor and transporter ligand pharmacology, the Krogsgaard-Larsen group has greatly expanded the tool box for isoxazole synthesis: Egebjerg, J.; Schousboe, A.; Krogsgaard-Larsen, P., Eds. *Glutamate and GABA Receptors and Transporters, Structure Function and Pharmacology*. Taylor and Francis: NY, NY, **2002**.
4. Pinho e Melo, T. M.V.D. *Current Org. Chem.*, **2005**, *9*, 925-958.
5. Trogu, E.; Cecchi, L.; De Sarlo, F.; Guideri, L.; Ponticelli, F.; Machetti, F. *Eur. J. Org. Chem.* **2009**, 5971–5978, and cited references.
6. Bode, J. W.; Hachisu, Y.; Matsuura, T.; Suzuki, K. *Org. Lett.*, **2003**, *5*, 391-394.

7. Bode, J.W.; Hachisu, Y.; Matsuura, T.; Suzuki, K. *Tetrahedron Lett.* **2003**, *44*, 3555–3558.
8. Han, X.; Li, C.; Mosher, M.D.; Rider, K.C.; Zhou, P.; Crawford, R.L.; Fusco, W.; Paszczynski, A.; Natale, N. R. *Bioorg. Med. Chem.* **2009**, *17*, 1671-1680.
9. Gajewski, M.P.; Beall, H.; Schnieder, M.; Stranahan, S. M.; Mosher, M. D.; Rider, K. C.; Natale, N. R. *Bioorg. Med. Chem. Lett.* **2009**, *19*, 4067-4069.
10. (a) Veiseh, M.; Gabikian, P.; Bahrami, S.-B.; Veiseh, O.; Zhang, M.; Hackman, R. C.; Ravanpay, A.C.; Stroud, M. R.; Kusuma, Y.; Hansen, S.J.; Kwok, D.; Munoz, N. M.; Sze, R.W.; Grady, W.M.; Greenberg, N. M.; Ellenbogen, R. G.; Olson, J. M. *Cancer Res.* **2007**; *67*: 6882-6888. (b) Smeltzer, C.; Cannon, M.J.; Pinson, P.; Munger, J.S.; West, F.G.; Grissom, C.B. *Org. Lett.* **2001**, *3*, 799-801. (c) McGreevy, J. M.; Cannon, M.; Grissom, C. B. *J. Surg. Res.* **2003**, *111*, 38-44.
11. Feuer, H., Ed, *Nitrile Oxides, Nitrones and Nitronates in Organic Synthesis*, John Wiley & Sons, Inc., Hoboken, New Jersey, 2008.
12. (a) Stork, G.; McMurry, J.E. *J. Am. Chem. Soc.* **1967**, *89*, 5461- 5462. (b) McMurry, J.E. *Org. Synth.* **1988**, *Coll. Vol. VI*, 582-594.
13. Natale, N.R.; McKenna, J.I.; Niou, C.-S.; Borth, M.; Hope, H. *J. Org. Chem.*, **1985**, *50*, 5660-6.
14. Zamponi, G.; Stephanie C. Stotz, Richard J. Staples, Rogers, T.A.; Nelson, J.K.; Hulubei, V.; Blumenfeld, A.; Natale, N.R. *J. Med. Chem.*, **2003**, *46*, 87-96, and cited references.
15. Bowles, K.D.; D.A. Quincy, D.A; Mallet, B.; McKenna, J.I.; Natale, N.R. *J. Chem. Ed.*, **1985**, *62*, 1118-20.
16. (a) Mosher, M.D.; Natale, N.R. *J. Heterocycl. Chem.*, **1995**, *32*, 779-781. (b) Han, X.; Twamley, B.; Natale, N.R. *J. Heterocycl. Chem.*, **2003**, *40*, 539-545.
17. Grundmann, C.; Dean, J.M. *J. Org. Chem.*, **1965**, *30*, 2809-2812.
18. (a) Beger, J.; Thielemann, C. *J. Praktische Chem.*, **1981**, *323*, 337-344. (b) Fujisawa, T.; Sato, T.; Takeuchi, M. *Chem. Lett.*, **1982**, *1*, 71-74.
19. Han, X.; Li, C.; Rider, K.C.; Blumenfeld, A.; Twamley, B.; Natale, N.R. *Tetrahedron Lett.*, **2002**, *43*, 7673-7677.
20. (a) Renzi, G.; Dal Piaz, V. *Gazz. Chim. It.*, **1965**, *95*, 1478-1491. (b) Renzi, G.; Pinzauti, S. *Il Farmaco Ed. Sci.*, **1969**, *24*, 885-892.
21. (a) Liu, B.; Liu, G.; Xin, Z.; Serby, M.D.; Zhao, H.; Schaefer, V.G.; Falls, D.; Kaszubska, W.; Collins, C.A.; Sham, H. L. *Bioorg. Med. Chem. Lett.* **2004**, *14*, 5223–5226 (b) Xin, Z.; Zhao, H.; Serby, M.D.; Liu, B.; Schaefer, V.G.; Falls, D.H.; Kaszubska, W.; Collins, C.A.; Sham, H.L.; Liu, G. *Bioorg. Med. Chem. Lett.* **2005**, *15*, 1201–1204.

22. Butler, J.D.; Coffman, K.C.; Ziebart, K.T.; Toney, M.D.; Kurth, M.J. *Chem. Eur J.*, **2010**, *16*, 9002-9005